

SOME ASPECTS OF OCEANIC VARIABILITY
IN THE UPPER LAYERS OF THE BAY OF BENGAL

by

K. V. SANIL KUMAR

Naval Physical and Oceanographic Laboratory
Cochin 682 021

Thesis submitted
in partial fulfilment of the requirements
for the degree of Doctor of Philosophy
in Physical Oceanography under the
Faculty of Marine Sciences

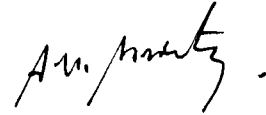
to

Cochin University of Science and Technology
Cochin 682 022

March 1995

C E R T I F I C A T E

This is to certify that the Thesis entitled 'Some aspects of Oceanic Variability in the upper layers of the Bay of Bengal' is an authentic record of research work carried out by Mr. K.V. Sanil Kumar under my supervision and guidance in the Naval Physical and Oceanographic Laboratory, Kochi for the Ph. D. degree of the Cochin University of Science and Technology and no part of it has previously formed the basis for the award of any other degree in any university.



Kochi
March 1995

Dr. A.V.S. Murty
(Research Supervisor)

C O N T E N T S

Preface		i - iii
List of Figures		iv - ix
Chapter I	Introduction	1 - 15
Chapter II	Thermohaline variability in the northern Bay of Bengal during the MONsoon Trough Boundary Layer EXperiment (MONTBLEX-90)	16 - 38
Chapter III	Salinity and currents in the northern Bay of Bengal during the Summer Monsoon Experiments	39 - 53
Chapter IV	Thermohaline and current variability off Visakhapatnam during summer monsoon season	54 - 67
Chapter V	Thermohaline and current variability off Andaman Islands during pre-monsoon season	68 - 80
Chapter VI	The hydrographic observations on the Western Boundary Current of the Bay of Bengal during March 1993	81 - 94
Chapter VII	Summary and Conclusions	95 - 103
References		104 - 121

P R E F A C E

Since the surface winds and currents reverse their direction seasonally, the Bay of Bengal is one of the best natural laboratories among the world oceanic regions to study the ocean-atmosphere coupling and related dynamics. In addition, the oceanographic environment in the northern Bay of Bengal, especially north of 15°N , is very complex due to the huge amount of river and sediment discharge. Moreover, the northern Bay is the only oceanic region where the monsoon trough extends into the sea. Consequently, intense convective activity and the genesis of monsoon depressions take place in this region which in turn control the rainfall events over east central India. The western and eastern boundaries of the Bay of Bengal are also characteristically different from the other world oceanic regions. In spite of all these typical features of the Bay of Bengal, it still continues as the least explored region.

With the advent of the satellites, oceanographers are able to monitor the synoptic variability of oceanographic parameters over a larger surface area. But, monitoring the subsurface oceanographic conditions and prediction of their short-term variability is still a challenging problem. In this regard, one-dimensional numerical models are helpful to a certain extent.

In this study, some aspects like short-term variability in the thermohaline and current fields at selected locations in the northern, western and east central Bay of Bengal and spatial variability of the recently identified (Legeckis, 1987) Western Boundary Current during March 1993 are studied. Two 1-D models of KTDM (Kraus and Turner, 1967 - Denman, 1973 - Miller - 1976) and NK (Niiler and Kraus, 1977) are also evaluated at the selected locations.

The thesis is divided into seven chapters with further subdivisions.

The first Chapter reviews the present knowledge on the major oceanographic features in the upper layers of the Bay of Bengal and gives a brief description about the objective of the present study.

The second Chapter deals with short-term thermohaline variability, genesis of meteorological disturbances and numerical simulation of the mixed layer characteristics in the northern Bay of Bengal during MONsoon Trough Boundary Layer EXperiment (MONTBLEX-90).

Short-term variability in the salinity and current fields in the northern Bay of Bengal during Summer Monsoon Experiments is examined in the Chapter III.

In the Chapter IV, a critical study is made to understand the short-term variability in the thermohaline and current structure, vertical mixing

characteristics of the water column and their effects on the mixed layer simulations off Visakhapatnam during summer monsoon season.

The Chapter V deals with the same aspects described in the Chapter IV, but at a different place in the east central Bay of Bengal, off the Andaman Islands.

The hydrographic features of the Western Boundary Current of the Bay of Bengal during March 1993 are described in the Chapter VI.

Finally, the Chapter VII summarizes all the important results and conclusions and points out the future scope of the work.

LIST OF FIGURES

- Fig. 1.1. The Bay of Bengal with bathymetry (m)
- Fig. 1.2. Monthly surface winds over the north Indian Ocean (Rao et., 1991)
- Fig. 1.3. The major rivers bordering the Bay of Bengal
- Fig. 1.4. Seasonal variation of salinity in the upper layers of the north Indian Ocean (Levitus, 1982)
- Fig. 2.1. Typical tracks of meteorological lows/depressions during July (India Meteorological Department, 1979) with spatial transects and the time series station of ORV Sagar Kanya during MONTBLEX-90.
- Fig. 2.2. Observed and estimated radiation using Lumb's (1964) scheme at 18.5°N & 89°E during August 1977 and at 18°N & 89.5°E during July 1979.
- Fig. 2.3. Schematic diagram to show the mixed layer physics (Denman, 1973).
- Fig. 2.4. Time series of surface pressure analysis - arranged columnwise in the chronological order from 15 August to 19 September 1990.
- Fig. 2.5. Time series of cloud imageries viewed by INSAT 1 D - arranged columnwise in the chronological order from 15 August to 19 September 1990.
- Fig. 2.6. Time series of surface meteorological parameters.
- Fig. 2.7. Time series of heat budget parameters.

- Fig. 2.8. Global MCSST analysis at 20°N and 90°E for 1990 (Legeckis, 1991). The figure in the inset represents the comparison between the MCSST analysis and sea truth data.
- Fig. 2.9. Annual cycle of temperature and salinity in the top most 250m water column at the time series station (based on Levitus, 1982).
- Fig. 2.10. Thermal structure along Leg1 and Leg2 based on XBT data.
- Fig. 2.11. (a) Mean vertical profiles of temperature, salinity and σ_t at the time series station (b) Temperature and salinity profiles at 3 hourly intervals in chronological order (c) Depth time section of temperature and (d) Depth-time section of salinity.
- Fig. 2.12. Depth-time section of Brunt-vaisala frequency (cycles/hour).
- Fig. 2.13. Depth-time section of temperature for the upper 40 m water column.
- Fig. 2.14. Time series of heat flux and heat content with respect to 28.7°C isotherm.
- Fig. 2.15. Time series of observed and simulated (using NK model) mixed layer depth.
- Fig. 2.16. Time series of observed and simulated (using NK model) mixed layer temperature.
- Fig. 2.17a. Time series of observed and simulated (using KTDM model) mixed layer depth.
- Fig. 2.17b. Time series of observed and simulated (using KTDM model) mixed layer temperature.
- Fig. 3.1. Stations occupied during the Summer Monsoon Experiments in the northern Bay of Bengal.

- Fig. 3.2. Temperature (T), salinity (S) and sigma-t (σ) for polygons of M-77 and M-79.
- Fig. 3.3. Brunt Vaisala Frequency (N) for polygons of M-77 and M-79.
- Fig. 3.4. Depth-time sections of salinity during M-77 and M-79.
- Fig. 3.5. Evaporation (E), precipitation (P), E-P, Σ E-P and salinity (S) at three stations of M-79.
- Fig. 3.6. Salinity for the upper 50 m, surface winds and currents on 18 July 1979 at W79.
- Fig. 3.7. Stick plots of surface winds and subsurface currents during M-77.
- Fig. 3.8. Stick plots of surface winds and subsurface currents during M-79.
- Fig. 3.9. Vectorially averaged surface winds and subsurface currents during M-77 and M-79.
- Fig. 3.10. Rotary spectra during M-77.
- Fig. 3.11. Rotary spectra during M-79.
- Fig. 4.1. Stations covered during June/July 1986 off Visakhapatnam.
- Fig. 4.2. Vertical sections of temperature along sections A and B.
- Fig. 4.3. Time series of meteorological elements at the deep (ST1) and shallow (ST2) station locations.
- Fig. 4.4. Time series of heat budget components at the deep (ST1) and shallow (ST2) station locations.

- Fig. 4.5. Temperature-time sections at the deep (ST1) and shallow (ST2) station locations.
- Fig. 4.6. Vectorially averaged surface wind and subsurface currents at shallow station (ST2).
- Fig. 4.7. Stick plots of surface winds and subsurface currents.
- Fig. 4.8. Time series of temperature (T), salinity (S) and offshore (U) and alongshore (V) components of currents at ST2.
- Fig. 4.9. Spectra of temperature (T), salinity (S), and offshore (U) and alongshore (V) components of currents.
- Fig. 4.10. Time series of Richardson number (Ri), Brunt Vaisala Frequency (N) and vertical current shear (SR) at ST2.
- Fig. 4.11. Time series of mixed layer depth (MLD) and mixed layer temperature (MLT) at ST1 and ST2.
- Fig. 5.1. Temperature and salinity distributions at different depths around the Andaman Islands.
- Fig. 5.2. Time series of meteorological elements.
- Fig. 5.3. Time series of heat budget components.
- Fig. 5.4. Composit plot of temperature, salinity and σ_t
- Fig. 5.5A. Depth-time section of temperature.
- Fig. 5.5B. Depth-time section of salinity.
- Fig. 5.6A. Vectorially averaged surface wind and subsurface currents.
- Fig. 5.6B. Stick plots of surface winds and subsurface currents

- Fig. 5.7. Time series of temperature (T), salinity (S) and east-west (U) and north-south (V) components of currents.
- Fig. 5.8. Spectra of temperature (T), salinity (S), and east-west (U) and north-south (V) components of currents.
- Fig. 5.9. Time series of Richardson number (Ri), Brunt Vaisala Frequency (N) and vertical current shear (SR).
- Fig. 5.10. Time series of mixed layer depth (MLD) and mixed layer temperature (MLT).
- Fig. 6.0. SST of the north Indian Ocean during the first week of February 1993 derived from the infra-red imageries of NOAA satellites.
- Fig. 6.1. Stations covered during March 1993 off the east coast of India along the sections 1 (11°N) to 8 (18°N) at 1° interval.
- Fig. 6.2. (a) The SST obtained from MICOM STD (9 - 23 March 1993)
 (b) Weekly averaged SST derived from the infrared imageries of NOAA satellites (15 - 22 March 1993)
 (c) Surface (5m) salinity (9-23 March 1993).
- Fig. 6.3. Vertical sections of temperature along sections 1 to 8. Contour interval is 1°C .
- Fig. 6.4. Vertical sections of salinity along sections 1 to 8.
- Fig. 6.5. Dynamic topography charts off the east coast of India during March 1993 relative to 500 db at (a) surface (5 db), (b) 100 db and (c) 200 db.
- Fig. 6.6. Geostrophic volume transport across the sections 1 to 8

- Fig. 6.7. TS diagrams for (a) region I, (b) region II, (c) region III and (d) region IV.
- Fig. 6.8. Temperature and salinity profiles at 12°N and 82°E .
- Fig. 6.9. Temperature, salinity, $\sigma_{s,t,p}$ and meridional flow along 14°N during May 1987.
- Fig. 6.10. Geostrophic volume transport across 14°N .

CHAPTER I

INTRODUCTION

The Bay of Bengal (area $\approx 2.2 \times 10^{12} \text{ m}^2$) is a portion of the north Indian Ocean bordering by Sri Lanka, India, Bangladesh, Myanmar, Thailand and Malaysia (Fig 1.1). The southern boundary of this basin can be considered at 6°N based on the geostrophic current structure (Varkey, 1986). The topography is conical in shape with its wider ($\approx 2000 \text{ km}$) and deeper ($\approx 4000 \text{ m}$) end towards south and narrower and shallower end towards north. The southeastern side of the Bay is enriched by a chain of Islands known as the Andaman and Nicobar Islands with complex bottom topography.

1.1. Major Oceanographic features of the Bay of Bengal

1.1.1. Surface winds

The basic source of surface wind information over the Bay comes from ships of opportunity supplemented by measurements from satellites, few island stations and coastal net work of observatories. Few climatological studies are available utilizing these observations (Hastenrath and Lamb, 1979; Rao et al., 1991). The distributions of surface winds (Rao et al., 1991) is shown in Fig. 1.2. During the peak of the winter monsoon (December/January), winds are northeasterly with an average speed of $\sim 4 \text{ m/s}$. The surface wind field reverses and strengthens with average speed of $\sim 8 \text{ m/s}$ during the height of summer monsoon (June/July/August). This reversal of wind direction from winter to summer is due to large scale movement of ITCZ over the Indian Ocean in response to differential heating between land and sea. The periods between the two monsoons are the transition phases. During the transition between summer and winter monsoons (October), winds are mainly anticlockwise in the Bay. However, by November winds south of 7°N becomes easterly and

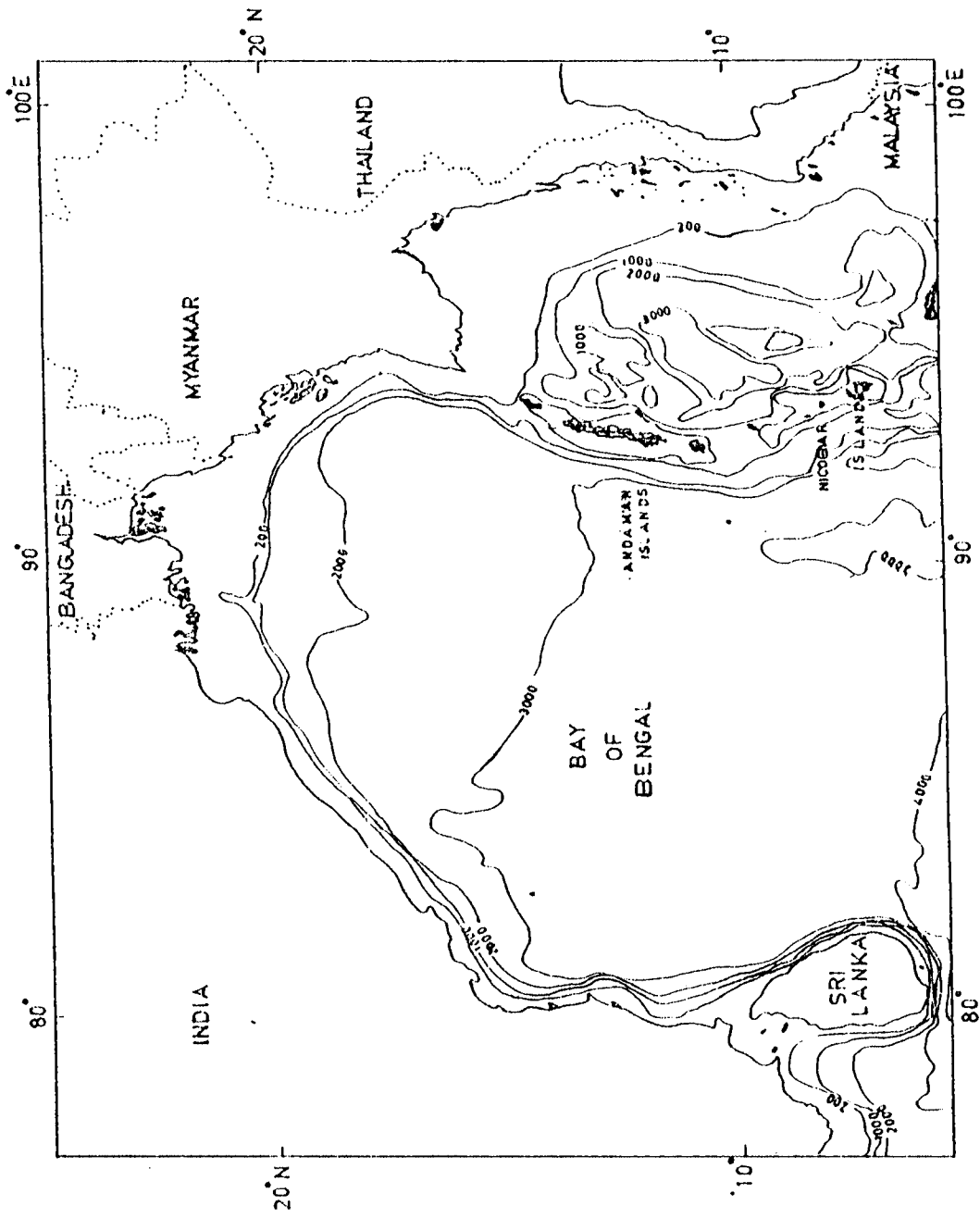


Fig.1.1.1 The Bay of Bengal with bathymetry (m)

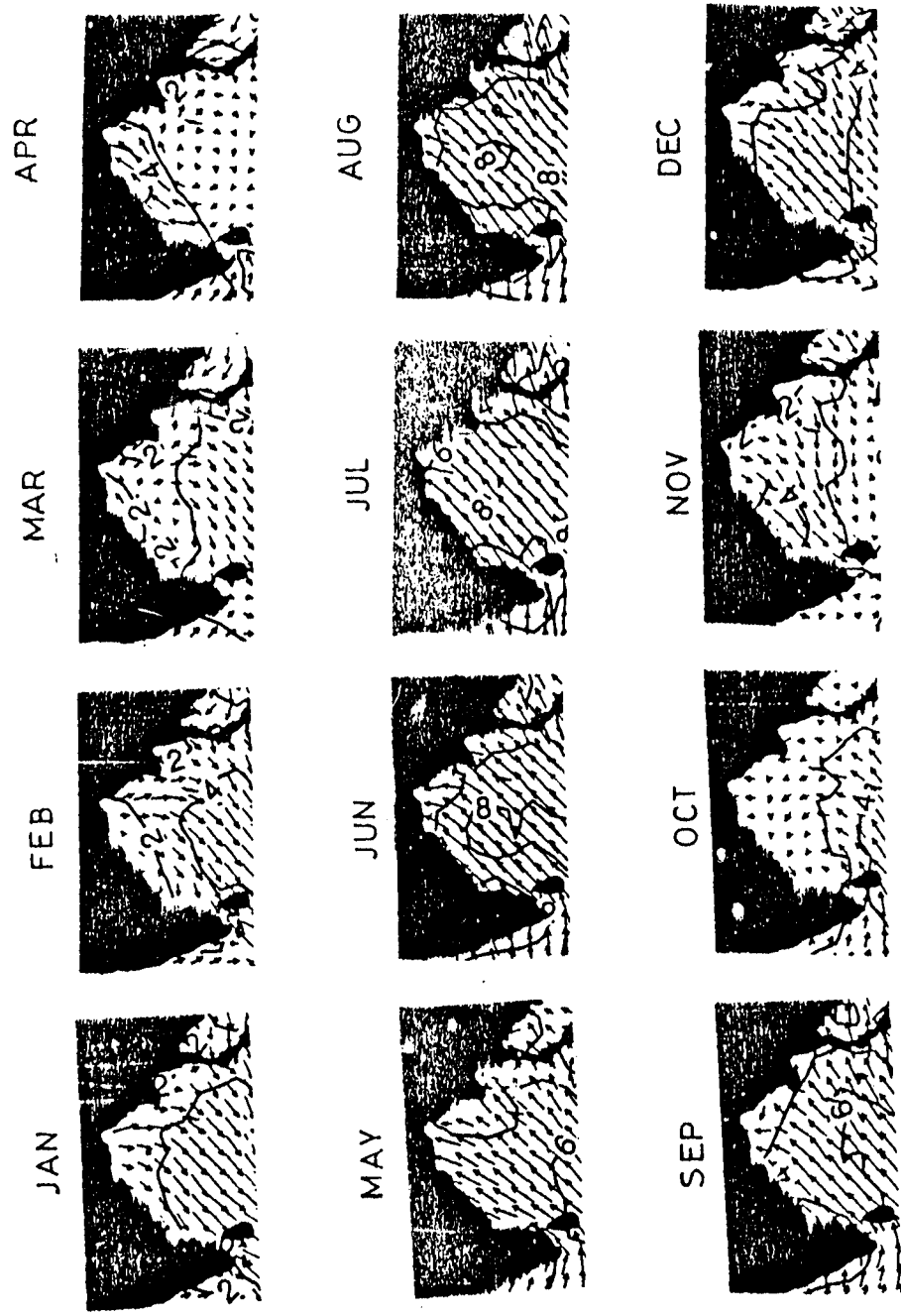


Fig. 1.2. Monthly surface winds over the north Indian Ocean (Rao et., 1991)

thus develops a positive wind stress curl around 7°N . The axis of this positive wind stress curl moves southward and crosses the equator with the progress of the season. During, the transition from winter to summer monsoon (March/April), the circulation is anticyclonic over the entire Bay which disappears with the arrival of the southwest monsoon. Thus the surface circulation is characterized by northeasterly and southwesterly winds during winter and summer monsoon seasons respectively with the alternate clockwise (March/April) and anticlockwise (October) circulation during the transition phases.

1.1.2. Surface currents

Following the winds over the Bay, surface circulation also shows a reversal in direction with season. In fact, all the information on the near-surface flow for this area is derived mostly from (i) monthly mean currents based on observations of ship drifts (KNMI 1952; U.S. Navy, 1976; Cutler and Swallow, 1984; Hastenrath and Greischar, 1989; Rao et al., 1991) (ii) charts of dynamic topography (LaFond and LaFond, 1968; Varadachari et al., 1968; Duing, 1970; Wyrтки, 1971; Murty et al., 1992; 1993; Suryanarayana et al., 1993; Shetye et al., 1993), (iii) physical properties (Gopalakrishna and Sastry, 1985), (iv) satellite imageries (Rao, 1974; Legeckis, 1987) and (v) model results (Potemra et al., 1991; Yu et al., 1991; Johns et al., 1992; McCreary et al., 1993). It is found that the winds are not the only factor influencing the circulation system. Spreading of the massive freshwater from river mouths to interior (Shetye and Shenoi, 1988; Shetye, 1993), coastal Kelvin waves and westward propagating Rossby waves from the eastern boundary

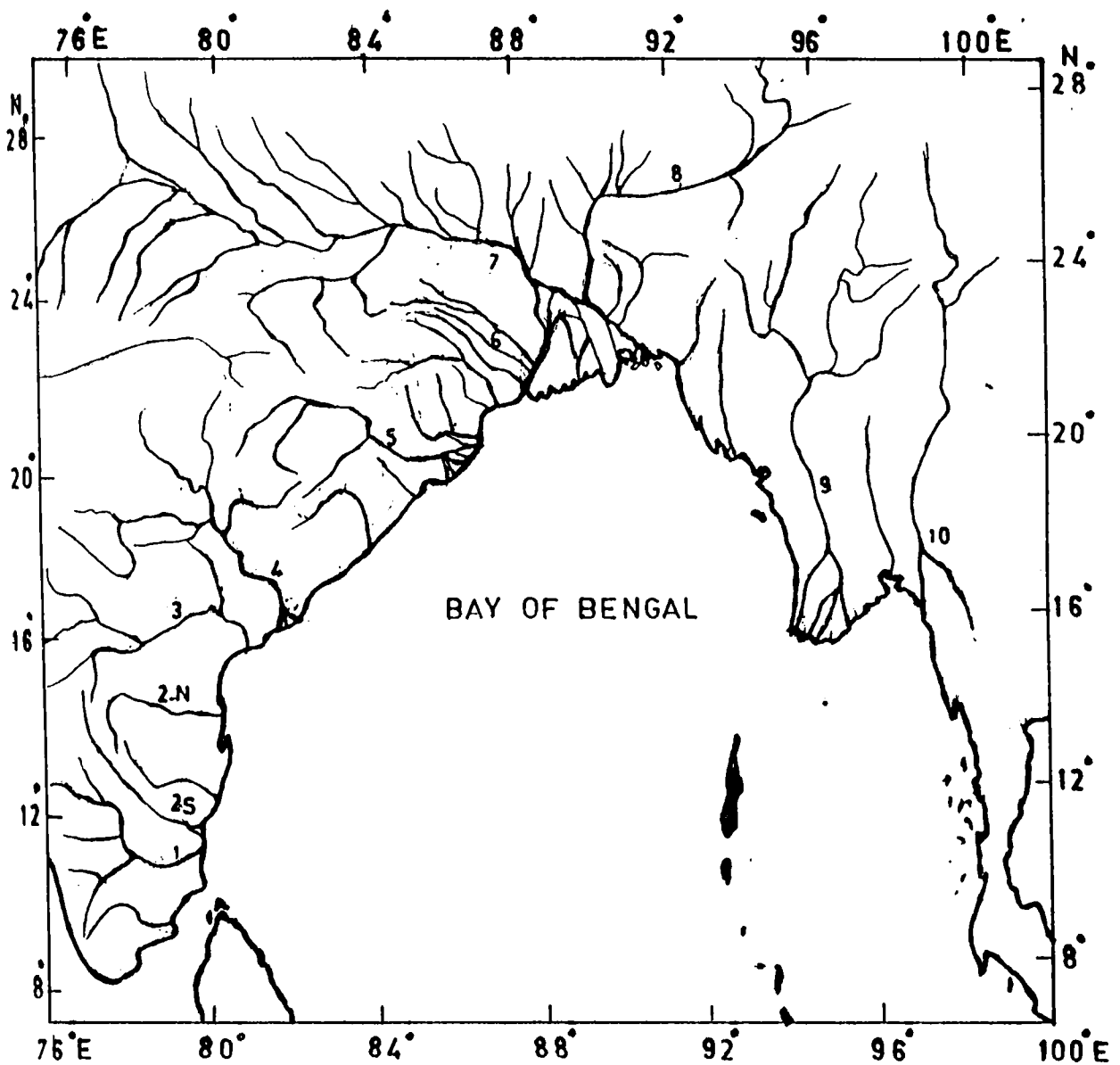
of the basin (Yu et al., 1991; Potemra et al., 1991; McCreary et al., 1993) etc. also make the system complex. Occasions of frequent cyclonic storms which is a characteristic feature of the Bay, also affect the system. The major features of the seasonal variability of the circulation are numerically modelled with boundary forcing derived from climatological monthly mean winds (Potemra et al., 1991). They found a very good comparison with Cutler and Swallow (1984). A large scale anticyclonic gyre begins to form during January and occupies the whole Bay by February. This gyre continues up to March. The western edge of this anticyclonic gyre shows the characteristic of a Western Boundary Current (WBC) similar to those of the other ocean basins (Legeckis, 1987; Potemra et al., 1991; Johns and Ali, 1992; Shetye et al., 1993). By April, the current at the eastern side, reverses its direction to northerly and the large scale gyre splits up into two cells as one an anticyclonic cell in the western half and the other as a cyclonic cell in the eastern half. By August, the eastern cyclonic gyre occupies the entire Bay. By September - October, two cells (anticlockwise in the western half and clockwise in the eastern half) develop again with southward currents along both coasts and northward current in the centre. Although, Wyrтки (1971) computed the bi-monthly dynamic topography charts for the Bay of Bengal, they did not reveal most of the features described above especially during the second half of the year mainly due to paucity of data in this region. However, the large scale anticyclonic gyre is clear from his study during the early half of the year. Recent hydrographic surveys (Murty et al., 1992; Suryanarayana et al., 1993) show detailed features of the circulation during both the summer and winter monsoons.

1.1.3. Eddies in the upper layers of the Ocean

Mesoscale/synoptic eddies of dimensions 200 to 500 kms are common feature of the circulation system of the Bay of Bengal. Existence of such eddies in the northern Bay is revealed from the satellite infra-red imageries (Rao, 1974; Legeckis, 1987). Some more observed evidences is available from the current meter data in the northwestern region (Rao et al., 1986). Both the cyclonic and anticyclonic eddies were revealed from the geostrophic computations at different areas for different seasons (Varadachari et al., 1968; Murty et al., 1993; Shetye et al., 1993; Suryanarayana et al., 1993). Babu et al. (1991) reported first time the existence of a subsurface eddy in the northwestern region. Its dynamics and influence on the sound propagation were described by Kumar et al. (1992). Thus it can be viewed that the Bay of Bengal is an energetic zone with rich eddy structure as suggested by Swallow (1983).

1.1.4. River and sediment discharge

The Bay of Bengal is one of the few ocean basins where the significant dilution takes place in the surface layers due to the copious amount of river discharge. The major rivers bordering the Bay (Fig 1.1) discharge over $10^{12} \times 10^9 \text{ m}^3$ (Table 1.1) fresh water annually into the Bay which is greater compared to many of the other major rivers in the world. For example, only three rivers - Amazon, Congo and Orinoco - have annual discharges greater than that of Ganges and Brahmaputra together (Shetye, 1993). The spreading and mixing of these freshwater make the ocean dynamics very complex.



- | | | |
|-----------------------|----------------|-------------------|
| 1. CAUVERY R. | 4. GODAVARI R. | 8. BRAHMAPUTRA R. |
| 2. S. SOUTH PENNER R. | 5. MAHANADI R. | 9. IRRAVADY R. |
| 2.N. NORTH PENNER R. | 6. DAMODAR R. | 10. SALWEEN R. |
| 3. KRISHNA R. | 7. GANGA R. | |

Fig. 1.3. The major rivers bordering the Bay of Bengal

Table.1.1. Seasonal run off volumes of major rivers bordering the Bay of Bengal (Varkey & Sastry, 1992)

River	Total run off volume ($\times 10^9 \text{ m}^3$)	
	SWM	NEM
Brahmaputra	252.9340	30.3672
Irrawady	217.2345	19.9660
Ganga	184.7363	24.4967
Salween	90.4615	8.3143
Meghna	65.8666	7.9079
Godavari	55.5646	2.2043
Krishna	33.7977	1.1397
Mahanadi	32.3198	1.1373
Damodar	5.8231	0.3174
Cauvery	2.8926	4.2447
Mahaweli	1.1594	3.0645
Penner	0.4139	0.6073
Total	943.2039	103.7673

NEM - northeast monsoon SWM - southwest monsoon

Table 1.2. Selected rivers of the world ranked by sediment yield (Holeman, 1968)

Name	Country	Average amount of suspended load x 1000 metric tons
Yellow	China	1,890,000
Ganges	India	1,452,000
Ganges & Brahmaputra	India/Bangladesh	2,179,000
Brahmaputra	Bangladesh	726,000
Yangtze	China	499,000
Indus	Pakistan	436,000
Ching	China	409,000
Amazon	Brazil	363,000

These rivers also carry huge amount of sediments into the Bay. Table 1.2 gives a comparison of the sediment discharge of the major rivers in the world. Ganges - Brahmaputra surpass all other rivers in the sediment transportation of which a good amount settles down and spreads towards south. Consequently, the bottom is formed into a deep sea fan known as the 'Bengal Deep Sea Fan' (Curry and Moore, 1971) with a gradual north-south slope.

1.1.5. Coastal Upwelling/downwelling

The western and northeastern boundaries of the Bay are the seasonal upwelling zones. Upwelling at the western boundary, commences by February and continues upto June/July under favourable winds (LaFond, 1954; 1957; Murty and Varadachari, 1968; Rao et al., 1986; Shetye et al., 1991). By September, the wind direction changes and consequently the downwelling becomes dominant. However, evidences are available for much early (by July/August) cessation of upwelling due to the spreading over of the massive fresh water discharge from the northern end of the Bay to the southwest (Gopalakrishna and Sastry, 1985; Johns et al., 1992; Rao et al., 1993). From the upwelling index computed from the climatological winds, the east coast is classified into three zones (Suryanarayana et al., 1992) viz. (i) northern (north of Visakhapatnam), (ii) central (Kakkinada to Machilipatnam) and (iii) southern (Nellore to Cuddalore). They found a decrease in upwelling index from southern to northern zones. However, observational evidence is available for stronger upwelling off Visakhapatnam than that off Madras (Murty et al., 1968). A spatial gradient of $> 3^{\circ}\text{C}$ in SST normal to the coast in the upwelling region was observed (Murty and

Varadachari, 1968; Rao et al., 1986) off Visakhapatnam during the summer monsoon season. Shetye et al. (1991) found 30 to 40 km wide upwelling band along with the shoaling of isotherms from a depth of 75 m off the east coast. The corresponding information on the upwelling along the northeastern boundary of the Bay, is however meager (LaFond and LaFond, 1968). It is to be noted that the intensity ($<10^{-3}$ cm/s) of upwelling on both sides of the Bay of Bengal is not comparable to that off Somalia or North and South American coasts ($>10^{-3}$ cm/s; LaFond and LaFond, 1968 and Progress in Oceanography, Vol 12, No.3, 1983) and off southwest coast of India (Mathew, 1983).

1.1.6. Heat fluxes across the air-sea interface

The distribution of monthly heat fluxes is presented in few works (Hastenrath and Lamb, 1979; Hastenrath and Greischar, 1989; Rao et al., 1989; 1991) in which they found positive net flux (gain by the sea) throughout the year over the Bay. The minimum gain is reported during the peaks of winter and summer monsoon seasons whereas the maximum occurs during the monsoon transition periods. Thus the heat flux distribution shows a bimodal distribution annually, with monthly averages ranging from 20 to 120 W/m².

1.1.7. Sea Surface Temperature (SST) distribution

Sea surface temperature (SST) is an important parameter for studies on air-sea interaction, climate, monsoons, fisheries, circulation etc.. Following the distribution of net heat flux, SST also shows a bi-modal distribution (Wyrtki, 1971; Colborn, 1974; Levitus, 1987; Robinson et al., 1979; Hastenrath and Lamb, 1979; Hastenrath

and Greischar, 1989; Rao et al., 1989; 1991) with maxima during May (30°C) and October (29°C) and minima during February and July/August (Fig. 1.4). Maximum annual range [between December (22°C) and May (29°C)] in the SST values is observed in the northern Bay. At the southern Bay the amplitude of variability is much less (3°C). This variability can be explained in terms of net heat flux through the ocean surface. However, other physical processes like upwelling, remote forcing, circulation, river discharge etc. may produce regional differences in the SST field (McCreary et al., 1993). For example, the seasonal boundary currents and upwelling could also be responsible for large annual variability (5°C) along the east coast of India. Similarly, low SST appears in the head of the Bay resulting from the river discharge of cold waters during winter (Legeckis, 1987).

1.1.8. Mixed Layer Depth (MLD)

Climatology of MLD is available only in few works (Colborn, 1975; Robinson et al., 1979; Hastenrath and Greischar, 1989; Rao et al., 1991). They found the deepest MLDs during January–March (70 m) and July–August (60 m) and shallowest in April–May (30 m) and November (40 m). These deepening and shoaling processes also appear to be correlated with the net heat gain by the sea. However, McCreary et al. (1993) pointed out the importance of the physical processes like advection, remote forcing etc., on the variability of MLD climatology at different regions. They found that the upwelling favourable wind during southwest monsoon and the WBC during January–May are the major factors responsible for the decrease of the MLD on the western side of the Bay.

During the northeast monsoon, the reverse process occurs due to northeasterly winds and southward coastal currents. During the summer monsoon, in the central Bay of Bengal, MLD shallows due to the reflected Rossby waves remotely forced from the equator (Yu et al., 1991; McCreary et al., 1993).

1.1.9. Salinity in the upper layers

Very few studies on salinity variability of Bay of Bengal is reported in the literature due to paucity of observations. The seasonal distribution of the salinity in the upper layers is available only from investigations (Wyrtki, 1971; Levitus, 1982; Hastenrath and Greischar, 1989). The seasonal variability described here (Fig. 1.4) is based on Levitus (1982). At the surface of the northern Bay, minimum salinity (< 33 PSU) occurs during the summer during the entire year. The amplitude of this annual variability is maximum at the northern Bay due to large seasonality in the river discharges. In the southern Bay, the salinity does not show much variability (between 33 and 34 PSU) because of less dilution. Another notable feature is the cellular structure in the surface salinity distribution during winter (Rao and Sastry, 1981). Seasonal variability and dilution is mainly limited to the upper 100 m (Murty and Rao, 1992; Murty et al., 1992).

1.1.10. Watermasses in the upper 500 m layers

Watermasses are formed at the sea surface because of certain physical processes like cooling, evaporation, precipitation, river discharge etc.. After the formation they move along with the local flow. While moving from the source region, they mix with the surrounding waters, but still

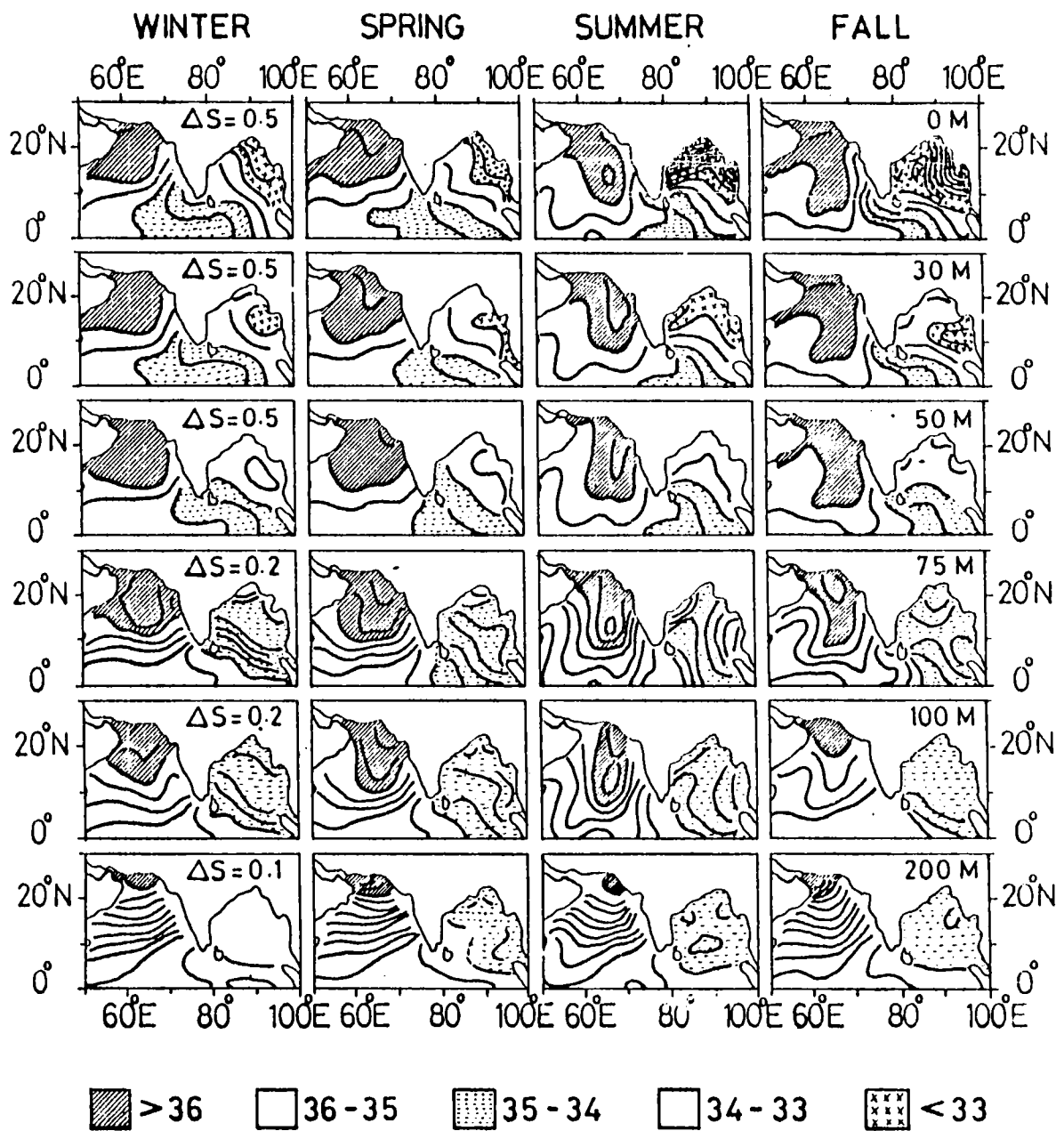


Fig. 1.4. SEASONAL VARIATION OF SALINITY IN THE UPPER LAYERS OF NORTH INDIAN OCEAN

retain their σ_t identity and sink/rise to maintain the stability of the water column. Excess evaporation over precipitation in the partially enclosed basins is the reason for the formation of the high saline Persian Gulf Watermass (PGW) and the Red Sea Watermass (RSW). But in the Bay of Bengal, the greater dilution causes the formation of low saline watermass in the upper layers ($\sigma_t = \simeq 21$). The Bay of Bengal is connected to the equatorial region at south, to the Arabian Sea at southwest and to the south China Sea at southeast through Malacca Strait. So all the watermasses which form in the neighbourhood regions are present in the Bay of Bengal at different depths. Watermasses originated from the Arabian Sea and were located (Rao, 1956; Balaramamurty, 1957; Rochford, 1964; Varadachari et al., 1968; Sastry et al., 1985; 1986; Premchand et al., 1986a; 1986b; Varkey and Sastry, 1992) in the Bay are (i) the Arabian Sea High Salinity Watermass ($\sigma_t = \sim 23.93$), (ii) the Persian Gulf Watermass ($\sigma_t = \sim 26.62$, depth of occurrence = 200 to 350 m), and (iii) the Red Sea Watermass ($\sigma_t = \sim 27$, depth of occurrence = >400 m). Another watermass observed is the Equatorial Watermass of which the σ_t is ~ 23.5 (Rochford, 1964).

1.1.11. Cyclogenesis over the Bay of Bengal

The Bay of Bengal is one of the regions of high cyclogenetic activity in the tropical ocean (Nieuwolt, 1977; INDIA METEOROLOGICAL DEPARTMENT, 1979). The mean frequency of the occurrence of the tropical cyclones per 10 years over the major ocean basins are given in Table 1.3 and all the cyclonic disturbances formed over the Bay during 1877-1976 are given in Table 1.4. These tables reveal the abundance of

the cyclones over the Bay and their monthly distribution. In the Bay of Bengal and the Arabian Sea, the cyclones move towards the continent soon after their formation. Therefore, their life spans are shorter than those of the other oceanic cyclones. These cyclonic storms are known to produce pronounced thermohaline variations in the upper layers of the Bay (Rao and Rao, 1986; Rao 1987; Rao et al., 1987). The specific reasons for the abundant cyclogenesis over the Bay and the prediction of their movement are still under investigation.

Table 1.3. Frequency of occurrence of cyclones per 10 years in the various ocean basins (Nieuwolt, 1977)

Ocean basin	Frequency
Northwest Pacific Ocean	208
North Atlantic Ocean, Carribbean	85
Bay of Bengal	75
Southwest Indian Ocean	41
Northeast of Australia	31
Northwest of Australia	23
Arabian Sea	19
Northeast Pacific Ocean	10

Table 1.4. Storms occurred in the Bay of Bengal in different months during 1877-1976 (Subbaramayya and Rao, 1981)

Jan	Feb	Mar	Apr	May	Jun	Jul	Aug	Sep	Oct	Nov	Dec	Total
3	2	6	29	81	46	55	33	60	105	131	60	614

1.2.Objectives of the Present Study

1.2.1.Short-term variability in the upper ocean

Most of the atmospheric processes are found to occur over a time scale of 1-5 days (Denman, 1973). In addition, active and inactive monsoonal spells cause short-term variability in the atmosphere over the north Indian Ocean during summer monsoon season (Pisharoty, 1964; Krishnamurti and Balme, 1976; Lau and Chan, 1988). Consequently, such variability can also be expected in the upper layers of the ocean. Understanding of this short-term variability ranging from few hours to few days has immense applications in the fields of forecasting of meteorological systems, underwater acoustic propagation studies, exploitation of fisheries and dispersal of pollutants etc.. However, studies on this aspect of temporal variability in the Bay of Bengal are quite few and are limited to selected locations mainly based on data collected during the summer monsoon experiments (Rao et al., 1981; Anto et al., 1982; Rao et al., 1983; Anto and Somayajulu, 1985; Rao et al., 1985; Rao and Rao, 1986; Rao, 1987; Rao et al., 1987; Rao and Mathew, 1988). Subsequently few more field observations were also made (Antony et al., 1985; Rao et al., 1986; Rao P. B. et al., 1987; Sarma et al., 1991). The short-term variability of some of the oceanographic parameters at few selected locations are studied here as the presently available information is inadequate.

1.2.2.Simulation of the mixed layer characteristics

Generally, the upper ocean thermal structure constitutes a near isothermal layer (known as mixed layer) capped over a thermocline. The mixed layer is controlled by

the variations in the surface wind stress, buoyancy flux, shear instability at the base of the mixed layer and horizontal and vertical advection. In the coastal waters, bottom friction, river discharges, upwelling/sinking etc., also modify the thermal structure. Prediction of the short-term variability in the mixed layer characteristics as depth (MLD) and temperature (MLT) is an important aspect for several oceanographic applications. A systematic approach to model the surface mixed layer characteristics was initiated by Kraus and Turner (1967) assuming that the energy inputs at the air-sea boundary and mass entrainment at the bottom of the layer mix uniformly within the mixed layer. Denman (1973) modified the model by incorporating the time dependent meteorological inputs. This concept was further extended by Miller (1976) to include the salinity effects. Several other authors also contributed to the development and evaluation of one dimensional numerical models (Denman and Miyake, 1973; Pollard et al., 1973; Niiler, 1975; Mellor and Durbin, 1975; Elsberry et al., 1976; Kim, 1976; Thompson, 1976; Garwood, 1977; Niiler and Kraus, 1977; Davis et al., 1981; Price and Weller, 1986; Price et al., 1986; Price et al., 1987). However, most of these studies are limited to Pacific and Atlantic Oceans where long time series measurements of temperature profiles and surface meteorological elements are made from weather ship stations and moored buoys. In the coastal waters off the west coast of India few studies were carried out utilising Miller's (1976) model during post-monsoon season with reasonably good agreement with the observations (Hareesh Kumar et al., 1990; Joseph et al., 1992; Murthy and Hareesh Kumar, 1991). In deep oceanic regions of the Arabian Sea, the same model was also evaluated

at certain selected locations (Rao, 1986; Rao and Mathew, 1990; Rao R. R. et al., 1993). Sanil Kumar et al. (1991) evaluated the Niiler and Kraus (1977) model at a station in the southern Arabian Sea during summer monsoon season. At a coastal station off Bombay, Niiler and Kraus (1977) model was found more suitable compared to Miller's (1976) model during south west monsoon period (Sanil Kumar et al., 1993). However, no attempts were reported in the literature to simulate the short-term variability in the thermal structure of the Bay of Bengal.

Therefore, an attempt is made in this study to understand the short-term variability as a coupling between local meteorological forcing and the upper layers of the Bay. Some numerical modelling attempts to simulate the observed short-term variation of mixed layer characteristics of selected locations are described in this study. Two 1-dimensional numerical models of Miller (1976) (extended version of Kraus and Turner, 1967 and Denman, 1973 - designated as KTDM) and of Niiler and Kraus (1977) (extended version of Niiler, 1975 - designated as NK) are employed to evaluate this performance in reproducing the observed scales of variability. The choice of these two models is based on the fact that these two models are simple and all the relevant physics are taken into account.

1.2.3. The Western Boundary Current of the Bay of Bengal (BBWBC)

Though the Bay of Bengal is characteristically different from the other oceanic regions, this basin is still known as the least explored region. Until recently, the BBWBC was unknown due to lack of both conventional and remotely sensed measurements. After the pioneering study of Legeckis

(1987), considerable interest was generated among the ocean modellers (Potemra et al., 1991; Yu et al., 1991; Johns and Ali, 1992; McCreary et al., 1993) to simulate this boundary current system. This brought out some theories including the 'remote forcing' for the formation of this seasonal phenomenon. However, in-situ measurements of the BBWC were made only once (Shetye et al., 1993) to describe and understand the sub-surface structure of the system in some detail. An independant analysis on this current system is provided in this study to suppliment the analysis of Shetye et al., 1993.

CHAPTER II

THERMOHALINE VARIABILITY IN THE NORTHERN BAY OF BENGAL
DURING THE MONSOON TROUGH BOUNDARY LAYER EXPERIMENT
(MONTBLEX-90)

2.1.Introduction

The intra-seasonal variability of summer monsoon over India is characterised by the movement and intensity of the seasonal monsoon trough extending from northwest India to the head of the Bay of Bengal. This trough is known to have organised structure with both lateral and vertical gradients in pressure, winds and organised moist convection and oscillates north-south corresponding to inactive and active regimes of the monsoon respectively (Raghavan, 1973; Rao, 1976). Majority of the monsoon depressions form in the oceanic region of the trough (the northern Bay), travel in north - westerly to westerly direction along the trough, dissipate over the land and produce significant rainfall over the Indo-Gangetic plains. The composite of the monsoon depression tracks for a 16 year period (INDIA METEOROLOGICAL DEPARTMENT, 1979) provides ample evidence on the genesis of meteorological disturbances over the head of the Bay of Bengal and their propagation along the monsoon trough (Fig. 2.1). Although some scanty information on the thermodynamic characteristics of this trough is available (Aanjaneyulu, 1969; Raman et al, 1978; Anto et al., 1982; Holt and Sethuraman, 1986; Mooley and Shukla, 1989), systematic observations covering the land and oceanic regions of the trough are lacking. Moreover, the meteorological and oceanographic conditions favourable for the genesis of the monsoon lows/depressions at this region still remain unknown. The summer monsoon experiments conducted during 1977 and 1979 provided some preliminary insight on this problem (Rao et al., 1981; Rao and Rao, 1986; Rao, 1987; Rao et al., 1987). Long continuous time series measurements of meteorological and oceanographic variables are essential to understand this

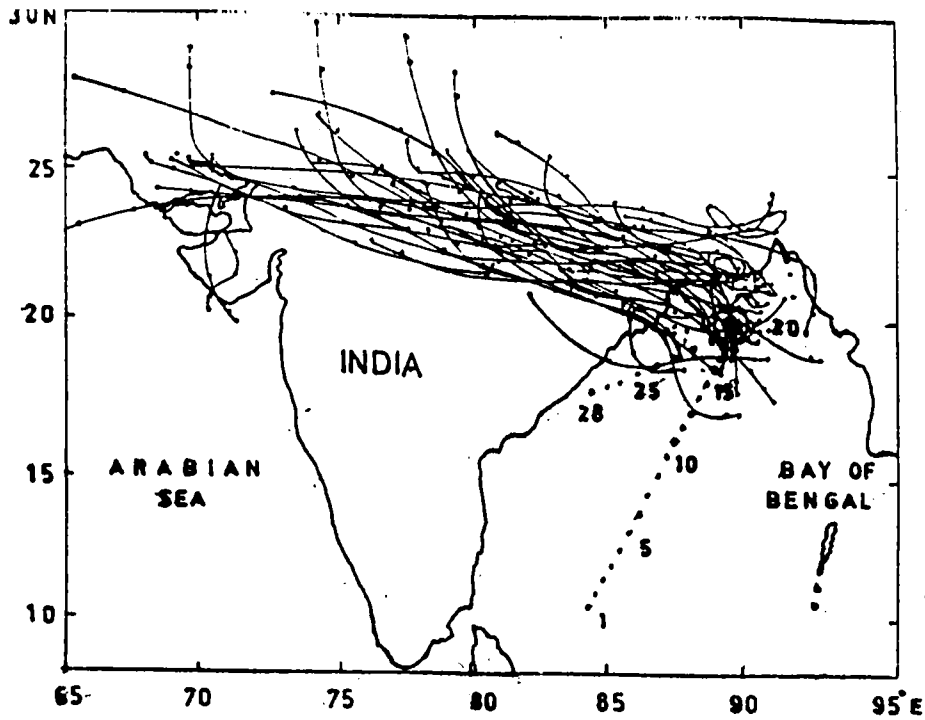


Fig. 2.1. Typical tracks of meteorological lows/depressions during July (India Meteorological Department, 1979) with spatial transects (.....) and time series station (●) of ORV Sagar Kanya during MONTBLEX - 90. Stations 1 to 19 and 19 to 28 are designated as Leg1 and Leg2 respectively.

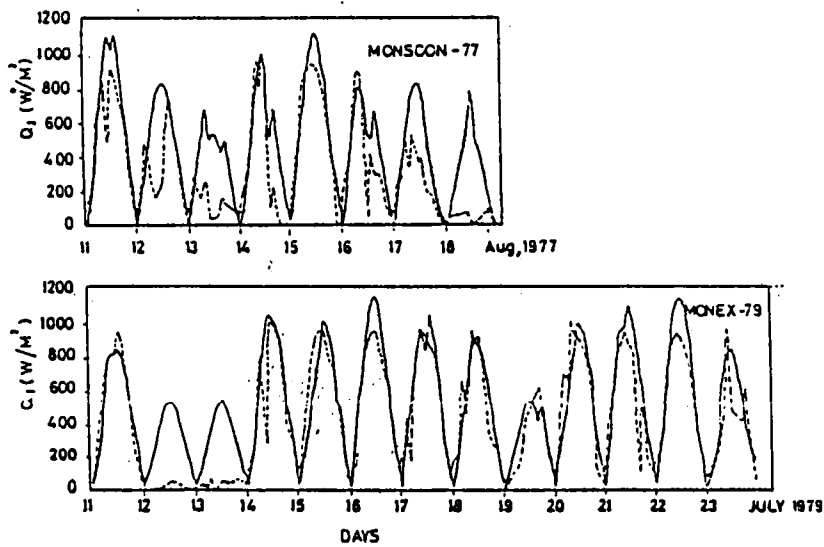


Fig. 2.2. Observed (---) and estimated (—) radiation using Lumb's (1964) scheme at 18.5 N & 89 E during August 1977 and at 18 N & 89.5 E during July 1979.

problem in greater detail.

To partially augment the above situation under a national programme, MONsoon Trough Boundary Layer Experiment (MONTBLEX) was carried out during the summer monsoon seasons of 1989 and 1990 (Goel and Srivastava, 1990). Various leading institutions of India participated in this programme. The atmospheric boundary layer was monitored at various locations in the monsoon trough region utilizing the instrumented towers, air-craft flights and routine meteorological observations. The oceanographic component was conducted during August and September 1990 by deploying ORV Sagar Kanya for time series measurements of atmospheric and oceanographic variables at a stationary location in the head of the Bay of Bengal.

The oceanographic data set thus obtained is first of its kind as there was no attempt to collect systematic time series measurements of surface meteorology and vertical profiles of temperature and salinity for such a long duration for any location in the Bay of Bengal during any season. The observational period represents both active and inactive regimes of the monsoon. Thus, this oceanographic data set is ideally suitable for the evaluation of one dimensional numerical models which can resolve the short-term variability caused in the upper layer thermal structure of the ocean resulting from local meteorological forcing (Sanil Kumar et al., 1995a).

An attempt is made in this chapter to understand the observed variability in the surface meteorological forcing and thermohaline structure in the upper layers of the ocean during MONTBLEX at the oceanographic station. An attempt is made to explain the genesis of meteorological

lows/depressions in terms of local surface meteorological forcing and thermal conditions of the upper layers. Two 1-dimensional numerical models, KTDM (Kraus and Turner, 1967 - Deman, 1973 - Miller, 1976) and NK (Niiler and Kraus, 1977), were used to simulate the observed mixed layer characteristics.

2.2. Data and methodology

ORV Sagar Kanya covered two spatial legs for XBT (Sippican) survey (stations 1-19:15 to 17 August 1990 and stations 19-28:1 to 2 September 1990) in addition to time series measurements of surface marine meteorological elements at hourly interval and vertical profiles of temperature and salinity at three hourly interval. The temperature and salinity were collected using a MICOM STD (TSK Japan; accuracy: temperature 0.05°C, salinity 0.04 PSU, depth 0.3 %) at a stationary location 20°N and 89°E (Fig. 2.1) from 18 August to 1 September 1990 (phase-I) and from 8 to 19 September 1990 (phase-II). The wind speed recorded onboard at 22.5 m height was reduced to 10 m height following Wu (1980).

2.2.1. Surface heat budget estimates

Heat exchanges across the air-sea interface are estimated to assess the relative importance of local meteorological forcing in producing the observed changes in the surface layer. As no direct measurements of these fluxes are available, empirical relationships were utilised to estimate all the terms of heat budget equation

$$Q = Q_I + Q_B + Q_S + Q_E \quad (2.1)$$

where Q is net surface heat flux reckoned positive when gained by sea, Q_I is solar radiation at sea surface, Q_B is net long wave radiation, Q_S is sensible heat flux and Q_E is latent heat flux. In the tropics, Q_I is positive and all the other terms (Q_B , Q_S and Q_E) generally are negative.

To estimate the solar radiation at sea surface, direct radiation at the top of the atmosphere (solar constant - Q_0), mean transmittivity of the atmosphere and the correction for cloudiness and reflectivity of the sea surface are required. Dobson and Smith (1988) evaluated a number of models for the estimation of insolation and found that the formulation of Lumb (1964) is more accurate and accordingly modified it for general use. This scheme which gained general acceptance (Dobson and Smith, 1988; Sanil Kumar et al., 1994; Harish Kumar and Mohankumar, 1995), is used in the present study. The amount of solar radiation incident on a unit horizontal area at the sea surface is

$$Q_I = Q_0 \sin(\alpha) (A_I + B_I \sin(\alpha)) \quad (2.2)$$

where Q_0 is 1368 Wm^{-2} (Frohlich and London, 1986), α is the elevation of sun, A_I and B_I are the regression coefficients for different cloud amounts (Table 2.1).

Table 2.1: Regression coefficients for different cloud amounts

cloud (octa)	1	2	3	4	5	6	7	8
A	0.517	0.474	0.421	0.380	0.350	0.304	0.230	0.106
B	0.317	0.381	0.413	0.486	0.457	0.438	0.384	0.285

$$\sin \alpha = \sin \phi \sin \xi + \cos \phi \cos \xi \cos h \quad (2.3)$$

$$\xi = -23.45 \cos(t+11) \quad (\text{Oke, 1987}) \quad (2.4)$$

$$h = 15 * (12 - t) \quad (\text{Oke, 1987}) \quad (2.5)$$

where ξ is the declination, h is the hour angle of the sun and t is the time in hrs. This scheme produced realistic estimates of observed radiation at two closeby stations during August 1977 and July 1979 (Fig. 2.2). The agreement between the observed and estimated radiation is very encouraging with exceptions during disturbed days when this scheme overestimated due to nonincorporation of cloud thickness.

The effective outgoing long wave radiation from ocean (Q_B) is the balance between the long wave radiation from the sea surface and from the atmosphere. The cloud cover, sea-air temperature difference, water vapour content of the atmosphere immediately above the sea surface are the important factors controlling Q_B . Several semi-empirical expressions are available to estimate Q_B . Following Fung et al (1984), the net long wave radiation (Q_B) was estimated employing the empirical expression developed by Berliand and Berliand (1952).

$$Q_B = \epsilon \sigma T_S^4 (0.39 - 0.05e^{0.5}) (1 - 0.59c1) + 4\epsilon \sigma T_S^3 (T_S - T_a) \quad (2.6)$$

where ϵ , emissivity of the sea surface (0.98); σ , Stefan-Boltzman constant ($5.67 \times 10^{-8} \text{ W.m}^{-2}\text{K}^{-4}$); T_S , sea surface temperature (K); T_a , air temperature (K); e , vapour pressure

(mb) at a height 10m; c_l , fractional cloud cover ($0 \leq c_l \leq 1$).

The turbulent heat fluxes from the ocean are the heat loss/gain due to latent heat (Q_E) and sensible heat (Q_S) fluxes. In the tropical ocean, Q_E contributes to the heat loss due to evaporation while Q_S can be either gain or loss. The latent and sensible heat fluxes are parameterised with widely used bulk aerodynamic method.

$$Q_E = \rho_a C_e L_e (q_s - q_{10}) V \quad (2.7)$$

$$Q_S = \rho_a C_h C_p (T_s - T_{10}) V \quad (2.8)$$

where ρ_a , density of air (Kg.m^{-3}); L_e , latent heat of evaporation (J.Kg^{-1}); q_s , specific humidity corresponding to T (Kg.Kg^{-1}); q_{10} , specific humidity at 10m (Kg.Kg^{-1}); V , wind speed (m.s^{-1}); C_p , specific heat of air at constant pressure ($\text{J.Kg}^{-1} \text{.}^\circ\text{K}$); and C_e and C_h are the non-dimensional transfer coefficients for moisture and heat respectively. The C_e and C_h are derived from a review of previous determinations following McCreary and Kundu (1989) and Friehe and Schmitt (1976) respectively. These formulae take into account of the atmospheric stability.

$$C_e = 0.0015 + 0.00033 (T_s - T_a) \quad (2.9)$$

$$C_h = \begin{cases} 0.97 \times 10^{-3}; T_a - T_s < 0 \\ 0.86 \times 10^{-3}; T_a - T_s > 0 \end{cases} \quad (2.10)$$

2.2.2. Heat content of the water column

The net heat gain Q causes increase/decrease of heat content (HC) of the upper layers of the water column and sea surface temperature (SST). The increase in the heat storage

in the sea appears to trigger the formation of meteorological systems and thus resulting into the release of the excess heat to atmosphere (Gray, 1975). Therefore the temporal distribution of Q, HC, SST and the events of meteorological lows/depressions were compared to identify the relation between them. The HC is more representative to atmospheric processes when it is computed with respect to a shallow isotherm depth compared to any fixed depth (Stevenson and Niiler, 1983). So the HC was computed for the water column from the sea surface and the depth of the warmest isotherm appeared throughout the observational period using the following equation:

$$HC = \rho C_p \sum_{i=1}^r (T_i - T_{ref}) dz \quad (2.11)$$

where ' ρ ' is density and ' C_p ' is specific heat of the water column, ' dz ' is depth slabs of 1 m thickness, T_i is the observed temperature and T_{ref} is the reference temperature. The shallowest isotherm present throughout the observed record is taken to identify the near surface heat content variability that has occurred during this period.

2.2.3. One dimensional numerical models

It is well known that during surface heating regime under light wind conditions, the mixed layer shoals with an increase in temperature and during cooling regime mixed layer deepens due to convective overturning. Under strong winds, even if there is net heating, the surface layer deepens and cools. These changes are caused by due to turbulent entrainment of colder and denser water into the mixed layer from below layer.

2.2.3.1. Assumptions

The ocean is assumed to be horizontally homogeneous, incompressible and stably stratified fluid (Boussinesq approximation). The 'wave' like dynamical effects such as gravitational, inertial and Rossby waves are ignored. The surface mixed layer is considered to be vertically homogeneous down to a level 'h' with a density discontinuity at the base (Fig. 2.3). All the heat and momentum are uniformly distributed throughout this layer by turbulent diffusion. The time scales for the distribution of these properties are small compared to the times over which the processes of interest are assumed to occur. Below the surface layer, a stable density profile is specified at $z=-h$.

The time dependent behaviour of the mixed layer at a stationary position is formulated from a set of differential equations based on equations of conservation heat, salinity and mechanical energy with appropriate boundary conditions. In the final equations, time derivatives of h (mixed layer depth), T (mixed layer temperature), S_m (mixed layer salinity), T_h (temperature immediately below the mixed layer) and S_h (salinity immediately below the mixed layer) are expressed in terms of the time-dependant boundary inputs, like surface wind stress, incoming solar radiation, net heat loss at the surface and the temperature and salinity (or density) gradients below the mixed layer.

2.2.3.2. Boundary conditions

i) At the surface

At the top of the surface layer, the radiative and turbulent heat fluxes are proportional to the net heat

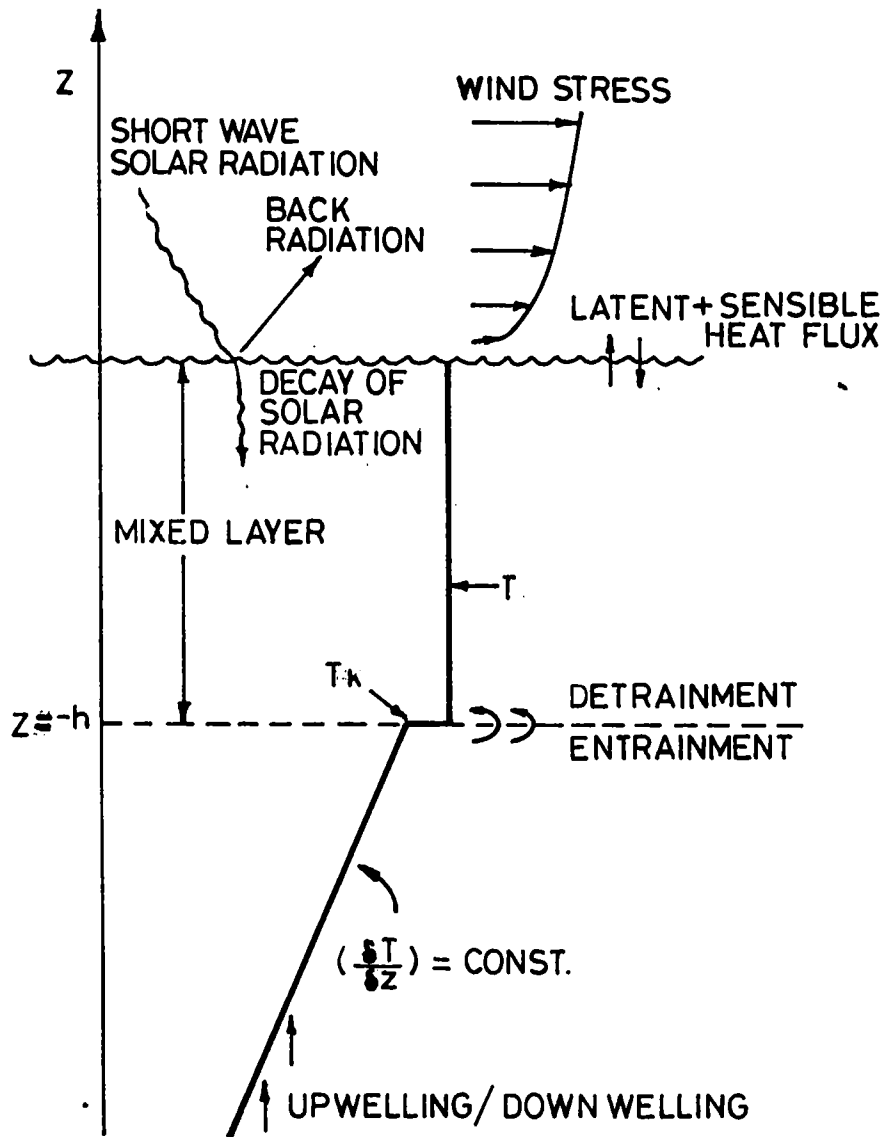


Fig. 2.3. Schematic diagram to show the mixed layer physics (Denman, 1973). The vertical temperature profile consists of a homogeneous mixed layer of thickness h and temperature T , followed by a temperature discontinuity ($T - T_h$), and a region with temperature gradient $(\delta T / \delta z)$. The surface fluxes are wind stress; incoming solar radiation; back radiation; latent heat and sensible heat flux together. The solar radiation decays in the mixed layer exponentially. A vertical velocity is prescribed below the mixed layer.

transfer through the ocean surface and fresh water flux is proportional to the difference between evaporation and precipitation.

ii) At the mixed layer base

The effect of diffusion across the stable interface at the bottom of the mixed layer is neglected and all the mixing processes are associated with the entrainment of the denser water into the mixed layer.

iii) Below the mixed layer base

In order to specify the system of equations completely, the temperature gradient below the mixed layer should be known. The assumptions made here are (a) no turbulent energy penetrates below $z = -h$ and (b) the local influence of surface forces acting on the ocean at a depth $z < -h$ is a small fraction of the forcing.

2.2.3.3. Integral equations of the Niiler and Kraus (1977) model

The final form of the major equations which determine the mixed layer characteristics of the model of Niiler and

Kraus (1977) are given below:

$$\underbrace{\frac{gh}{2} (\rho_h - \rho_m)}_{(A)} \frac{dh}{dt} = \underbrace{m_1 \rho U_*^3}_{(B)} + \underbrace{m_2 S}_{(C)} + \frac{\alpha g}{C_p} \left[\underbrace{\int_{-h}^0 q(z) dz}_{(D)} - \right.$$

$$\left. \underbrace{\frac{h}{2}(Q - q_h - r_h) - m_3 \frac{h}{4} (Q - |Q|)}_{(E)} \right] \quad (2.12)$$

$$h \frac{dT}{dt} + (T - T_h) \frac{dh}{dt} = \frac{1}{\rho C_p} (Q - q_h - r_h) \quad (2.13)$$

$$h \frac{dS_m}{dt} + (S_m - S_h) \frac{dh}{dt} = S_m (E - P) \quad (2.14)$$

$$\frac{dT_h}{dt} = \gamma R e^{-\gamma h} - L_T \frac{dh}{dt} \quad (2.15)$$

$$\frac{dS_h}{dt} = -L_s \frac{dh}{dt} \quad (2.16)$$

where U_* , frictional velocity ($U_* = \sqrt{\tau/\rho}$ where τ is surface wind stress); α , coefficient of thermal expansion; g , acceleration due to gravity; ρ , mean density of the water column; ρ_m , mean density of the mixed layer; ρ_h , density just below the mixed layer; C_p , specific heat of sea water; q_h , heat flux into the thermocline; r_h , radiative heat flux into the thermocline; L_T , temperature gradient below the mixed layer; L_s , salinity gradient below the mixed layer and

m_1, m_2 and m_3 are the coefficients represent the fractions of wind, shear and convection energy available to change the potential energy of the water column. These unknown tuning coefficients of this model do not have universally acceptable values.

The term A is rate of energy that needs to agitate entrained water; B, rate of work done by surface wind; C, rate at which energy of mass velocity field is reduced by mixing across the layer base; D, rate of potential energy change produced by penetrating solar radiation; and E, rate of potential energy produced by fluxes across the sea surface. When the wind speed changes rapidly, inertial current in upper ocean produces a sharp velocity gradient across the layer base and then the term C determines the rate of shear mixing at the interface. Following Price et al. (1978) and Paulson and Simpson (1977), the terms S and $q(z)$ in equation 2 may be written as

$$S = \frac{\rho}{2} |V - V_h|^2 \frac{dh}{dt} + \frac{1}{2} (V - V_h) \tau_h \quad (2.17)$$

$$q(z) = Q_I [R e^{\gamma_1 z} + (1-R) e^{\gamma_2 z}] \quad (2.18)$$

where V is velocity of current in mixed layer, V_h is velocity of current below the mixed layer base, R is a constant which varies with the water type, τ_h , momentum flux into the thermocline; and γ_1 and γ_2 are extinction coefficients of light attenuation for long and short wave length respectively. The terms involving q_h , r_h and τ_h are small quantities and never exceed 10 % of the principal terms. So they were significant only in the case of deep convective regime or for long term integration. Hence they were

neglected in the present study.

2.2.3.4. Comparison between NK (Niiler and Kraus, 1977) and KTDM (Kraus and Turner, 1967 - Denman, 1973 - Miller, 1976) model

The NK is analogous to KTDM, when the shear production term $m_2 S$ is ignored and convective efficiency parameter m_3 is chosen as unity. The remaining unknown coefficient in KTDM is only m_0 analogous to m_1 . The important factor in $m_2 S$ is δv^2 i.e. $|V - V_h|^2$, square of the magnitude of velocity difference across the base of the mixed layer. An explicit expression for δv^2 is given by Price et al. (1978) as

$$|V - V_h|^2 = \frac{2U_*^4}{h^2 f^2} (1 - \cos(ft)) \quad (2.19)$$

where 'f' is coriolis force and 't' is time. In KTDM, U_* alone is considered as the relevant scale velocity in determining the MLD. The inclusion of δv^2 produces more realistic results in the case of mixed layer deepening under strong wind events or long term integration. Following Paulson and Simpson (1977) double exponential term (eq. 18) is used in NK for the absorption of solar radiation at different depths instead of the single exponential term in KTDM (ie. $q(z) = Q_I e^{-\gamma h}$).

Equations 2.12 to 2.14 were integrated using Runge-Kutta numerical integration scheme with a time step of 5 min. When dh/dt is < 0 , terms involving below layer gradient lose the significance (no entrainment) and 'h' is found out using Newton's iterative technique. The MLD is taken as the deepest depth where a drop of 0.1°C occurs from the SST in the observed vertical temperature profiles (Davis

et al., 1981). Since the temperature values of MICOM STD close to surface are not reliable, the temperature at 5 m depth was considered to represent the mixed layer temperature.

2.3. Weather Summary of the Observational Period (15 August to 19 September 1990)

The time sequence of maps of surface pressure analysis (India Meteorological Department) over India and the Bay of Bengal corresponding to 0830 IST for the period 15 August to 19 September 1990 is shown in Fig. 2.4. The corresponding time sequence of cloud imageries viewed by INSAT 1D is also shown in Fig. 2.5. The genesis, intensification and landward propagation of meteorological disturbances characterised by close isobars and organised massive cloud cover are evident from Figs. 2.4 and 2.5. During this observational record, five meteorological lows formed over the head of the Bay of Bengal and traversed in west-northwesterly direction along the monsoon trough. Only one of these 5 systems intensified into a deep depression. The average life of these disturbances was about 5 days. Thus the observations collected during this experiment provided typical signatures of both active and inactive regimes of the monsoon. The time sequence of satellite imageries (Fig. 2.5) show the evolution of the cloud cover over the Bay of Bengal and the Indian subcontinent during the observational period. In general, massive cloud cover appeared southwest of the monsoon lows. The cloud cover shows a broad correspondence with the intensity of the monsoon trough and the strength of meteorological disturbances.

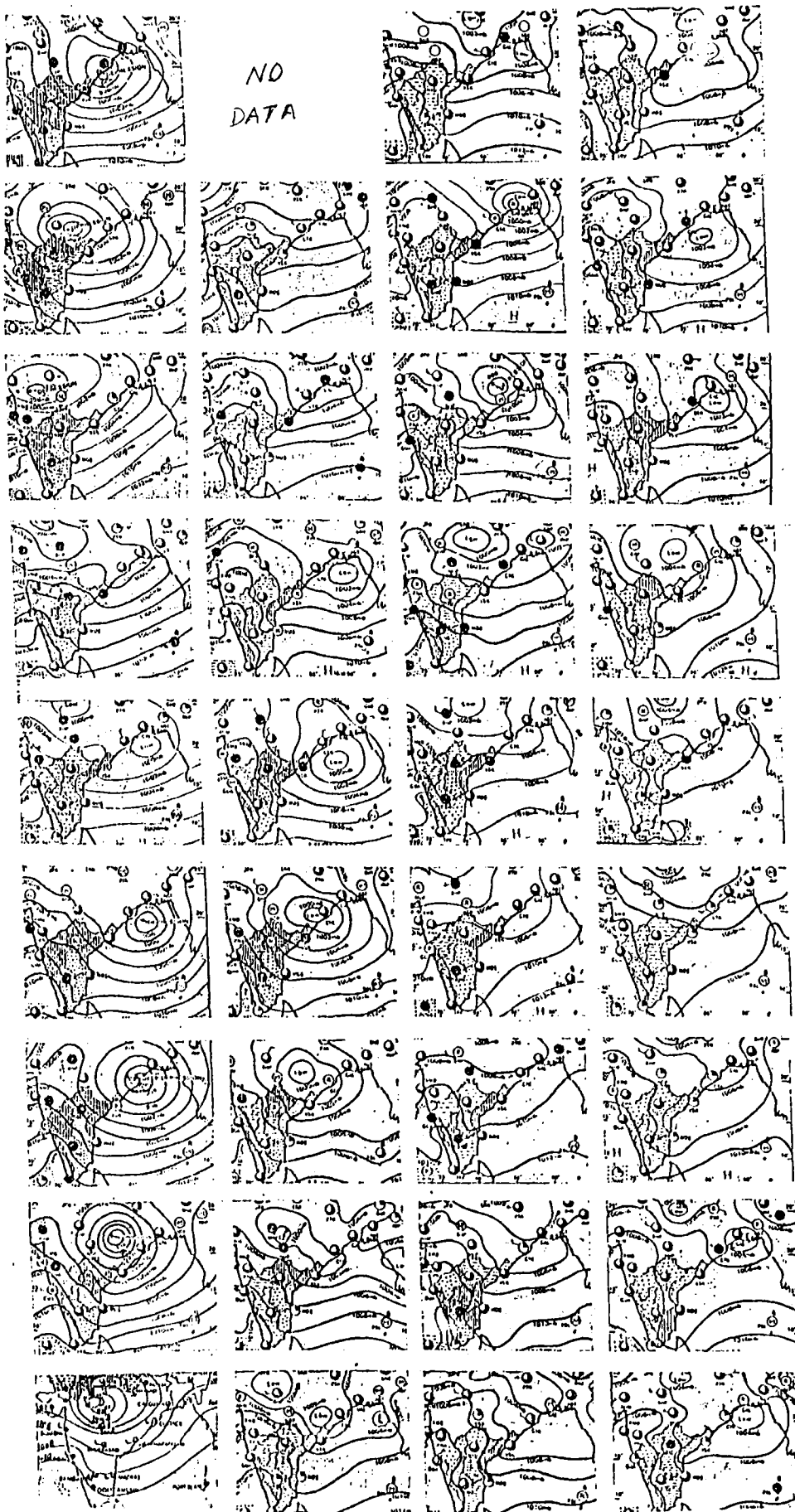


Fig. 2.4. Time series of surface pressure analysis - arranged columnwise in the chronological order from 15 August to 19 September 1990.

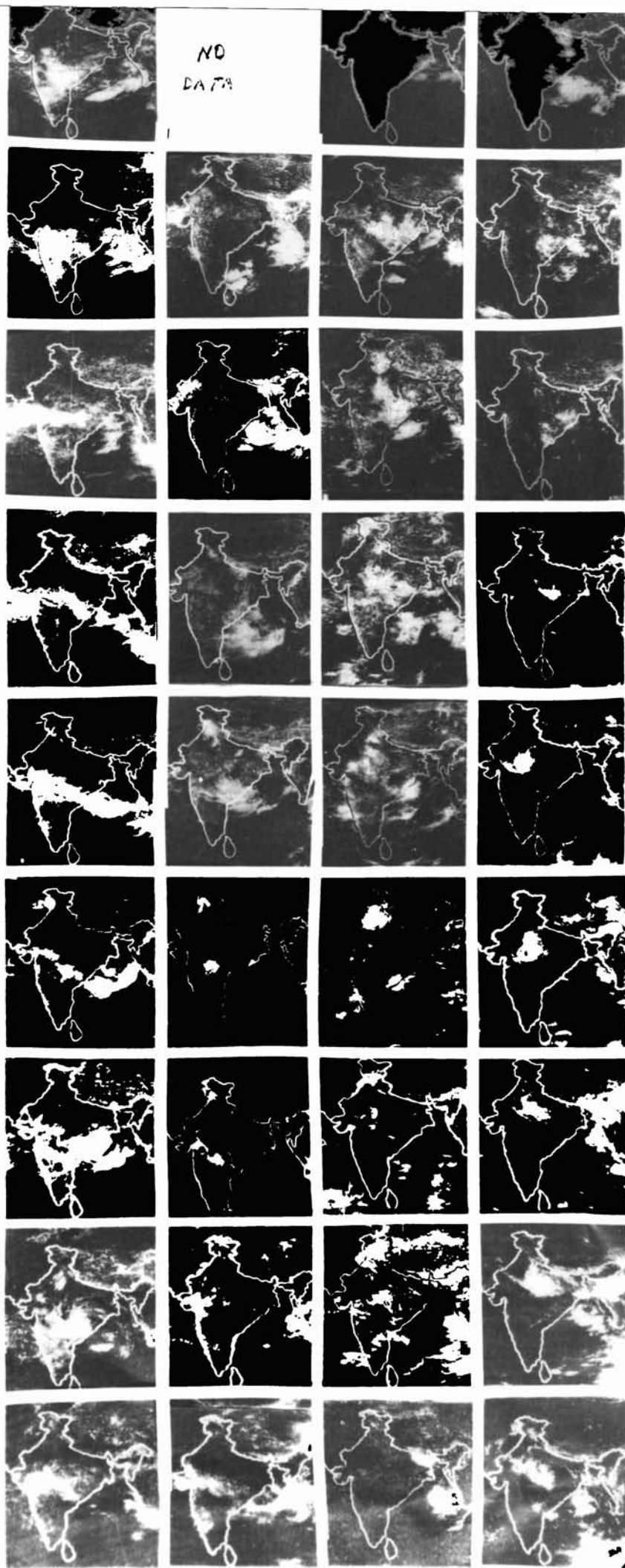


Fig. 2.5.
 Time series
 of cloud
 imageries
 viewed by
 INSAT 1 D -
 arranged
 columnwise in
 the
 chronological
 order from 15
 August to 19
 September
 1990.

2.4. Surface meteorology and heat budget estimates

The hourly march of time series of the standard marine meteorological parameters as surface pressure (PR), wind direction (DD) and speed (FF), visually observed cloud cover (CL), dry (DB), wet bulb (WB) and sea surface temperatures (SST) are shown in Fig. 2.6. The perturbations caused by the meteorological disturbances are best captured in PR, DD, FF and SST distributions. The winds strengthened during disturbed weather conditions with sudden changes in direction. The DB and WB did not reflect any regular cyclic variations as noticed in other elements. However, violent fluctuations are noticed in DB and WB in association with rapid variations in wind direction. In general, SST showed an inverse relationship with surface pressure with an approximate time lag of 2 days. A broad correspondence between strengthening of winds and lowering of SST is also noticed during disturbed conditions.

The heat budget components were estimated with the hourly observed marine meteorological data and then daily averaged. The daily march of these components are shown in Fig. 2.7. In general, Q_I was mostly in excess of 150 W/m^2 and showed synoptic scale fluctuations corresponding to variations in cloud cover due to disturbed and undisturbed regimes of the monsoon. The Q_B was almost invariant during both the phases with an average value of 35 W/m^2 . The most dominant heat loss term for the tropical oceans is Q_E which showed dramatic increase in association with deep depression (270 W/m^2) on 20 August 1990 and meteorological lows on 28 August, 11-13 and 18 September 1990. Occurrence of weak Q_S suggests near neutral conditions during most of the observational period. The net heat flux Q was positive

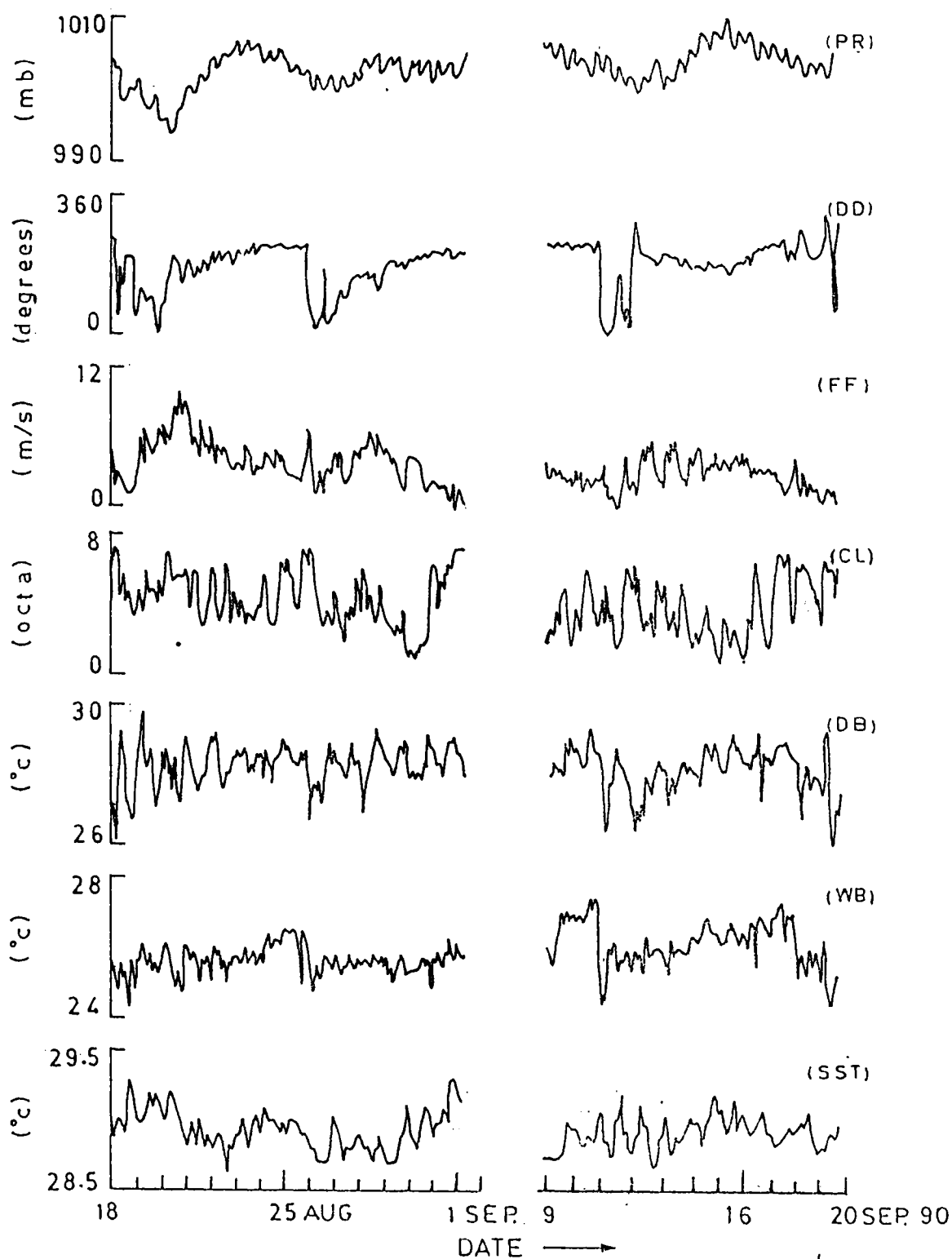


Fig. 2.6. Time series of surface meteorological parameters.

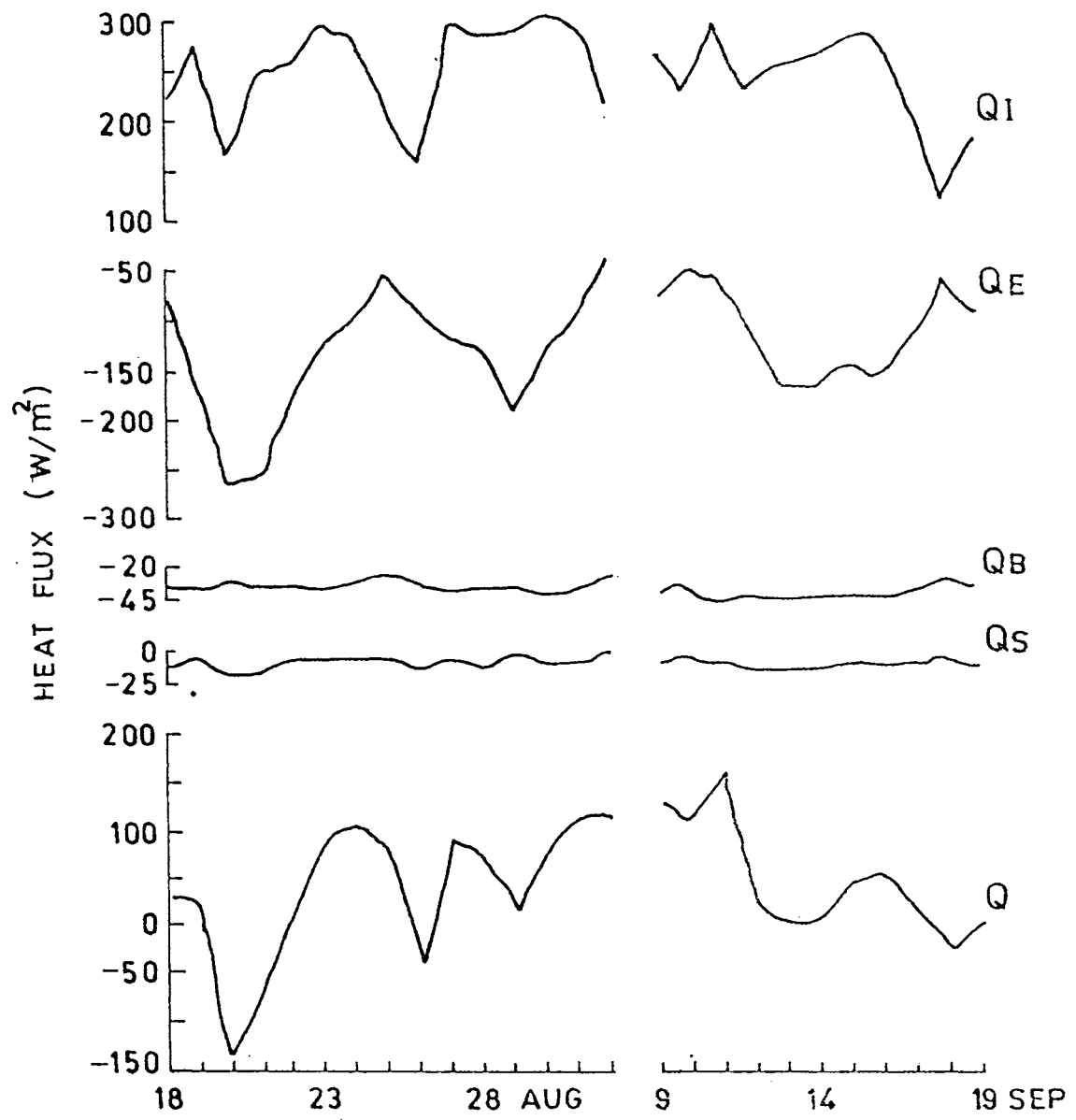


Fig. 2.7. Time series of heat budget parameters.

throughout with exceptions corresponding to the days of disturbed weather conditions (20,27 August and 18 September 1990). In general the net heat gain fluctuated between 0 and 100 W/m^2 .

2.5. Thermohaline variability

The annual cycle of the SST as revealed by global MCSST analysis (100 km x 30 days) for 1990 (Legeckis, 1991) is characterised by strong heating from February to May followed by a moderate cooling during June and July (Fig. 2.8). Another phase of moderate warming is noticed from August to October followed by an intense cooling during November to January. The near surface water column is also characterised by a variation of $\sim 5^\circ\text{C}$ in the annual cycle. The near surface waters are warmer than 28°C from April to November and showed only little variation during summer monsoon season contrary to the Arabian Sea. The daily averaged SST is presented for the observational periods for comparison with the satellite measurements in the inset of Fig. 2.8. The agreement is quite encouraging with a root mean square difference of 0.25°C .

The annual cycle of the observed temperature and salinity in the top most 250m water column at the time series station constructed from the data sets derived from Levitus (1982) is shown in Fig. 2.9. It must be cautioned that very few data are available for this region and hence these representations may not be very robust. However, the features are quite discernable. The thermal structure is characterised by a near surface mixed layer which is variable in depth and temperature. Maximum MLD ($\sim 50 \text{ m}$) is found during winter. The salinity field shows the presence of a very sharp halocline

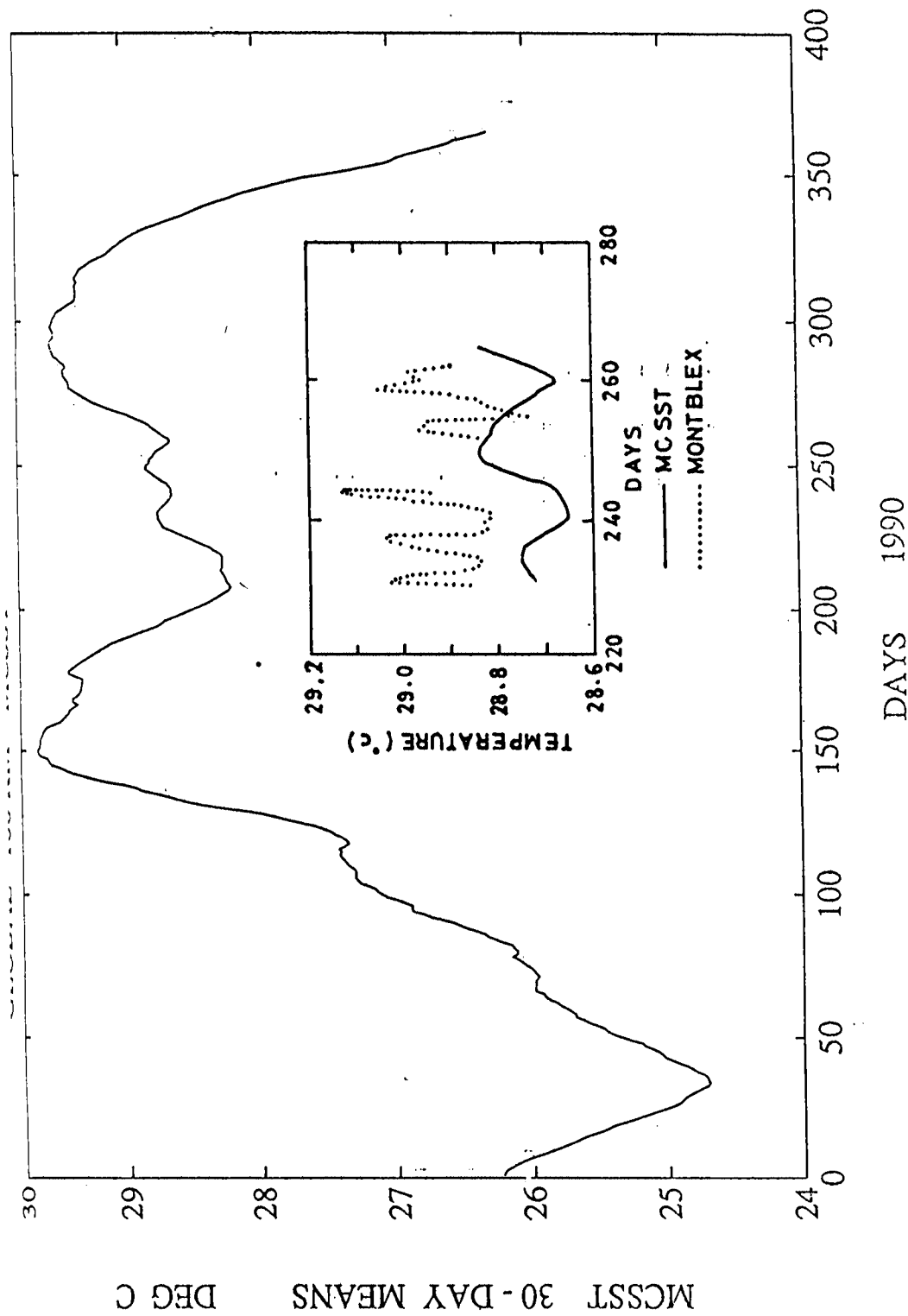


Fig. 2.8. Global MCSST analysis at 20°N and 90°E for 1990 (Legeckis, 1991). The figure in the inset represents the comparison between the MCSST analysis and sea truth data.

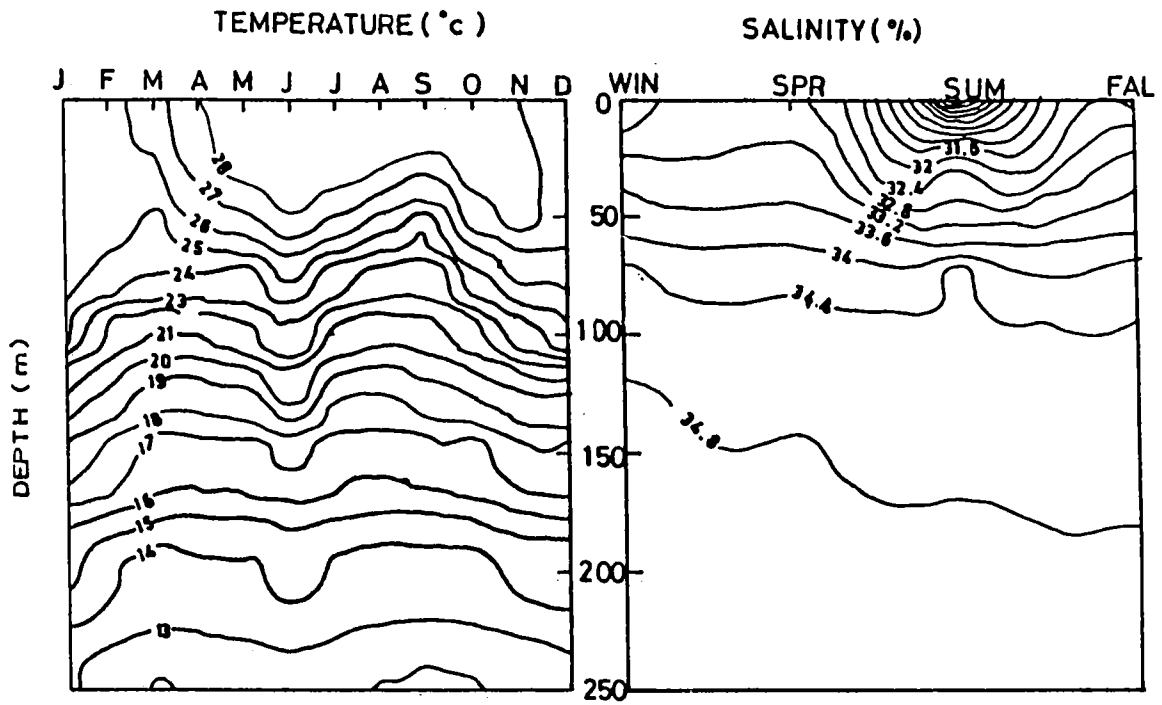


Fig. 2.9. Annual cycle of temperature and salinity in the top most 250m water column at the time series station (based on Levitus, 1982).

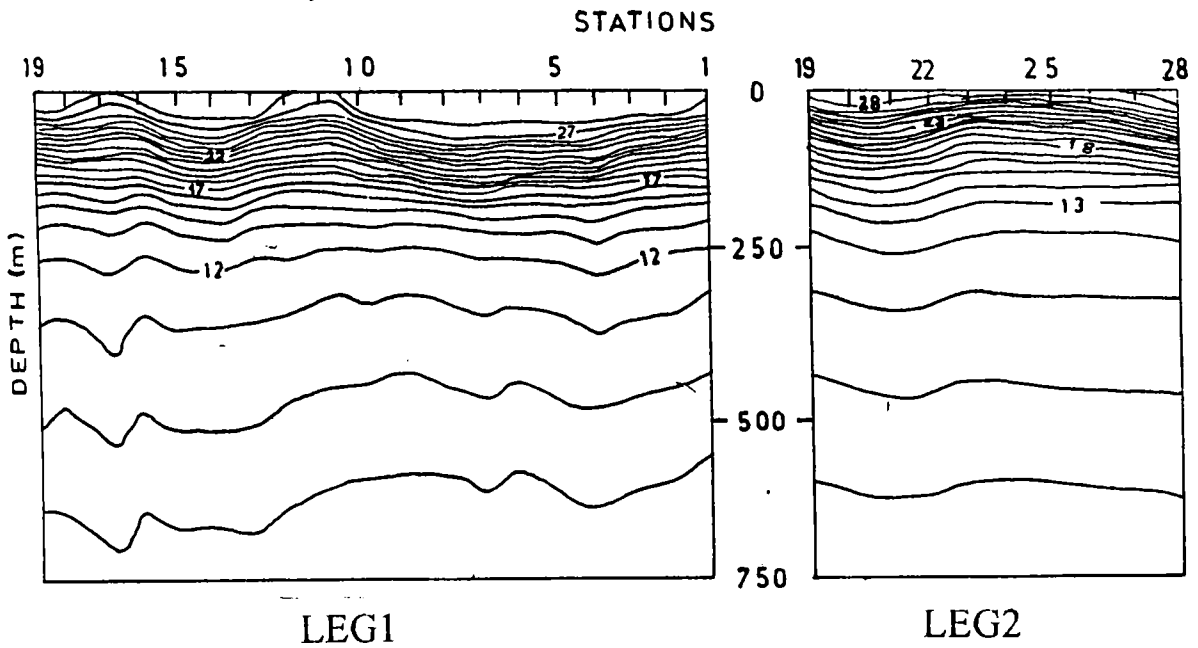


Fig. 2.10. Thermal structure along Leg1 and Leg2 based on XBT data.

in the near surface water column during the summer monsoon season due to massive fresh water discharges from the Ganges and Brahmaputra rivers. While the salinity below 100m depth varied only marginally throughout the year. Thus the station covered during MONTBLEX represents a very typical oceanographic setting where the salinity effects are expected to play prominent role on the near surface layer characteristics.

The horizontal variability of the thermal structure in the top 750m water column constructed with XBT data corresponding to two transects of MONTBLEX (Fig. 2.1) is depicted in Fig. 2.10. The thermal structure is distinctly characterised by a strong stratification in the upper 200m water column beneath the near surface mixed layer. In addition, the wavy nature of isotherms in the thermocline also suggests the presence of mesoscale eddy circulation or of propagating waves with horizontal scales of the order of 300 kms which is typical of mesoscale eddies in the Bay of Bengal (Rao, 1974; Swallow, 1983; Legeckis, 1987). The vertical extent of these perturbations is limited to about 250m of water column.

The mean vertical profiles of temperature, salinity and σ_t based on 7 CTD casts representing both the phases are shown in Fig. 2.11a. The temperature profile is characterised by a shallow near surface isothermal layer capped over a steep thermocline extending upto 200 m depth. A very sharp halocline is also present between surface and 175 m depth below which salinity remained invariant with depth. The corresponding density profile reflects strong pycnocline in the top 200 m water column.

The synoptic scale evolution of thermal structure in

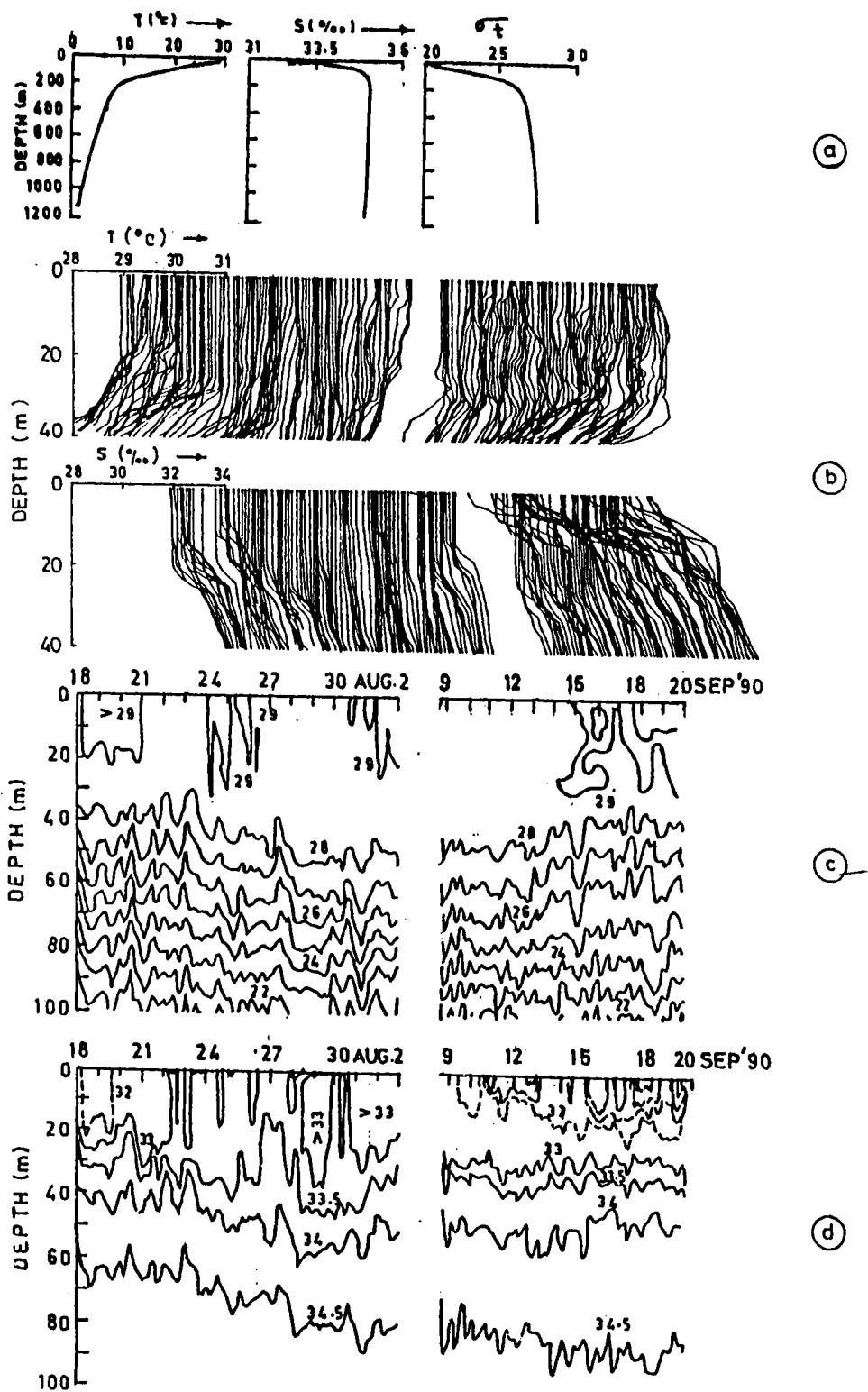


Fig. 2.11. (a) Mean vertical profiles of temperature, salinity and σ_t at the time series station. (b) Temperature and salinity profiles at 3 hourly intervals in chronological order. (c) Depth time section of temperature. (d) Depth-time section of salinity.

the top 100 m water column at the stationary position is shown in Fig. 2.11b and c. The analysis is based on time series measurements of vertical temperature profiles recorded by MICOM STD system. Isotherms were drawn at 1°C interval. The thermocline showed a descent during phase-I and an ascent during phase-II. These trends in the vertical motion of isotherm topography within the thermocline suggest a possible influence of either a moving clockwise eddy or a propagating wave. Eddy of dimension of more than 440 km in the northern Bay of Bengal during the summer monsoon period of 1979 (Chapter III). Hence it is probable that a similar eddy might have been presented in this case too. However, the available data are inadequate to address this problem in greater detail. The embedded short period fluctuations in the isotherm topographies suggest the influence of internal tides and inertial oscillations. The corresponding variability noticed in the salinity field is depicted in Fig. 2.11b and d. The isohaline contours were drawn at 0.5 PSU interval for values greater than 32 PSU and at 1 PSU interval for values less than 32 PSU to avoid congestion in the diagram. A great deal of small scale structure is evident in the topmost 20m water column throughout the observational period and this is more so during phase II. This type of small scale variability is caused by local rainfall, variations in river discharges and associated complex circulation regimes. The halocline also showed a descent during phase-I and an ascent during phase-II in accordance with thermal regime. The high frequency oscillations show a great deal of correspondence with the isotherm fluctuations.

The vertical stability regime represented by the Brunt-Vaisala frequency was computed utilising the vertical

profiles of temperature and salinity and the corresponding depth-time section is shown in Fig. 2.12. The contours were drawn at 3 cycles/hour interval. The pycnocline is characterised by a strong stability regime with values in excess of 10 cycles/hour. During phase-II, strong stratification occurred very close to the surface on account of strong gradients and rapid fluctuations in the salinity field. On the whole, the stratification in the pycnocline did not differ significantly between phase-I and phase-II.

2.6. Genesis of meteorological lows

As the thermal conditions of the near-surface water column are known to play a key role in the convective activity of the overlying atmosphere (Gray, 1975; Gadgil et al., 1984; Graham and Barnett, 1987), focus is laid on small scale thermal fluctuations within the isothermal layer in relation to disturbed and undisturbed weather conditions (Fig. 2.15). The 29°C isotherm appeared on 5 occasions (18-20 and 23-25 August, 31 August- 1 September, 11 and 15-18 September 1990) during the entire observational record, each lasting approximately for 1 to 3 days. The vertical extent and duration of these mini-warm pockets also varied from one event to another. A very clear correspondence is noticed between the occurrence of these mini-warm pockets and subsequent genesis of meteorological disturbances (19-22, 27-28 August, 1-2, 11-13 and 18-19 September 1990). The genesis and sway of these meteorological disturbances resulted in surface cooling (SST around 28.7°C) by extraction of available surplus thermal energy. Warming of water beyond 29°C appears to trigger instability in the overlying atmosphere towards the formation of disturbed weather. Higher

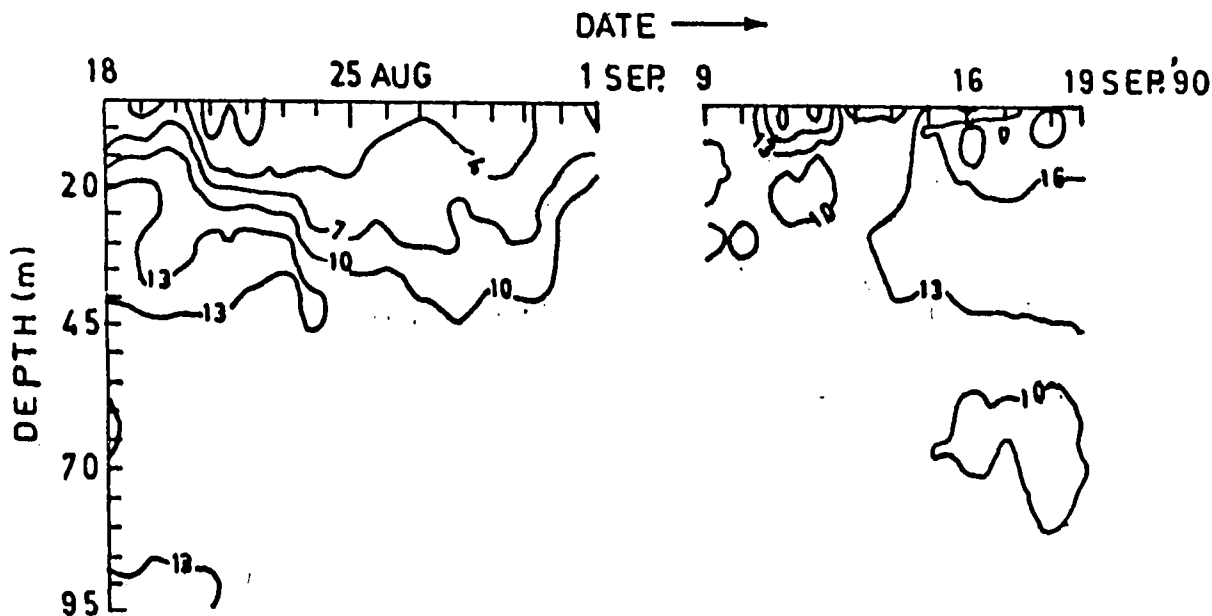


Fig. 2.12. Depth-time section of Brunt-vaisala frequency (cycles/hour).

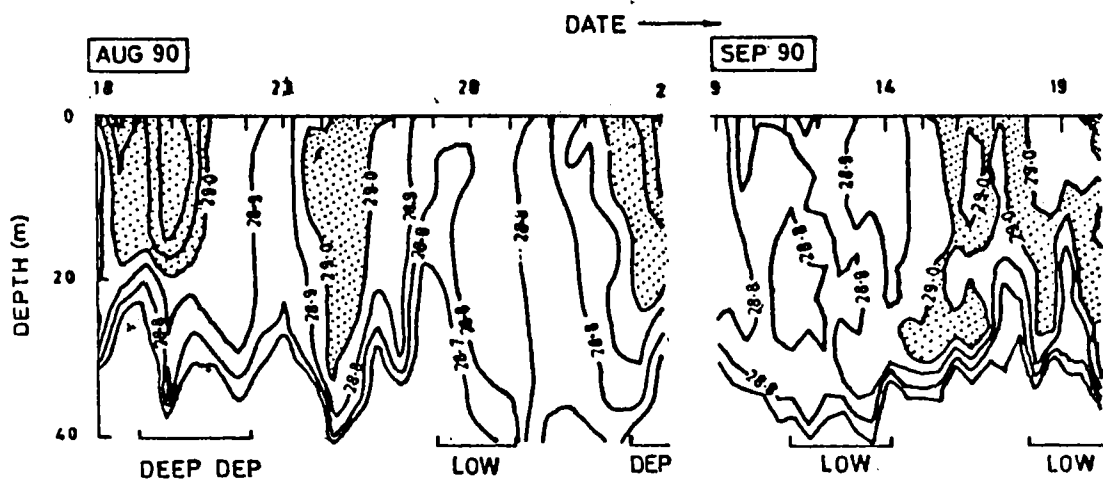


Fig. 2.13. Depth-time section of temperature for the upper 40 m water column. 'Dep' for depression and 'low' for meteorological low pressure systems.

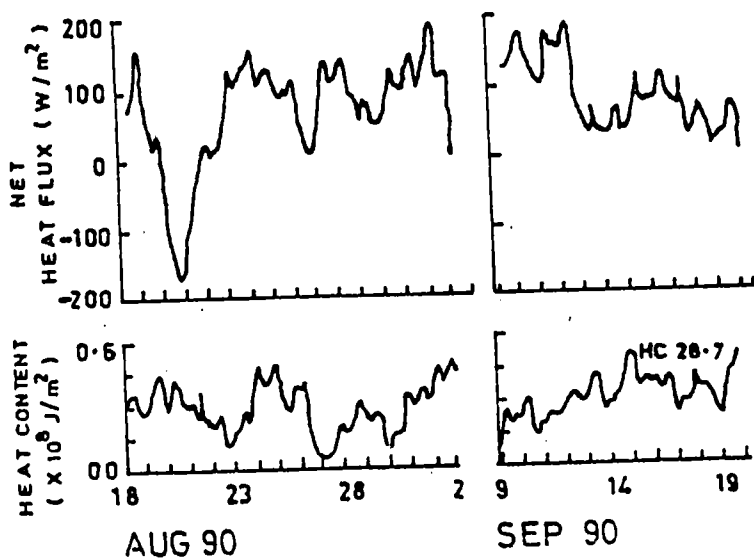


Fig. 2.14. Time series of heat flux and heat content with respect to 28.7 C isotherm.

SST is already known as a favourable condition for the genesis of tropical cyclones (Gray, 1975; Graham and Barnett, 1987). In the monsoonal seas, SST of 28°C has been found as the threshold value for the generation of organised convection in the atmosphere (Gadgil et al., 1984). However, due to the averaging of the daily cloudiness (area considered - 2.5° x 2.5° square) and monthly SST (area - 5° x 5° square) for larger area, Gadgil et al. (1984) could not establish the exact threshold value of SST for the genesis of the atmospheric disturbances. The MONTBLEX experiment has provided an unique opportunity to collect time series of thermal profiles using high accuracy instrument (MICOM STD) at closer time intervals during a monsoon regime represented by both disturbed and undisturbed conditions. When considering the fact that the SST fluctuation even within 0.3°C (28.7°C to 29°C) appears to control the atmospheric stability. The accuracy of instrument being 0.05°C with a vertical resolution of 1 m amply meets the requirement.

The accumulation of net heat flux at the surface is expected to increase the heat content of the near-surface water column. The heat content with respect to 28.7°C isotherm (the warmest isotherm present throughout the observational period) was estimated (Fig. 2.14) to identify correspondence with local surface heat fluxes and the formation of the meteorological disturbances. Whenever the heat content of the water column exceeded $\sim 0.4 \times 10^8 \text{ J/m}^2$, the ocean released energy to the atmosphere, leading to cooling of the surface waters. These events remarkably coincided with the formation of the meteorological disturbances except for the low pressure system formed during 11-13 September 1990. Rao and Rao (1986) and Rao et al. (1987) reported such a

correspondence between the genesis of a depression and an increase in the heat content of the upper layers in the head of the Bay of Bengal. A close agreement between the distributions of Q and HC, with a time lag of 1-2 days (HC lagging Q) during phase I, suggests the importance of local heat exchange in regulating the thermal variability of the upper layers. The weak agreement during phase II is probably due to circulation patterns causing a complex thermohaline structure (Fig. 2.11b).

2.7. Numerical simulation of mixed layer characteristics

Among the coefficients, m_1 and m_2 represent the fraction of turbulent energy production due to (i) interaction of the surface stress and near surface current shear and (ii) interaction of entrainment stress and shear at the mixed layer base. The coefficient ' m_1 ' depends on the atmospheric and oceanic stability, sea state and surface roughness. In addition to these factors, m_2 depends on the stratification of water column. The correct dependence of these variables on the above mentioned factors is not known exactly (Bush, 1971). Therefore, it is a common practice (Davis et al., 1981; Sanil Kumar et al., 1994) to assign constant values by trial and error with bounds determined by laboratory and field experiments. The value for m_3 (0.83) (convective efficiency parameter) has been determined fairly well by the experiments of Deardorff et al. (1969). Considering the uncertainty in m_1 and m_2 , in this study, NK model was run with different combinations of values drawn from Davis et al. (1981).

The results (simulated hourly time series of MLD and MLT) of these combinations represent minimum and maximum

values of the parameter range are presented Figs. 2.15 and 2.16. The disagreement between the simulated and observed series of MLD progressively reduced with progressive increase of ' m_1 ' and ' m_2 ' (Fig. 2.15). This is also equally true for MLT (Fig. 2.16). Better simulation with larger coefficients imply that mixing both at near-surface and mixed layer base was important in mixed layer variability at the northern Bay under the alternate rough and fair weather conditions. However, during phase II, the disagreement between the observed and simulated values were higher. Prominent small scale variability in both temperature and salinity profiles was evident during phase II (Fig. 2.11b). This variability showed the dominance of internal dynamic processes rather than the one dimensional processes and thus explain the reasons for larger departures between the observed and predicted values.

The ' m_0 ' in KTDM model, is analogous to m_1 in NK model and hence its dependence on environmental factors is also similar. A wide range of values for m_0 are available in the literature varying from 0.009 to 0.01 (Kato and Phillips, 1969; Turner, 1969; Denman, 1973). However, in the present study a value of 0.009 was chosen after making a few trial runs. The corresponding simulated values of MLD and MLT are given in Fig. 2.17a and b. In general, KTDM model predicted deeper MLD while NK model predicted lower MLD. Also the shoaling events were comparatively well captured in NK model. Another notable point is that during the period of deep depression, the deepening rate of MLD was simulated reasonably well by NK; whereas it was poorly done by KTDM. For obtaining an overall picture of the variations between the observed and simulated values of MLD and MLT, the root

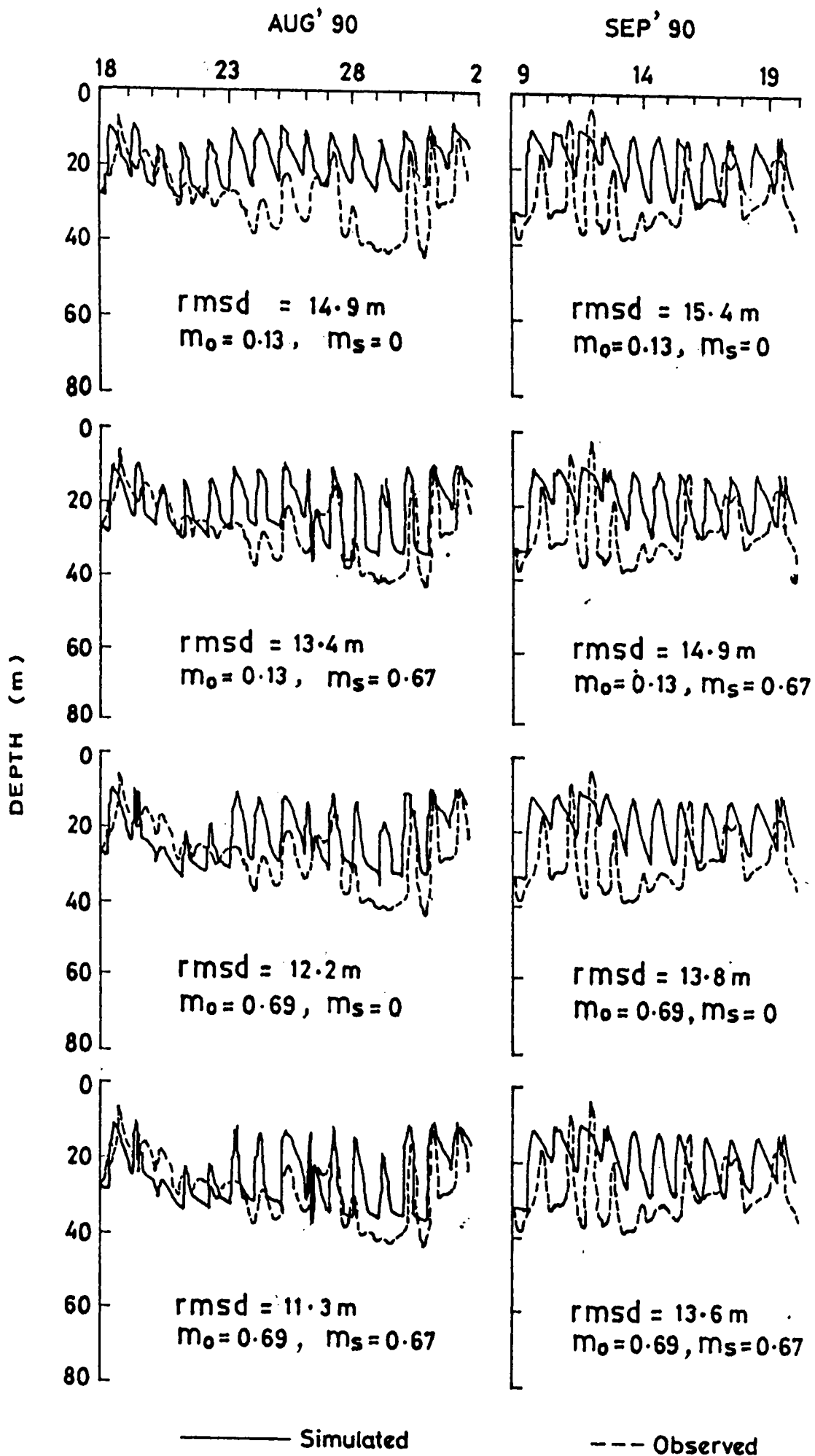


Fig. 2.15. Time series of observed and simulated (using NK model) mixed layer depth.

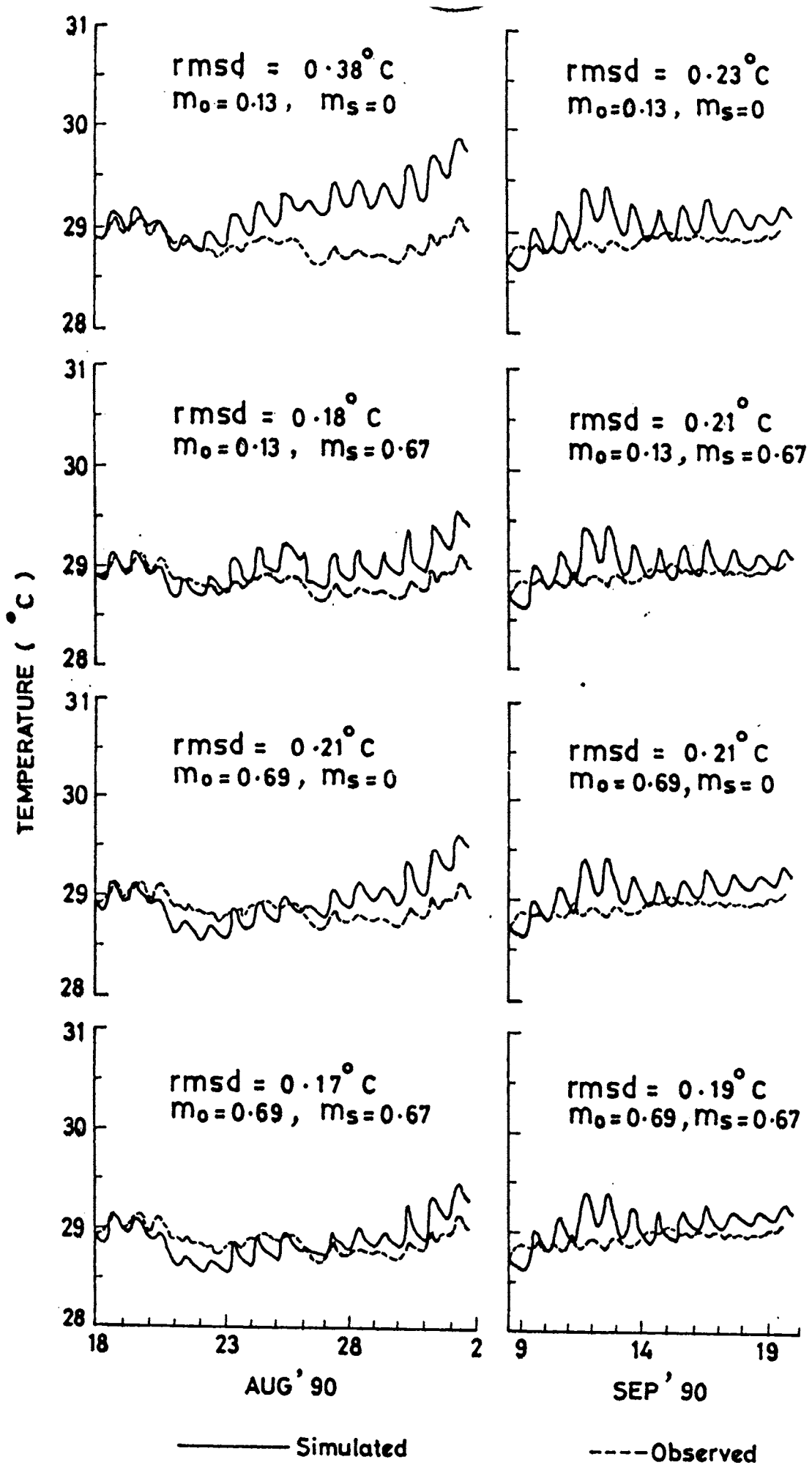


Fig. 2.16. Time series of observed and simulated (using NK model) mixed layer temperature.

Kraus - Turner - Denman - Miller

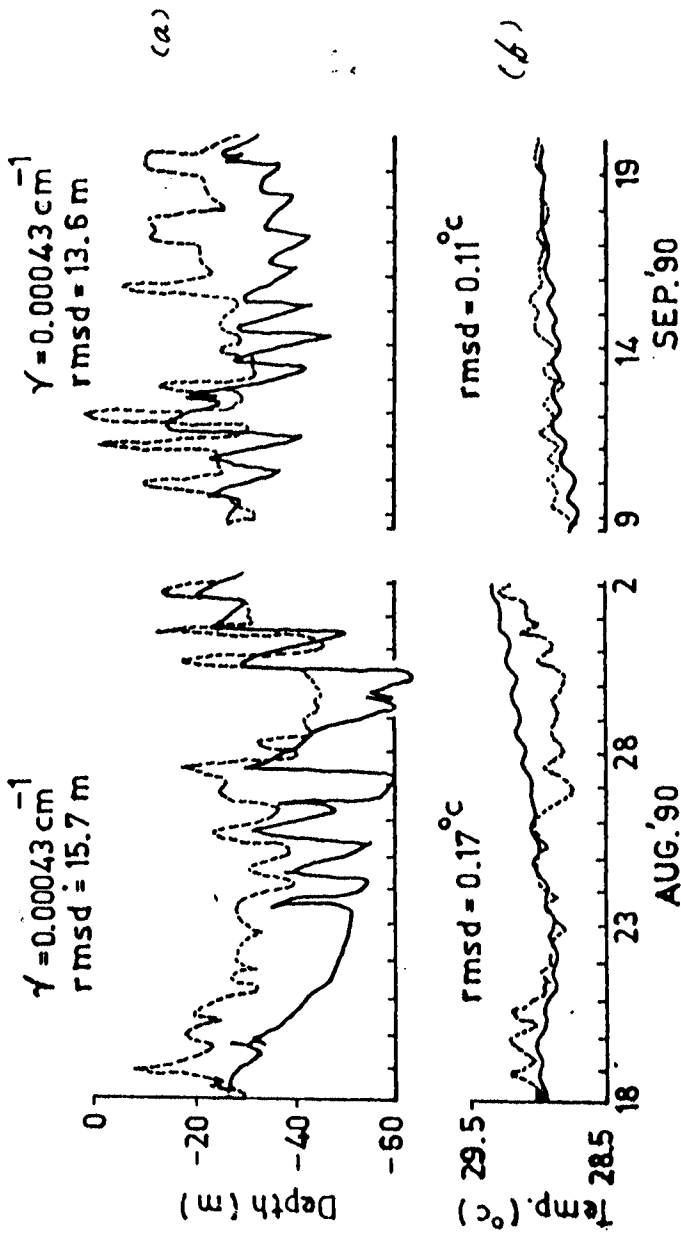


Fig. 2.17a. Time series of observed and simulated (using KTDM model) mixed layer depth.

Fig. 2.17b. Time series of observed and simulated (using KTDM model) mixed layer temperature.

mean square (RMS) errors were computed (Table 2.2). In general, NK is found to perform better than KTDM for the northern Bay during summer monsoon period. Since the differences between NK and KTDM are mainly in the parameterization of the terms of shear production at the layer base ($m_2 S$), the convective efficiency (m_3) and the absorption of solar radiation at different depths [$q(z)$], the relatively better performance of NK can be explored in terms of these terms. The ' δv^2 ' in $m_2 S$, is important in the case of strong wind events. In the present case, the strongest wind event occurred on 20 August 1990 in association with the deep depression and the NK model performed better. So it is quite evident that the inclusion of δv^2 in NK model improved the performance of the model. The other possible factors are m_3 and $q(z)$. In NK, m_3 is restricted to 0.83 instead of 1 in KTDM. This implies that in KTDM, 100 % of the surface energy flux is utilized for the mixed layer cooling while in NK, only 83 % is used. Since the overcooling was not noticed in MLT with KTDM, it is concluded that the difference in the parameterization of m_3 is not very significant for the present data set. But, under different environmental conditions (when heating was weak), unrealistic cooling was observed with KTDM (Alexander and Kim, 1976; Sanil Kumar et al., 1993). The differences between the simulated values occurred using these two models during shoaling events of the mixed layer, can be explained in terms of the parameterization of $q(z)$. In KTDM, the solar radiation absorption at different levels is parameterized based on single exponential decay of the insolation, while in NK, the absorption is based on double exponential decay. It seems that the parameterization of $q(z)$ in NK appears to improve

Table- 2.2

Kraus-Turner-Denman-Miller

Secchi disc depth (m)	γ (cm ⁻¹)	r m s deviation			
		mld (m)		mlt(°C)	
		phase1	phase2	phase1	phase2
10	0.0017	14.9	16.4	1.0	0.97
20	0.00085	12.0	11.5	0.49	0.31
30	0.00056	12.2	11.1	0.25	0.09
40	0.00043	15.7	13.6	0.17	0.11

Niiler-Kraus

m_o	m_s	r m s deviation			
		mld(m)		mlt(°C)	
		phase1	phase2	phase1	phase2
0.13	0.0	14.9	15.4	0.38	0.23
0.13	0.67	13.4	14.9	0.18	0.21
0.69	0.0	12.2	13.8	0.21	0.21
0.69	0.67	11.3	13.6	0.17	0.19

the performace of the model.

The lack of exact coincidence between the observed and simulated mixed layer characteristics with these two models, suggests that one dimensional forcing can not explain the entire observed variance as this area is characterised with rich eddy fields and associated complex mesoscale circulation (Legeckis, 1987; Chapter III) with overwhelming small scale structure evident from the high resolution vertical temperature and salinity profiles (Fig. 2.11b).

CHAPTER III

SALINITY AND CURRENTS IN THE NORTHERN BAY OF BENGAL
DURING THE SUMMER MONSOON EXPERIMENTS

3.1.Introduction

The northern Bay of Bengal (north of 15°N) deserves special attention during summer monsoon season (June to September). More than 90 % of the total river input into the Bay of Bengal, takes place at the boundaries of this water body (Table 1.3). This much water can raise the sea level of the Bay by 0.34 m (Varkey and Sastry, 1992). The whole water spreads over the southern Bay and dilutes the upper layers. As a result, a monotonous increase of salinity occurs towards the southern Bay and towards the subsurface layers. Sharp salinity fronts can also form at different locations of the Bay during different periods (Amos et al., 1972). In addition to the spatial variability, temporal variability on a synoptic scale is also expected to be very conspicuous due to the variability in river discharge resulting from energetic pulses of monsoon rainfall (Pisharoty, 1964; Krishnamurti and Balme, 1976). This variability in salinity can affect tropical ocean models (Cooper, 1988), mixed layer characteristics (Sprintall and Tomczak, 1990) and other surface layer dynamics (Toole and Raymer, 1985; Harenduprakash and Mitra, 1988; Shetye, 1993). So the understanding the salinity variability in the northern Bay of Bengal becomes very important. However, we had no field observations to study the variability of the salinity field on shorter temporal scales prior to 1977.

It is well known that the circulation in the northern Bay of Bengal is very much complicated due to the fresh water discharge (Shetye, 1993), seasonal reversal of winds (Shetye et al., 1993) and remote forcing (Potemra et al., 1991; Yu et al., 1991; McCreary et al., 1993). So the indirect methods

like geostrophic computations, wind driven models etc. may not be appropriate, especially during the summer monsoon season. Only the direct measurements using the moored instruments would provide an accurate picture on the prevailing circulation. However, no direct current measurements were made in the northern Bay of Bengal prior to 1977.

Though the northern Bay of Bengal possesses very complex oceanographic environment, no systematic field observations had been conducted to probe the synoptic scale oceanographic and atmospheric variability until 1977. During 1977 and 1979, as a part of the First Global GARP (Global Atmospheric Research Programme) Experiment, field observations were conducted in the north Indian Ocean known as MONSOON-77 and MONEX-79 (designated as M-77 and M-79 respectively in the following discussion). During both the expeditions former USSR deployed four-ship stationary polygons in the northern Bay of Bengal to collect time series measurements of temperature, salinity and currents. Utilizing these data sets, thermal structure and its response to atmospheric variability was studied in great detail earlier (Anto et al., 1982; 1985; Rao et al., 1981; 1983; 1985; 1987; Rao and Rao, 1986; Rao, 1987; Rao and Mathew, 1988). In this chapter, the focus is mainly laid to investigate the observed salinity and current variability.

3.2.Data and methodology

The stations occupied by the ships during both the experiments and the respective observational periods are given (Fig. 3.1 and Table 3.1). The approximate physical

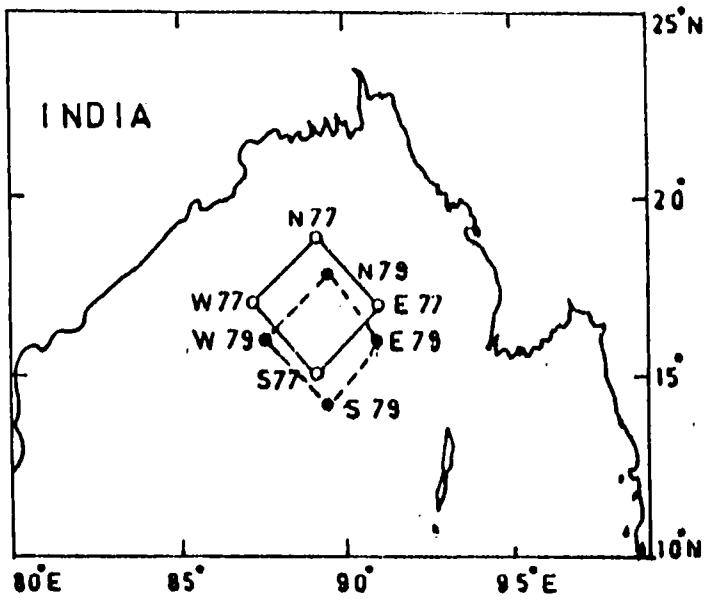


Fig. 3.1. Stations occupied during the Summer Monsoon Experiments in the northern Bay of Bengal.

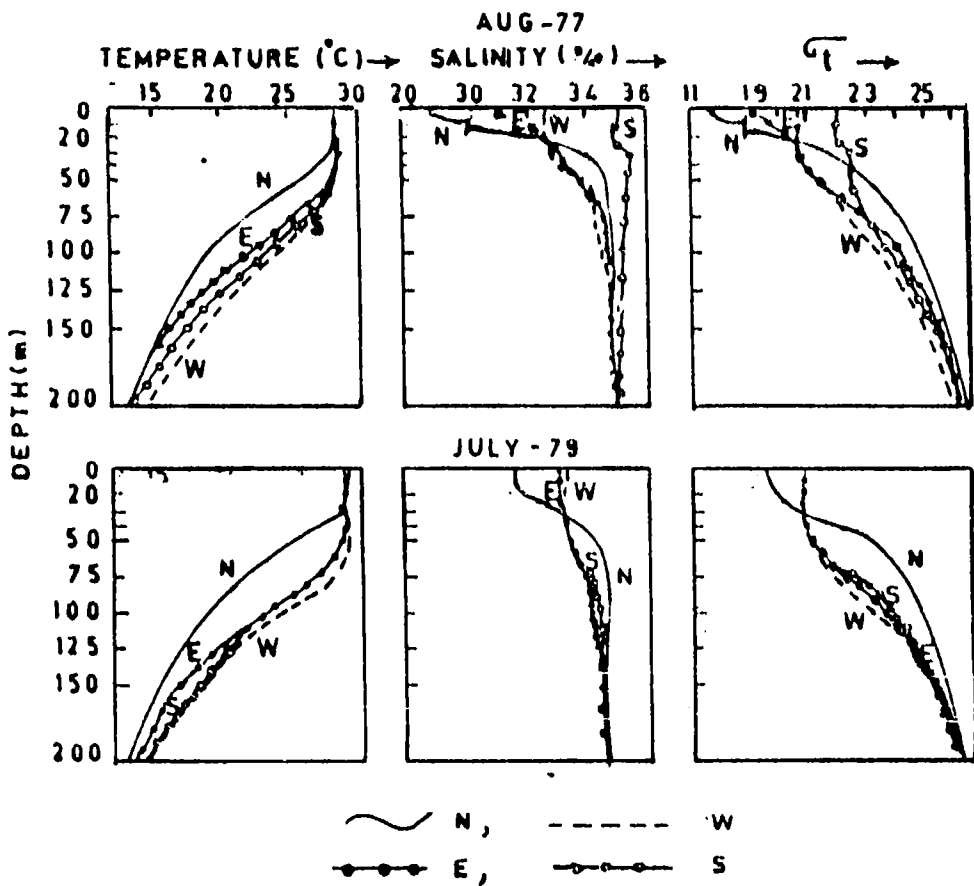


Fig. 3.2. Temperature (T), salinity (S) and sigma-t (σ_t) for polygons of M-77 and M-79.

separation between respective corners of each polygon was of the order of about 60 nautical miles. Three or six hourly time series of Nansen cast data at standard depths (during M-79 data were reported at irregular depths), one hourly standard surface meteorological elements, half hourly currents at selected depths and daily totals of rainfall are the main inputs to this study. Vertical profiles of salinity at 5 m interval were interpolated (Borowski and Goulat, 1971) and used in the vertical sections as the daily averages for the top 200 m water column. The accuracy of salinity and temperature measurements were 0.003 PSU and 0.02°C. Current

TABLE 3.1: Station locations and the observational periods during the summer monsoon experiments in the northern Bay of Bengal.

Station designation in the text	Location	Observational period
N77	19.0 N & 89.0 E	11 - 18 August 1977
E77	17.0 N & 91.0 E	
S77	15.0 N & 89.0 E	
W77	17.0 N & 87.0 E	
N79	18.0 N & 89.5 E	11 - 23 July 1979
E79	16.2 N & 91.1 E	
S79	14.4 N & 89.5 E	
W79	16.2 N & 87.7 E	

meter data were collected at 25, 50, 100, 150 and 200m depths at half hourly intervals for durations of the order of 1-2

weeks. These data were reported at a resolution of 1° in direction and 1 cm/s in speed. The corresponding surface wind data at 10 m height were also collected at one hourly intervals. In the following discussion the stations at northern, eastern, southern and western corners of the polygon are designated as N, E, S and W respectively.

3.2.1. Brunt-Vaisala frequency (N): -

N is a measure for static stability and is defined as

$$N^2 = \frac{-g\Delta\rho}{\rho \Delta Z} \quad (3.1)$$

where g is the acceleration due to gravity, ΔZ is the spacing between the current meters, $\Delta\rho$ is the density difference and ρ is the average density of the layer between the sensors. The water column is considered neutral for zero values of N , stable for positive values and unstable for negative values of N^2 .

3.2.2. Rotary Spectra :-

Observed current records usually consist of harmonic oscillations of different frequencies. Spectral analysis is an effective tool to delineate the frequency components embedded in these data. This technique can be used for both scalar and vector series. But, for vector series, because of the earth's rotation, an asymmetry in the Fourier components of the horizontal plane can be expected. In the rotary spectral method, this asymmetry will be resolved as the difference in energy levels in clockwise (S_-) and anticlockwise (S_+) spectra (Gonella, 1972). Therefore the

rotary spectral method is more appropriate for the analysis of current meter data.

Any discrete time series data, $U(t)$ for a vector length 'j' varies from '1' to 'm' and sampled at 'T' time interval can be transformed into Fourier series as follows:

$$U(t) = \sum_{j=1}^m (a_j \cos \omega_j t + i b_j \sin \omega_j t) \quad (3.2)$$

where 't' is time, $\omega_j = 2\pi j/mT$, and a_j and b_j are the coefficients representing amplitude of the wave component of frequency ω_j . 'a_j' and 'b_j' can be found out using the formulae given below:

$$a_j = \sum_{j=0}^{m-1} x(t) \cos \omega_j t \quad (3.3)$$

$$b_j = \sum_{j=0}^{m-1} x(t) \sin \omega_j t \quad (3.4)$$

But a vector series, $U(t)$ can be split up into two scalar series of $u_1(t)$ and $u_2(t)$ in a horizontal rectangular cartesian system. These scalar series are converted into two Fourier series. Thus we get

$$u_1(t) = \sum_{j=1}^m (a_{1j} \cos \omega_j t + i b_{1j} \sin \omega_j t) \quad (3.5)$$

$$u_2(t) = \sum_{j=1}^m (a_{2j} \cos \omega_j t + i b_{2j} \sin \omega_j t) \quad (3.6)$$

Then

$$P_{u_1 u_1}(f_j) = \langle a_{1j}^2 + b_{1j}^2 \rangle \quad \text{autospectra for } u_{1j} \quad (3.7)$$

$$P_{u_2 u_2}(f_j) = \langle a_{2j}^2 + b_{2j}^2 \rangle \quad \text{autospectra for } u_{2j} \quad (3.8)$$

$$P_{u_1 u_2}(f_j) = \langle a_{1j} a_{2j} + b_{1j} b_{2j} \rangle \quad \text{cross spectra} \quad (3.9)$$

$$Q_{u_1 u_2}(f_j) = \langle a_{1j} b_{2j} - a_{2j} b_{1j} \rangle \quad \text{quadrature spectra} \quad (3.10)$$

where the symbol $\langle \rangle$ represents the average over all the segments of vector length 'm' and f_j is the frequency ($f_j = j/mT$, $0 \leq j \leq m-1$).

Gonella (1972) derived the following relationship utilizing the above spectra (equations 3.5 to 3.8):

$$S_{-}(f_j) = \frac{1}{8} \{ P_{u_1 u_1}(f_j) + P_{u_2 u_2}(f_j) - 2Q_{u_1 u_2}(f_j) \} \quad (3.11)$$

$$S_{+}(f_j) = \frac{1}{8} \{ P_{u_1 u_1}(f_j) + P_{u_2 u_2}(f_j) + 2Q_{u_1 u_2}(f_j) \} \quad (3.12)$$

$$S_t(f_j) = S_{-}(f_j) + S_{+}(f_j) = \frac{1}{4} \{ P_{u_1 u_1}(f_j) + P_{u_2 u_2}(f_j) \} \quad (3.13)$$

where S_{-} , S_{+} and S_t are the clockwise, anticlockwise and total spectra respectively.

3.2.2.1. Procedure adapted in the spectral analysis:-

The procedure adapted in the spectral analysis in this study is based on Ahmed and Natarajan (1983). The data set was centered to a zero mean by subtracting the mean of the record from each data point. For example

$$\bar{u}_1(j) = u_1(j) - \frac{1}{m} \sum_{j=1}^m u_1(j) \quad (3.14)$$

where $\bar{u}_1(j)$ is the zero mean series of $u_1(j)$. This new series was low pass filtered with a cut off frequency of 0.08 cph (12.5 h) to remove frequencies greater than that of semi-diurnal tide. Then each $\bar{u}_1(j)$ was multiplied by a window sequence $w(j)$ to combat a phenomenon known as 'leakage'. In this analysis Hanning window is used.

$$\text{ie. } w(j) = 0.5 [1 - \cos(2\pi j/m - 1)] \quad (3.15)$$

These processed series were used for the Rotary spectral analysis. The results [$U_1'(fj)$] were affected by power loss due to the windowing processes. To account for the power loss, $U_1'(fj)$ was divided with the average power in the window sequence (W). Here

$$W = \frac{1}{m} \sum_{j=0}^{m-1} w^2(j) \quad (3.16)$$

The desired power density spectrum was then computed as

$$p_{u_1 u_1}(fj) = \frac{1}{mW} U_1'(fj) \quad (3.17)$$

Similarly $p_{u_2 u_2}$, $p_{u_1 u_2}$ and $Q_{u_1 u_2}$ were also computed.

3.3. Results and discussion

The behaviour of the monsoon during 1977 and 1979 was contrasting. During 1977, the monsoon behaviour was above normal (Anon. 1978) while in 1979 it was below normal (Awade et al. 1988). Consequently, the freshwater inputs through

rainfall and river discharges into the Bay are expected to differ during the monsoon seasons of both the years. Added to these differences, the observations during M-79 were collected one month earlier to those of M-77.

3.3.1. Observed mean hydrography :- The mean distributions (corresponding to the observational period) of the vertical profiles of observed temperature, salinity and σ_t for the polygons of M-77 and M-79 are shown in Fig. 3.2. The most notable feature is that the σ_t profiles of all locations followed salinity profiles but not the temperature profiles in the upper $\simeq 50$ m which is quite uncommon to the other world oceanic regions. This shows the importance of salinity distribution influencing the dynamics of the northern Bay of Bengal. During M-77 the salinity differences within the polygon area were relatively larger in the upper layers (30m) compared to those of M-79. The salinity was also lower during M-77 compared to M-79. Higher river discharges resulting from the better monsoon might have probably produced these differences. The lowest surface salinity (<22 PSU) and strong halocline occurred at N station during 1977 because of its close proximity to the river mouths of Ganges and Brahmaputra. All the other locations showed relatively higher salinity with isohaline layers extending from surface to about 20 to 30m depth. These spatial differences in the vertical salinity distribution within the polygon are mainly attributed to the relative distance of the stations from the river mouth and local mesoscale circulation patterns causing differential advection of salinity. Very large spatial variability in the observed salinity field at the Head of the

Bay during M-77 and M-79 was also reported by Sarma et al.(1988). During both the experiments the salinity profiles below 50m depth resembled each other with diminishing spatial differences. This result suggest that the year to year variability in the salinity field is probably limited to the upper 50 m.

Brunt-Vaisala frequency (BVF) was calculated utilizing the mean temperature and salinity profiles for each observational period for all the locations (Fig. 3.3). Relatively large values of BVF are noticed during M-77 at N and E locations in the near surface layers due to the development of strong halocline caused by freshwater discharges at the Head of the Bay. The observed spatial variability of BVF was also large during M-77 in the upper layers within the observational array. The variability of BVF was insignificant below 100m. During M-77, the large values of BVF and a sharp decrease in the topmost 50m water column is prominently seen only at N location (closest station to the river mouth). In the near surface layers the BVF values decreased in a clockwise manner suggesting the reduction of dilution from N to W locations. However, the situation during M-79 was more or less similar to that of open ocean conditions with the only exception at N location due to its proximity to the river mouth as inferred from low salinity values there.

3.3.2.Short-term variability in the salinity field :-

The day to day variability observed in the top 100m water column at all the four corners of the stationary polygons during M-77 and M-79 is depicted in Fig. 3.4. Daily averaged salinity profiles are utilized to construct

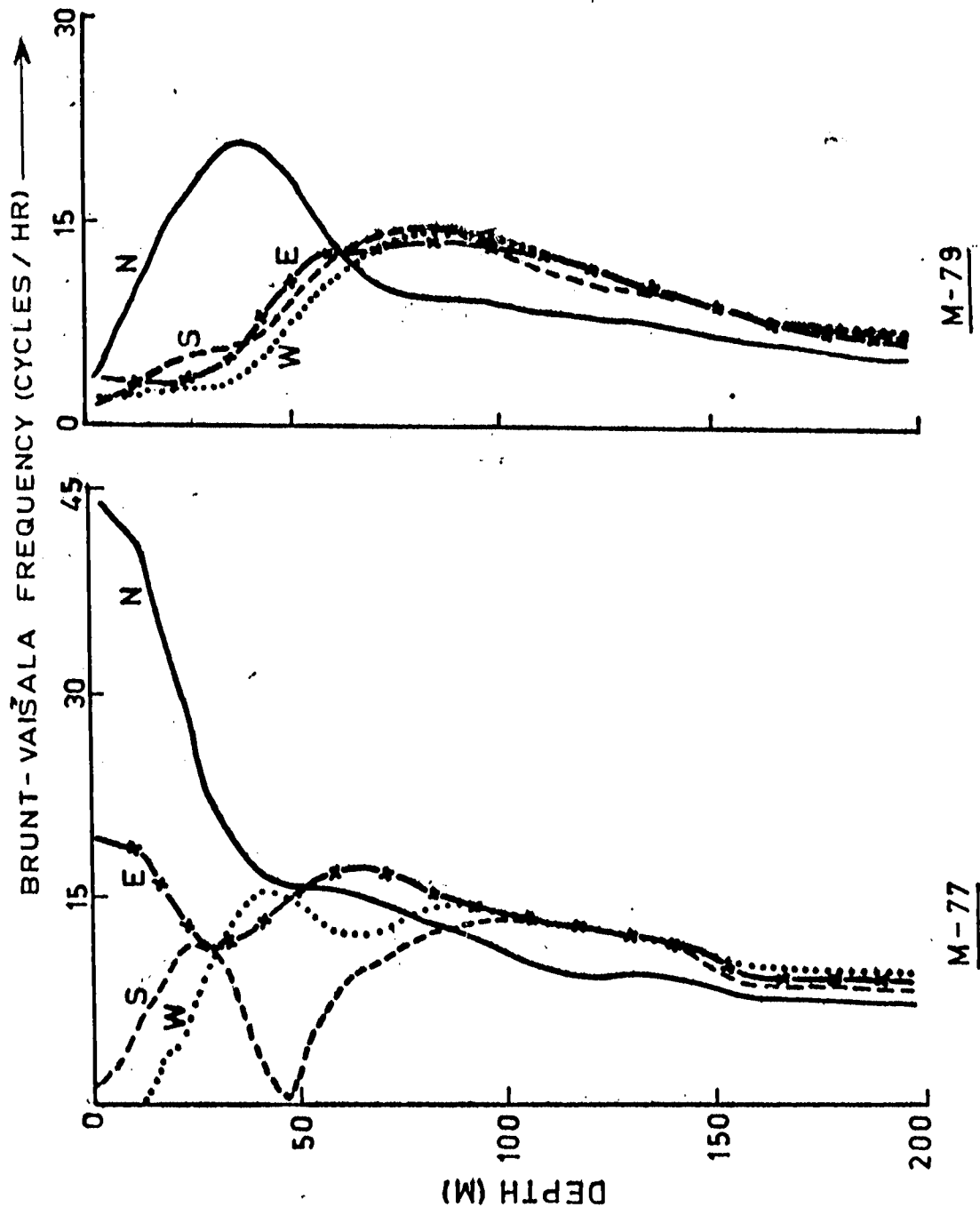


Fig. 3.3. Brunt Vaisala Frequency (N) for polygons of M-77 and M-79.

depth-time sections. The isopleths were drawn at interval of 2 PSU for salinities < 33 PSU and at interval of 0.25 PSU for salinities >33 PSU for M-77. But they were drawn at constant interval of 0.25 PSU for M-79 as the vertical salinity gradients were weak during M-79.

During the observational period, the surface salinity at N during M-77 showed a dramatic reduction by as much as 8 PSU within a week. Such variability is quite unusual in a deep oceanic region. Contrary to this, during the same period the surface salinity at E registered an increase by 4 PSU.

Rainfall was measured onboard three ships only during M-79. The daily march of estimated evaporation E (following Rao and Basil Mathew, 1988), observed rainfall P , $E-P$, cumulative $E-P$ and observed surface salinity at three stations of M-79 are shown in Fig. 3.5. As $E-P$ was mostly positive with occasional exception on rainy days, the surface salinity is expected to show an increase. However, the rainfall occurred at S during 18-22 July 1979 seemed to have lowered the surface salinity. But the impact of the heavy rainfall event of 18 July at W is not noticed in the daily-averaged surface salinity. However, a closer examination of the diurnal variation of salinity in the topmost 50 m water column on 18 July at W (Fig. 3.6) revealed the influence of rainfall event limiting to the top 20 to 30m water column. In the surface layer a mild increase in salinity by about 0.08 PSU for 0000 hr to 1200 hr may be attributed to the eastward advection of saline waters (observed eastward flow at 25 m was 55 cm/s and the mean salinity of the topmost 20 m water column was higher at W than that at E). The sudden drop of salinity from 1200 hr to

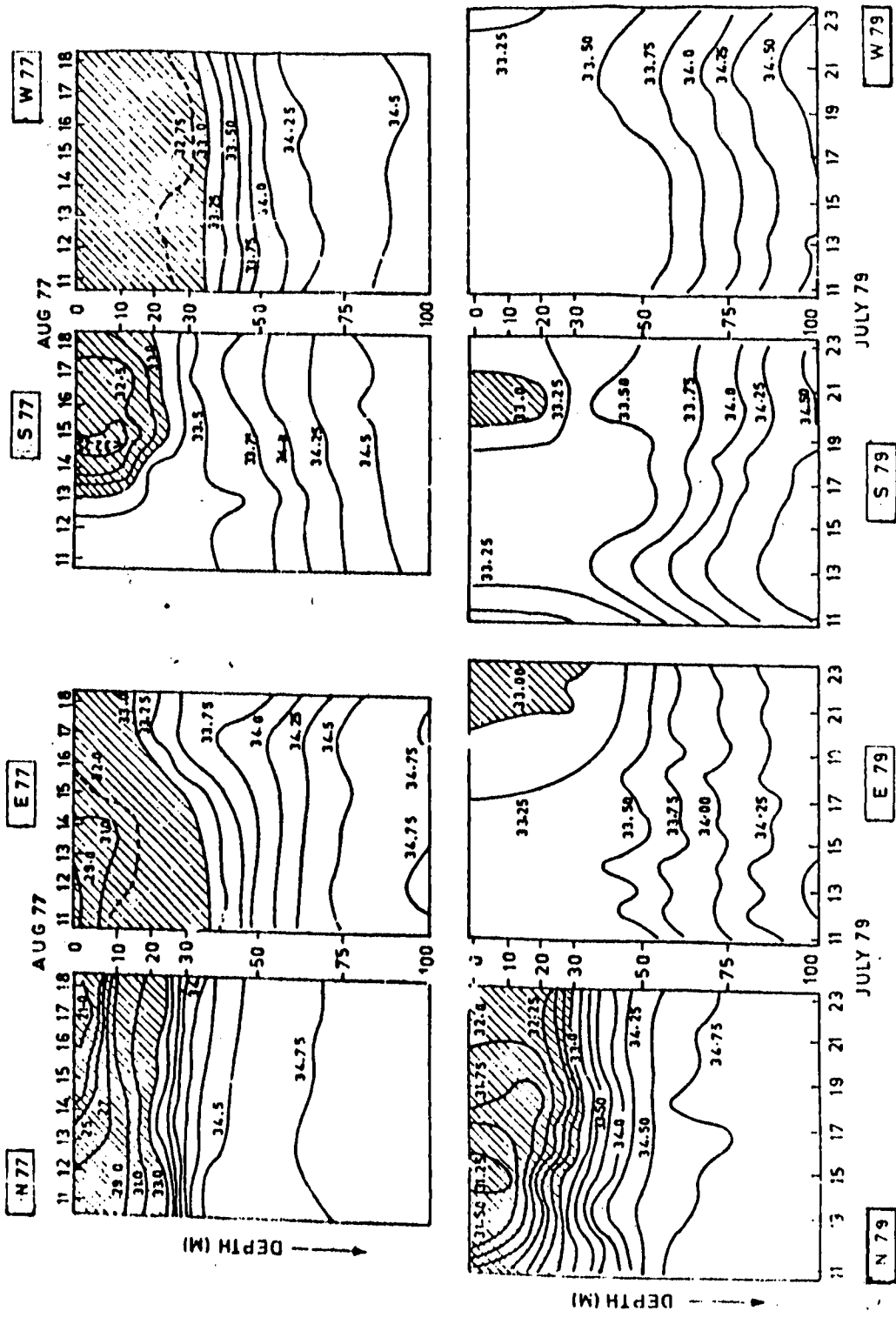


Fig. 3.4. Depth-time sections of salinity during M-77 and M-79.

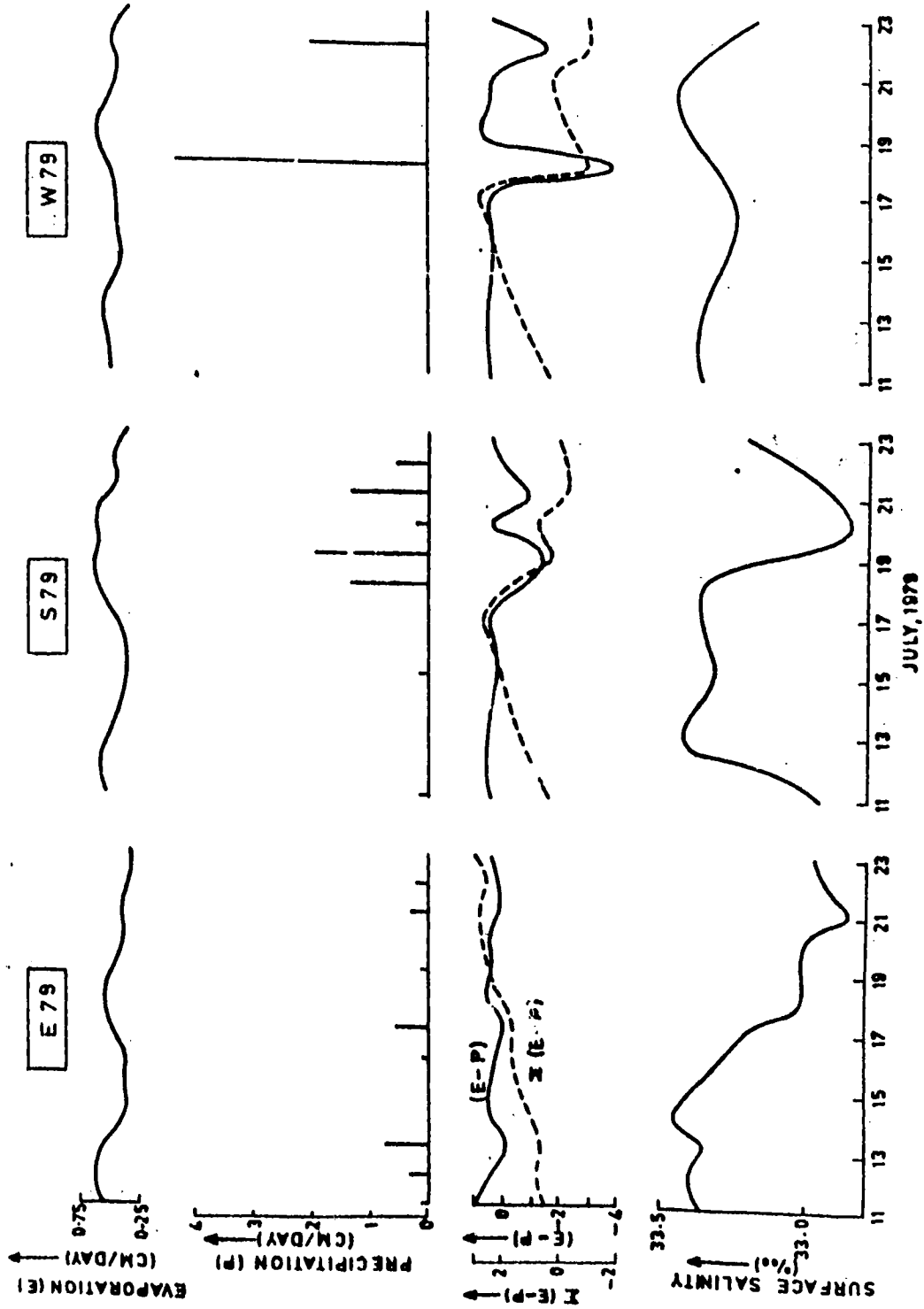


Fig. 3.5. Evaporation (E), precipitation (P), E-P, Σ E-P and salinity (S) at three stations of M-79.

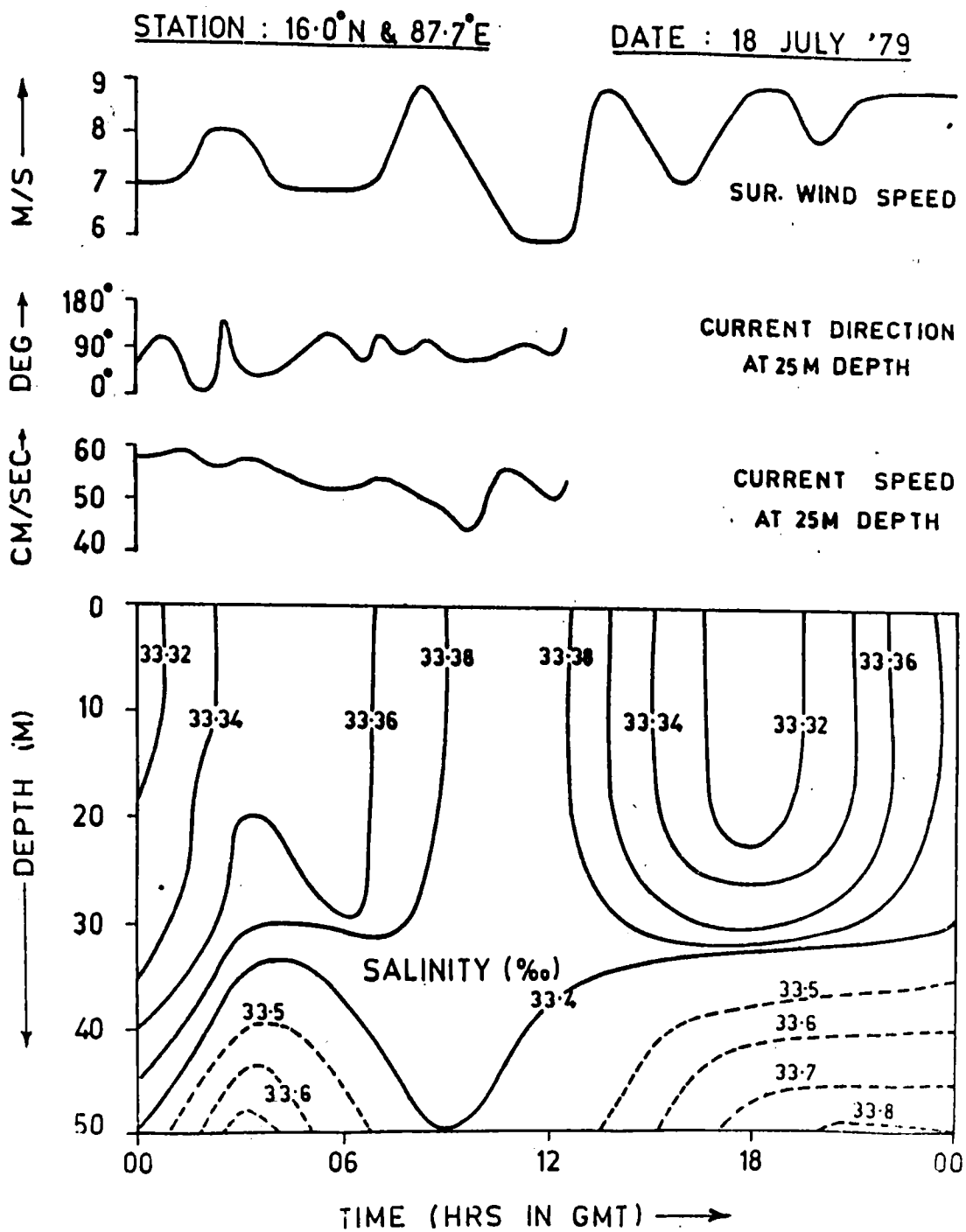


Fig. 3.6. Salinity for the upper 50 m, surface winds and currents on 18 July 1979 at W79.

1800 hr by about 0.09 PSU in the upper 20 m water column could be attributed to rainfall (4.2 cm of rainfall from 1315 hr to 1455 hr) at W. After the cessation of rainfall, the salinity again showed an increase from 1800 hr to 0000 hr. Before the occurrence of the rainfall event a well-marked halocline is evident between 20 and 30 m depths at 1800 hr. During the following 6 hours this stratification weakened probably under the influence of surface wind (~8 m/s) and wave mixing. The dilution caused in the upper 20m water column due to this rainfall event is estimated utilizing the following equation.

$$\Delta S = [(E-P)/h]\bar{S} \quad (3.18)$$

where ΔS is salinity change; \bar{S} the average salinity of the 20 m water column before the occurrence of rainfall (33.39 PSU); and h , the isohaline layer depth (20 m). The computed value of ΔS 0.067 PSU against the observed change of 0.09 PSU is in reasonable agreement.

3.3.3. Short term variability in the current field:-

Direct measurements of currents at half hourly intervals were utilized to describe the short term variability in the flow regime at selected depths in the top 200m water column. These data provide a good description of the vertical structure of velocity field in the upper 200m water column. The current meter data were filtered to remove the variance with periods less than semidiurnal (M2) tide i.e. 12.5 hrs (0.08cph). The smoothed data are shown as sticks for all the 4 locations in Figs. 3.7 and 3.8 for M-77 and M-78 respectively. The observed surface wind data were also

subjected to similar processing and the wind sticks are shown in the topmost panels of Figs. 3.7 and 3.8. During M-77, the surface winds were predominantly southwesterly at all locations with an average speed of 9 m/s, implying a nearly steady wind forcing over the observational array (Fig. 3.7). However, the subsurface current field showed some interesting variations in space and time. The overall flow was towards southeast at N and S locations, and towards northwest at E and W locations suggesting convergence in the northeastern sector and divergence in the southwestern sector. The flow weakened very rapidly with depth only at N and E locations while the weakening was moderate at S and W locations. This rapid downward decay of current strength only at N and E locations may be attributed to weak downward transport of surface wind stress due to strong stratification in the pycnocline. During M-79 the surface winds were also from southwest at all locations with an average speed of 7 m/s (Fig. 3.8). The flow at N and W was towards northeast while at E and S locations it was towards southwest. A close examination of the current sticks indicates the presence of a clockwise eddy circulation extending from 25m to 200m depth. Swallow (1983) inferred a weak clockwise eddy of 400-500 km diameter at this area from the temperature field. This eddy was centered near S location where the 20°C isotherm was depressed by 30m. The reduction in the current speed with depth at N and E locations is smaller in magnitude compared to that noticed during M-77. It is to be noted that the density stratification was also less during M-79 compared to that of M-77. This perhaps clearly demonstrates the importance of local stratification in the downward transport

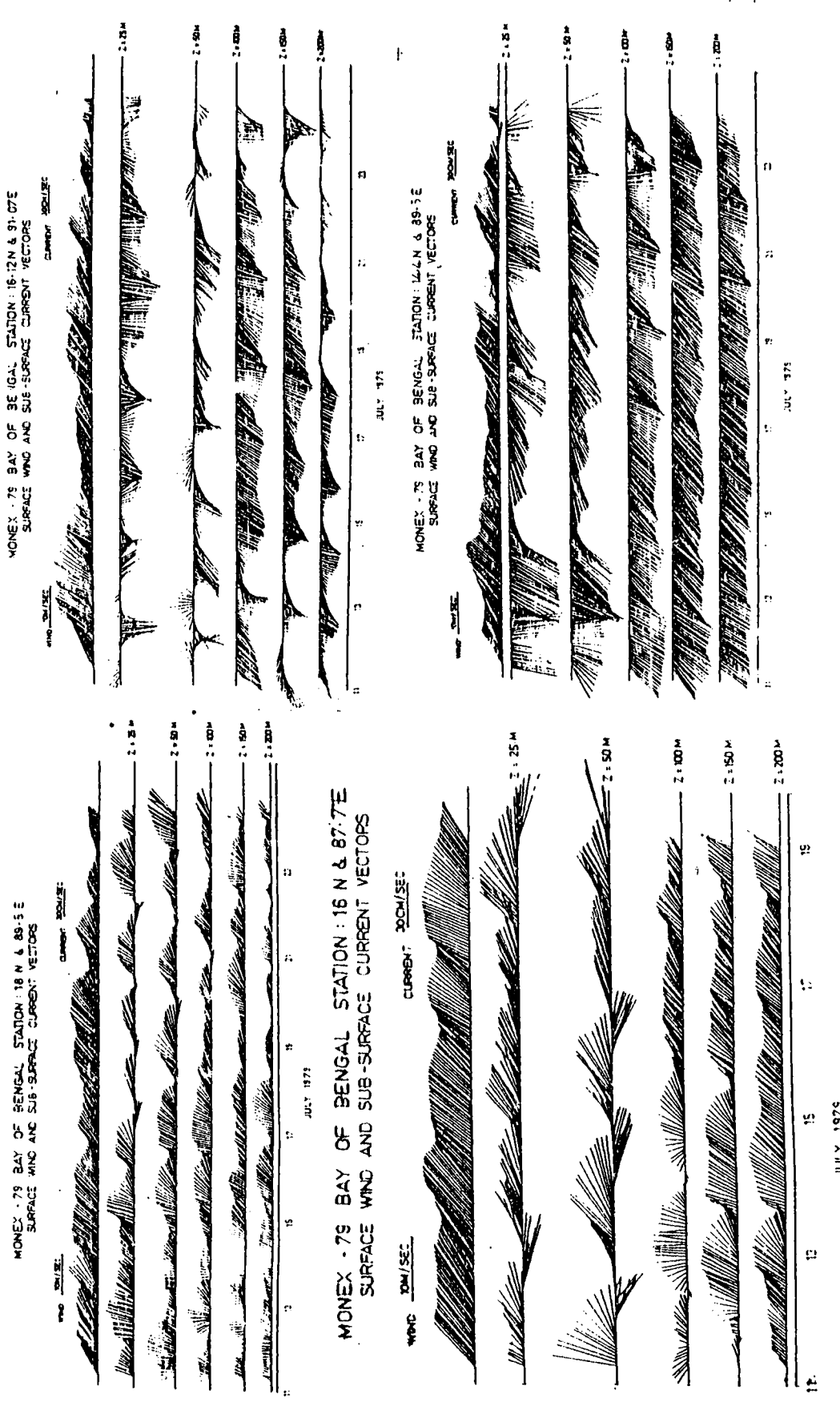


Fig. 3.8. Stick plots of surface winds and subsurface currents during M-79. Both the wind and current vectors start from the origin.

JULY 1979

of surface momentum. Flow was strong and steady throughout the 200m water column only at the S location. During both the experiments the flow regime exhibited a well defined energetic oscillatory nature. These synoptic scale fluctuations show an excellent correspondence with the local inertial periods. Pollard and Millard (1970) successfully demonstrated the importance of local wind forcing on the amplitude of inertial oscillations beneath the mixed layer. The amplitude of these inertial oscillations also appeared to be related to the local stratification.

3.3.4. Mean wind and current patterns:-

The surface wind and subsurface current data were vectorially averaged for the total observational period and the mean vectors are presented for M-77 and M-79 in Fig. 3.9. During both M-77 and M-79 the surface winds were predominantly from southwest with average speeds of 9m/s and 7m/s respectively. But the observed current vectors during both the experiments do not resemble each other. A well defined clockwise circulation is evident only during M-79 with no significant variation either in direction or in speed with depth. Apparently no Ekman type of balance is noticed during either of the experiments with the only exception at S location during M-77. The forcings produced by thermohaline gradient and massive river discharges might have been significant in producing the observed flow patterns in the upper 200m water column. The significant weakening of the flow from the mixed layer to thermocline noticed at N and E locations during M-77 was not noticed during M-79 when the pycnocline at N and E locations was relatively weaker. On the

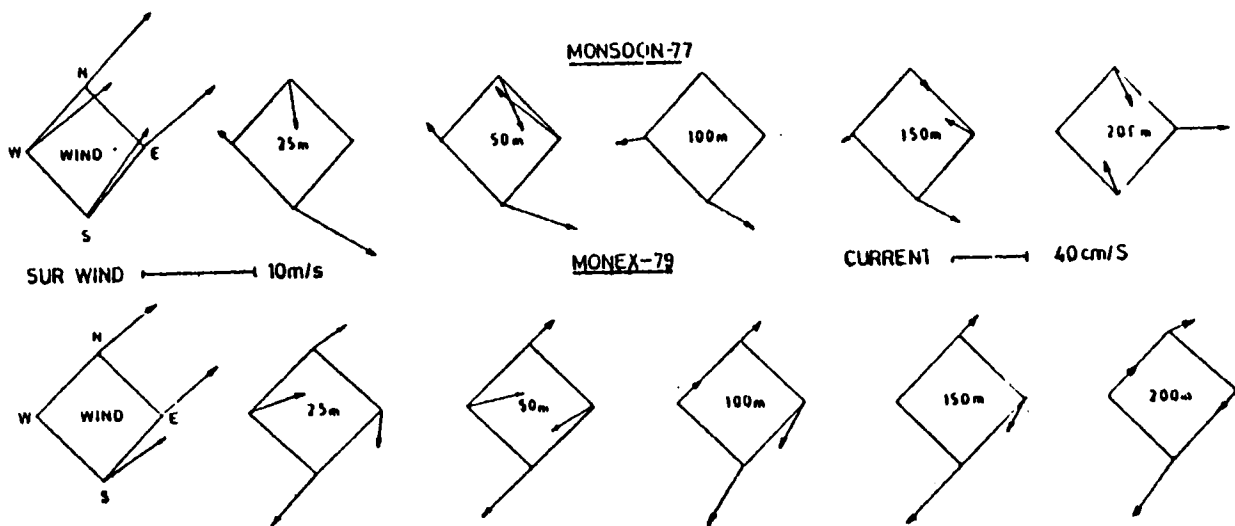


Fig. 3.9. Vectorially averaged surface winds and subsurface currents during M-77 and M-79.

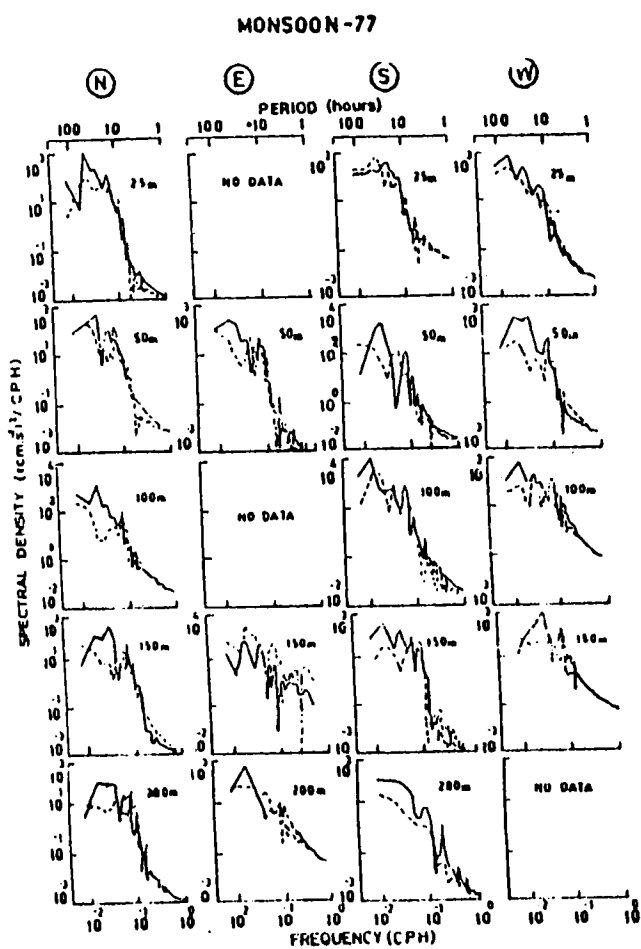


Fig. 3.10. Rotary spectra during M-77.

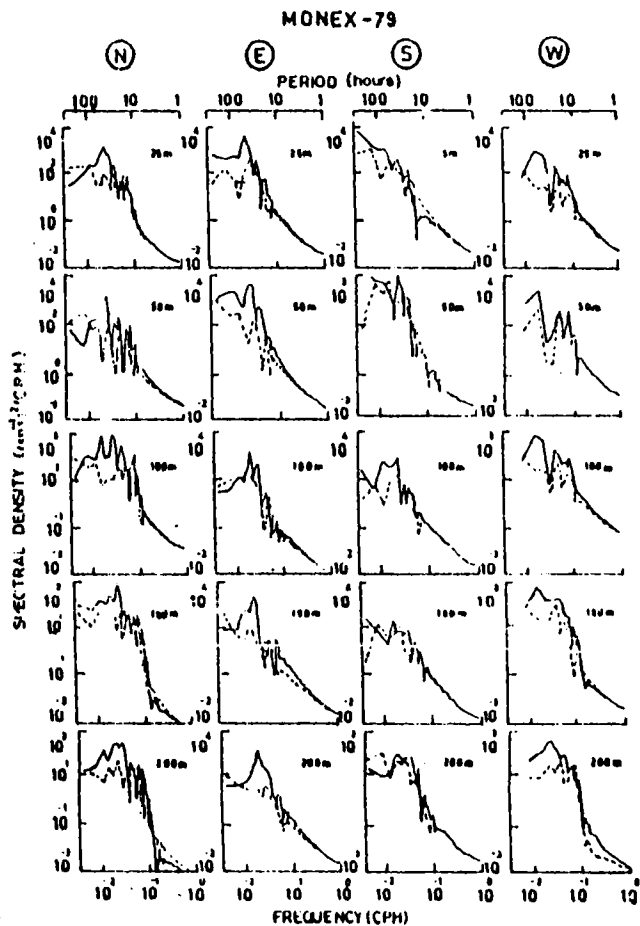


Fig. 3.11. Rotary spectra during M-79.

other hand, during M-79 the flow was uniformly stronger throughout the 200m water column at all the four locations. This feature suggests the importance of the strength of pycnocline in determining the vertical structure of the flow beneath the mixed layer base. The clockwise circulation can also be inferred from the mean flow field only during M-79. The stronger flow regime noticed at S location also suggests that the centre of the clockwise eddy was located towards south within the observational array which is in accordance with an earlier inference of Swallow (1983). This eddy circulation is noticed throughout the 200m water column.

3.3.5. Rotary spectral analysis :-

Rotary spectra were computed to examine the nature of embedded periodic oscillations in the current field over a range of frequencies of positive (corresponding to velocity vectors that rotate anticlockwise with time) and negative (corresponding to velocity vectors that rotate clockwise with time) components of the flow. These clockwise (continuous line) and anticlockwise (dashed line) spectral estimates for all the locations and depths for M-77 and M-79 are presented in logarithmic scale in Figs. 3.10 and 3.11 respectively. The most striking feature of the rotary spectra is the dominance of the clockwise component over anticlockwise component during both M-77 and M-79 especially in the low frequency band. In general the spectral energy is about an order of magnitude higher in the clockwise spectra compared to the anticlockwise spectra. The peaks in the clockwise spectra mostly correspond to inertial, diurnal and semidiurnal periodicities. However, the inertial peak is insignificant in

the anticlockwise spectra as the inertial flow is clockwise in the northern hemisphere (Pollard and Millard, 1970). In general, a spectral peak of 128 hr period is dominant in the clockwise spectra while another peak of 85 hr period is noticed in the anticlockwise spectra at N, E and S locations during M-79. These peaks correspond to approximately 3-5 day oscillations in the current field. Such periodicities in the observed outgoing longwave radiation representing active weather over this region during summer monsoon season was reported earlier (Lau and Chan, 1988). However, these peaks could not be resolved for W location during M-79 and for all locations during M-77 due to short data lengths. During M-79, the inertial peak in the clockwise spectra was prominent at E and S locations compared to other locations. During M-77 and M-79 the peaks corresponding to diurnal and semidiurnal periods are well resolved in both clockwise and anticlockwise spectra revealing the importance of tidal forcing in producing these oscillations. However these peaks were less prominent at E and S locations. At N location where the stratification was strongest, multiple peaks in the low frequency band are noticed both in the clockwise and anticlockwise spectra only during M-79. The absence of such a feature at N location during M-77 may be attributed to low resolution of spectra due to short data length (6 days).

CHAPTER IV

THERMOHALINE AND CURRENT VARIABILITY OFF VISAKHAPATNAM
DURING SUMMER MONSOON SEASON

4.1. Introduction

Western boundaries of the Bay of Bengal and Arabian Sea are unique because of the occurrence of seasonal upwelling and Boundary Currents associated with the seasonally reversing winds. All the major coastal upwelling zones are located at the eastern boundaries of the oceans except in the Bay of Bengal and Arabian Sea. In the western Arabian Sea, the upwelling processes are intense during summer monsoon and can not be explained in terms of local wind forcing alone (Schott, 1983). Remote forcing by offshore windstress curl and southern hemispheric trades are also the factors to be taken into consideration (McCreary and Kundu, 1985). In contrast to this, evidence is available for upwelling in the western Bay, driven by local winds alone as seen in the eastern boundaries of the oceans (LaFond, 1957; Murty and Varadachari, 1968; Unnikrishnan and Bahulayan, 1991; Shetye et al., 1991; Johns et al., 1992; Rao et al., 1993). In general, in the Bay of Bengal, upwelling takes place during February to August. With the onset and progress of the summer monsoon, the massive river discharge into the head of the Bay, dampens the upwelling in the northern Bay (Gopalakrishna and Sastry, 1985; Shetye et al., 1991; Johns et al., 1992; Rao et al., 1993). When the monsoon winds recede, sinking takes place all along the western boundary starting from the northern Bay and extending to the southern Bay. This process, continues from August to December (LaFond, 1958b; LaFond and LaFond, 1968).

Other than upwelling, the major seasonal feature in the western boundaries of the north Indian Ocean is the Western Boundary Currents (WBCs). Poleward WBCs (Somali

Current) appear in the Arabian Sea during the summer monsoon; whereas it occurs in the Bay of Bengal during January to May (Chapter - VI).

In addition, the western boundary of the northern Bay experiences tidal currents, high amplitude internal waves and fresher water inflow (LaFond and LaFond, 1968; LaFond and Moore, 1972; Shetye et al., 1991).

Under the influence of the above mentioned physical processes, significant seasonal and short-term variability in the oceanographic characteristics is to be expected in the western Bay of Bengal. Some studies were carried out to understand the seasonal and spatial variability in the western Bay (Ganapati and Murthy, 1954; LaFond, 1954; 1958a; 1958b; Rao, 1956b; LaFond and Rao, 1954; Ramasastry and Balaramamurty, 1957; LaFond, 1972; LaFond and Moore, 1972; Shcherbinin et al., 1979; Gopalakrishna and Sastry, 1985; Rao et al., 1986; Rao et al., 1987; Raju et al., 1992; Rao and Sadhuram, 1992; Suryanarayana and Rao, 1992; Banse, 1990; Babu et al., 1991; Shetye et al., 1991; 1993; Kumar et al., 1992). However, information on the short-term variability in the current and thermohaline fields are sparse. Previously, few direct current measurements were made as follows: (i) for few hours off Godavari during September 1980 (Sarma and Rao, 1986), (ii) in the vicinity of Krishna river mouth during June/July 1982 (Antony et al., 1985), (iii) off the rivers Krishna, Godavari and Mahanadi and off New Moore island during June/July 1982 (Rao K. H. et al., 1987) and (iv) off Visakhapatnam for every month for a tidal cycle each (Rao P. B. et al., 1987). Apart from these studies, no information is available on the observed current structure from the

continental shelf region of the western Bay of Bengal either seasonally or synoptically. It is to be noted that all those measurements were made by hanging sensors from onboard platforms. Moreover, the informations on the short-term variability in the thermohaline field for longer than one full tidal cycle is practically null.

To partially augment our knowledge on the short-term variability, a cruise was conducted off Visakhapatnam during the summer monsoon of 1986 (Sanil Kumar et al., 1989). The experimental site off Visakhapatnam was selected because of the reasons that it is almost at the middle of the east coast of India and the wind field with respect to the coastline is stronger and highly favourable for upwelling during summer (Murthy et al., 1968).

In this investigation, an attempt is made to study the short-term variability in the air-sea interaction and thermal structure at a deep and a shallow station off Visakhapatnam during the summer monsoon. The mixed layer response to the atmospheric forcing is simulated using KTDM and NK Models. At the shallow station, currents, thermohaline variability and the associated mixing characteristics in the water column are studied using moored vector averaging current meters at different levels.

4.2.1. Data and methodology

Twelve stations were occupied in the coastal zone off Visakhapatnam during cruise No. 170 of *RV Gaveshani* from 23 to 30 June 1986 (Fig. 4.1). At each station subsurface temperature profiles were taken using MICOM BT (TSK, Japan. Accuracy: temperature - 0.05°C ; depth - 3 m for 100 m depth)

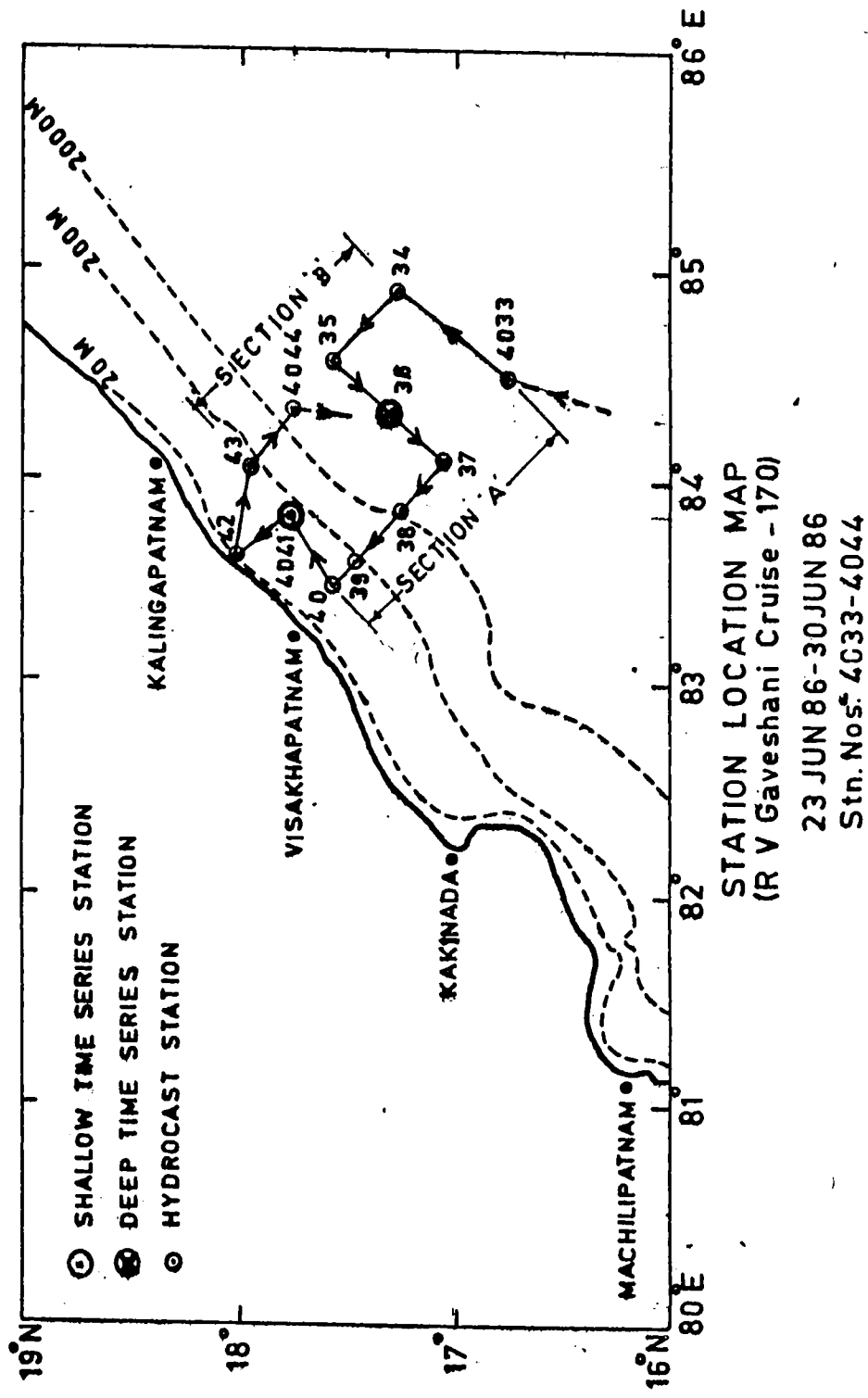


Fig. 4.1. Stations covered during June/July 1986 off Visakhapatnam.

while Nansen casts provided data on temperature and salinity at discrete depths. In addition to this, hourly subsurface temperature and standard marine meteorological observations were made at $17^{\circ}20' \text{ N}$ and $84^{\circ}20'$ (depth $>2000 \text{ m}$; deep station - designated as ST1) from 24 to 27 June 1986 and at $17^{\circ}45' \text{ N}$ and $83^{\circ}50' \text{ E}$ (depth $\sim 90 \text{ m}$; shallow station - designated as ST2) from 27 to 30 June 1986. At the shallow station, 4 Aanderaa current meters (accuracy: speed - 4 cm/s ; direction - 5° ; temperature - 0.05°C and salinity - 0.03 PSU) were moored for recording temperature, salinity and current speed and direction at every 10 minutes interval. The current meters were moored in such a way that 2 were positioned in the mixed layer (10 to 25 m), one in the pycnocline (50 m) and the last one close to the bottom (85 m). Stations perpendicular to the coast on either side of the mooring location are referred as section A and B.

4.2.2. Power Spectra:-

A Fast Fourier Transform (FFT) algorithm following Ahmed and Natarajan (1983) was used to compute power spectral energies embedded in different bands of offshore (U), alongshore (V), temperature (T) and salinity (S) fields. Due to the restriction on the number of data points to be used in an FFT (fast fourier transform) algorithm, data length was limited to 64 h (384 points at 10 min interval). The data were smoothed by a 3 point moving average to remove the frequencies greater than $1/30 \text{ cycles/min}$. The procedure adapted for computing power spectra is given in chapter 3 (3.2.2). First set of spectral values was computed from the data points 1 to 256 and the second set from 127 to 384

points by allowing 50 % overlapping. The resultant two sets were averaged over the same frequencies and presented in this chapter as logarithmic plots of frequency versus spectral density.

4.2.3. Vertical shear (S):-

S represents the dynamic stability and is given by the equation

$$S^2 = \left(\frac{\Delta U}{\Delta Z} \right)^2 + \left(\frac{\Delta V}{\Delta Z} \right)^2 \quad (4.1)$$

where ΔU and ΔV are the differences in the offshore and alongshore components of the flow.

4.2.4. Richardson Number (Ri):-

A dimensionless quantity, Richardson number

$$Ri = N^2 / S^2 \quad (4.2)$$

measures the relative importance of both density (static stability) and mechanical (dynamic stability) effects in mixing. The transition from waves to turbulence occurs (Munk, 1966; Phillips, 1966) when Ri is less than 0.25.

Mixed layer simulation was carried out using the methodology described in Chapter II and the Brunt vaisaala frequency was computed using Eq. 3.1.

4.3. Results and Discussion

4.3.1. Thermal structure on either side of the stationary locations:-

Vertical sections of temperature along sections A and

B on either side of the stationary locations are presented in Fig. 4.2. The surface temperature was low ($\sim 26^{\circ}\text{C}$) near the coast along both sections and increased to over 28°C offshore. Throughout the upper 100 m water column upsloping of isotherms towards the coast indicated upwelling. Upwelling starts off Visakhapatnam by February and continues upto June/July under the favourable winds (LaFond, 1954; 1957; LaFond and LaFond, 1968; Murty and Varadachari, 1968; Rao et al., 1986; Shetye et al., 1991). Observational evidence is reported on the occurrence of spatial gradient of $> 3^{\circ}\text{C}$ in temperature within 30 to 40 km wide upwelling band due to upwelling off Visakhapatnam during summer monsoon (Murty and Varadachari, 1968; Rao et al., 1986; Shetye et al., 1991). By July/August, the massive fresh water discharge at the head of the Bay inhibits the upwelling processes (Gopalakrishna and Sastry, 1985; Johns et al., 1992; Rao et al., 1993).

4.3.2.1. Observations at stationary locations:-

Surface meteorological elements at deep (24 to 27 June 1986) and shallow (27 to 30 June 1986) stations for the observational periods are shown in Fig. 4.3. In general, oscillations with varying amplitudes and periods were prominent in all the elements at both the stations. The surface pressure (PR) fluctuations were comparatively more periodic (at semi-diurnal periodicity) at ST2. The maximum drop of 8 mb occurred in the pressure field at ST2 on 24 June 1986. The speed (FF) of the southwesterly wind was higher than 10 m/s most of the time and had crossed 15 m/s occasionally. Cloudy (> 5 octa) to overcast (> 7 octa) sky was seen during the entire observational period except on 30 June

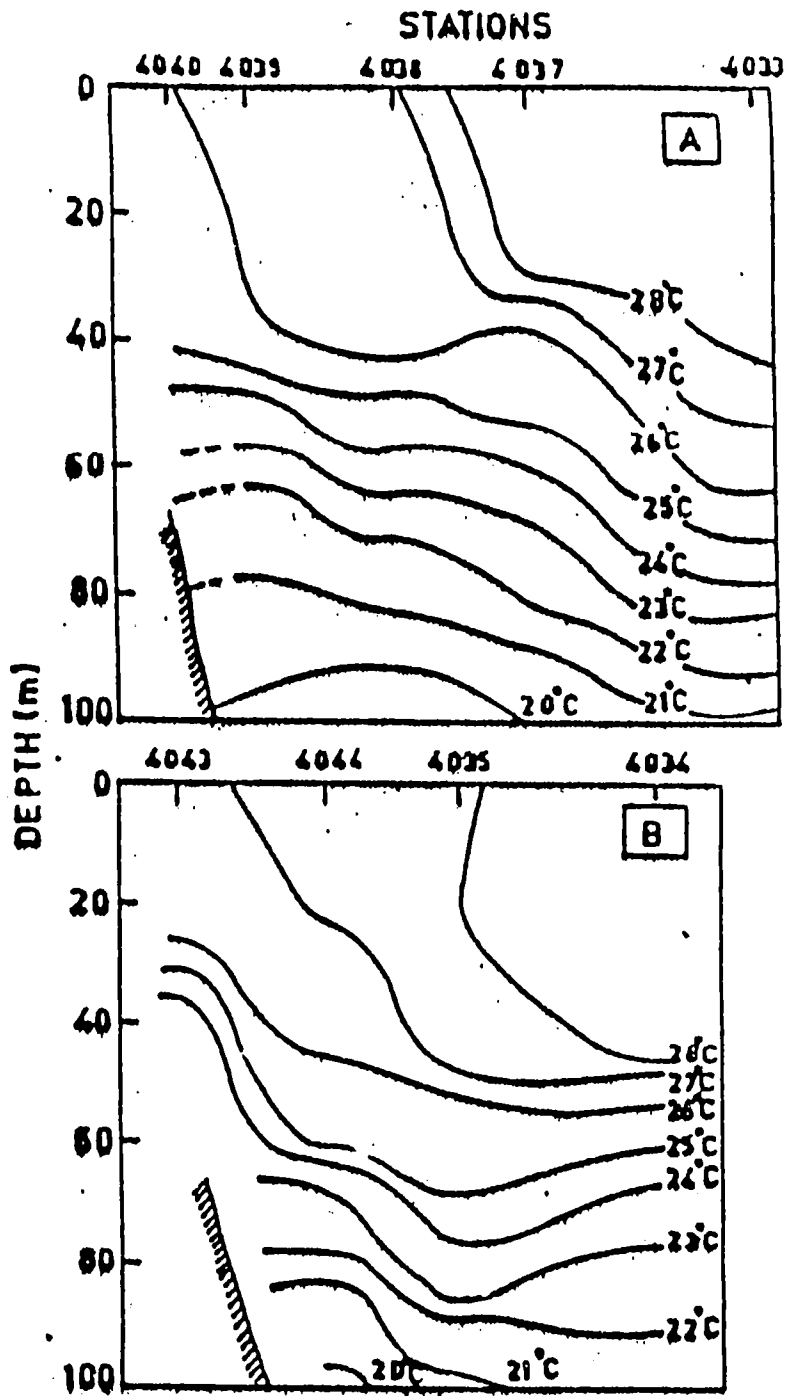


Fig. 4.2. Vertical sections of temperature along sections A and B.

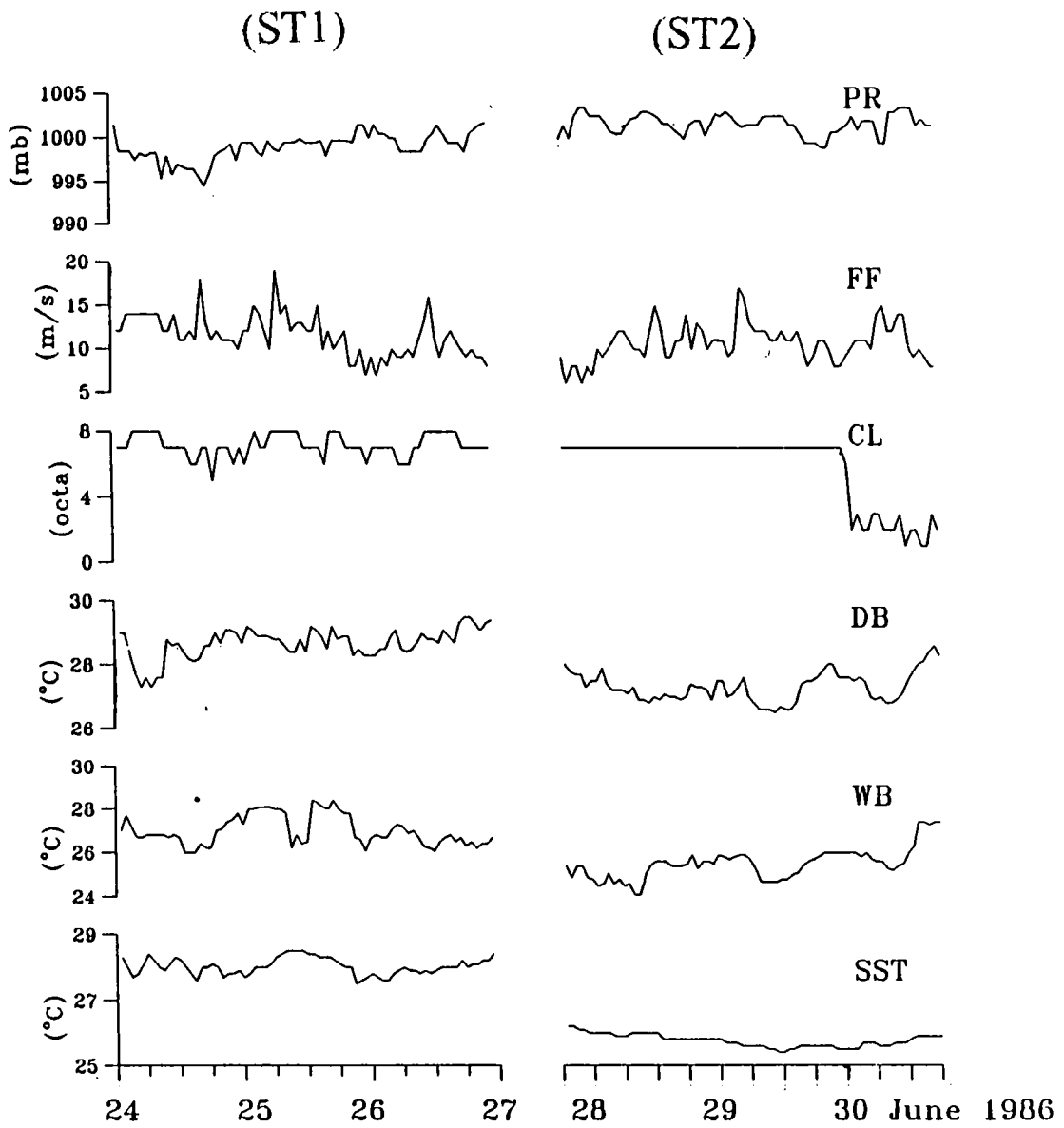


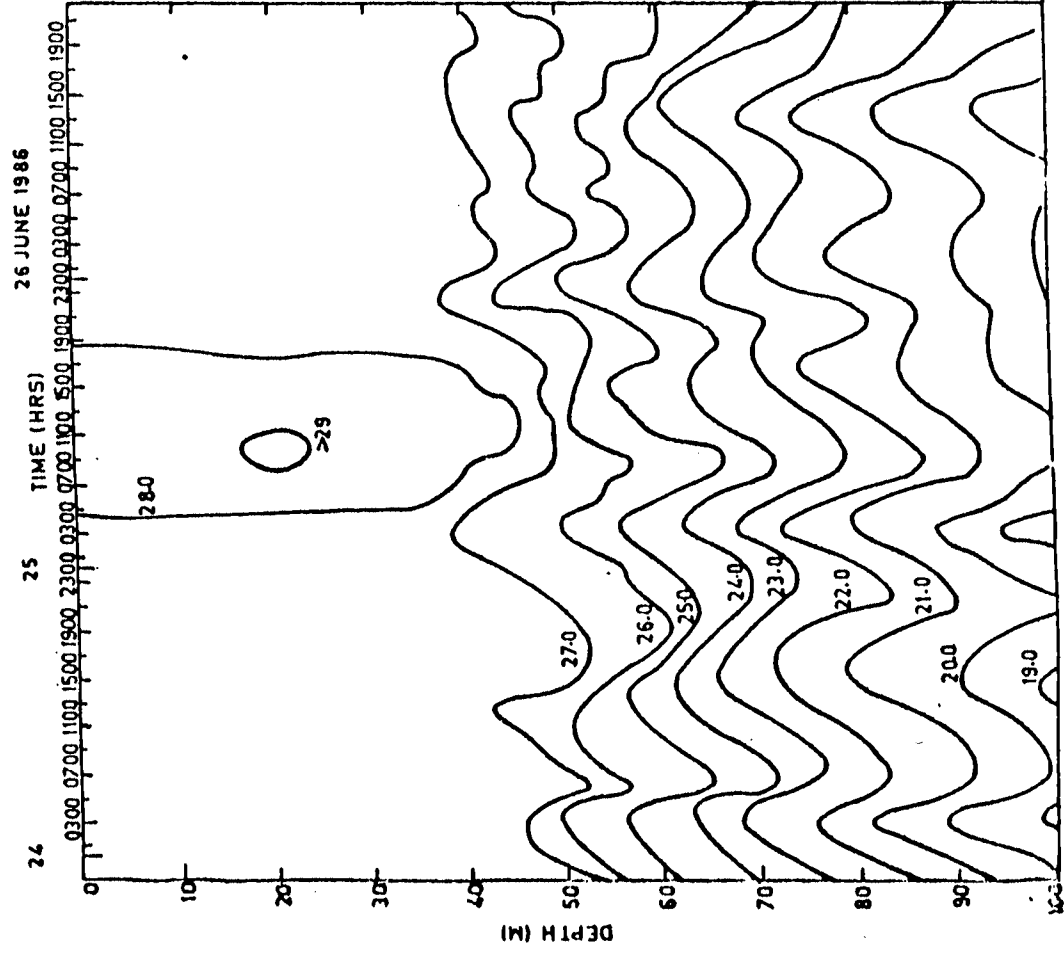
Fig. 4.3. Time series of meteorological elements at the deep (ST1) and shallow (ST2) station locations.

1986 at ST2. On 30 June, the sky became clear and the air (DB), wet bulb (WB) and sea surface temperature (SST) increased considerably. DB, WB and SST were lower at ST2 compared to those of ST1. The low temperature ($\sim 26^{\circ}\text{C}$) at the shallow station was due to the existing upwelling as evidenced from Fig. 4.2.

Time series of hourly heat budget components (Q_I , Q_E , Q_S and Q_B) and net heat flux (Q) are shown in Fig. 4.4. The day time peaks of Q were less than 800 W/m^2 due to the massive cloud cover except on 30 June 1986 when the peak reached upto 1200 W/m^2 . The minimum of the peak was $\sim 500 \text{ W/m}^2$, observed on 26 June 1986. Thus the Q showed wide range in day to day variation with the diurnal maxima between 500 and 1200 W/m^2 . It can be seen that the Q followed mainly Q_I as expected for the tropical oceans. Maximum differences between Q and Q_I were observed on 24 and 26 June 1986 when the heat loss due to Q_E was maximum. The other two terms (Q_S and Q_B) had not influenced much on Q .

Temporal variability in the thermal field at TS1 and TS2 is inferred from Fig. 4.5. An important observation at TS1 was the appearance of warmer water ($>28^{\circ}\text{C}$) in the surface layers with an inversion (29°C) at 20 m. Since the heating due to surface heat flux starts from the surface, the inversion layer appeared at subsurface has to be viewed as the manifestation of the advected warmer water. Also it has to be noted that even though Q was more on 24 June 1986, the corresponding warmer layer was absent. These observations suggest the one dimensional vertical heat flux was not the only major controlling factor of the thermal variability at the deep station. The isotherms at shallow station was found

(ST1)



(ST2)

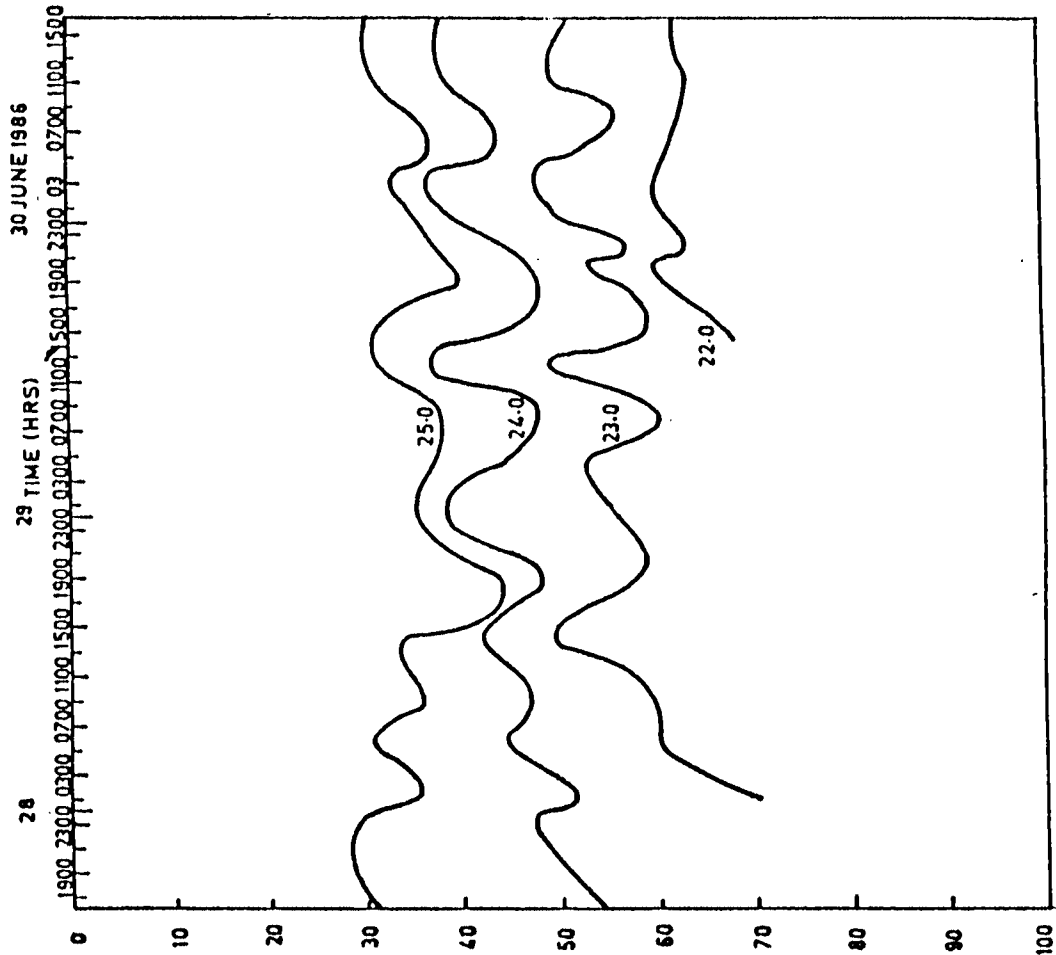


Fig. 4.5. Temperature-time sections at the deep (ST1) and shallow (ST2) station locations.

to be pushed upwards by 25 to 30 m when compared with those of at deep station. For example, 25°C isotherm was around 60 m at deep station; whereas it was around 35 m at the shallow station. This uplifting of the isotherms can be attributed to the prevailing upwelling (Fig. 4.3). The wavy isotherms with amplitudes of 15 to 20 m indicated the influence of internal tides.

The residual surface wind and subsurface currents at 10, 25, 50 and 85 m for the entire observational period at the shallow station are presented as the vector averaged plots (Fig. 4.6). The wind direction was southwesterly with an average speed of ~12 m/s. The current at 10 m was southeasterly and was stronger (~41 cm/s) with respect to the currents at deeper levels. The direction of residual flow changed to southwesterly with a sizable reduction in speed (~10 cm/s) in the pycnocline (50 m depth). This reduction in speed might have resulted from the weak vertical transport of wind induced momentum into the stratified pycnocline. In the present study the clockwise rotation and diminishing magnitude of current vectors (when looked from top) clearly suggest the influence of wind induced Ekman type circulation. As expected the currents at 85 m were weak due to bottom frictional effects. The direction of surface currents fairly agreed with the derived currents from wind field utilizing a barotropic model (Bahulayan and Varadachari, 1986). Those currents showed northeasterly flow during June with a speed of 30 cm/s. During the summer monsoon of 1978, the surface currents derived off Visakhapatnam from density distribution also showed a northeasterly component. But, south of Visakhapatnam no well-defined field of motion could be seen

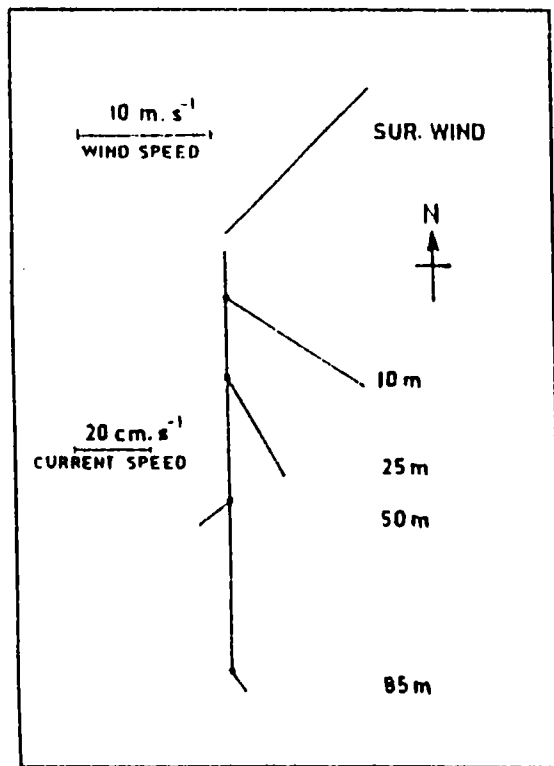


Fig. 4.6. Vectorially averaged surface wind and subsurface currents at shallow station (ST2). Both the wind and current vectors start from the origin.

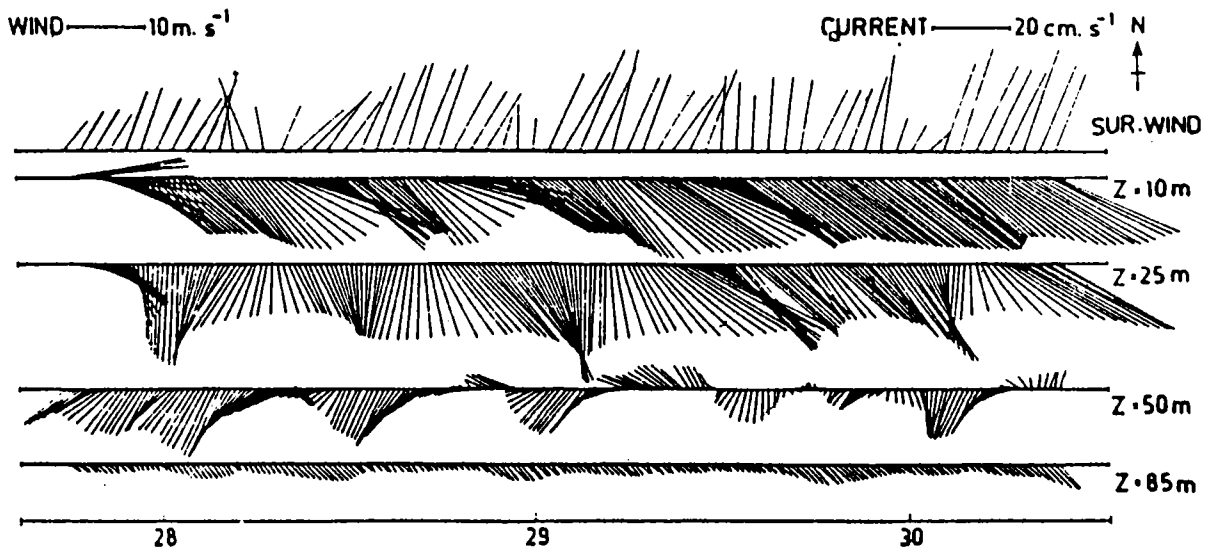


Fig. 4.7. Stick plots of surface winds and subsurface currents at ST2. Both the wind and current vectors start from the origin.

(Gopalakrishna and Sastry, 1985). However, the geostrophic currents during July/August 1989 (Shetye et al., 1991) revealed a northerly current very near to the coast and a southeasterly current offshore. The southeasterly current was observed as a part of the cyclonic eddy in the offshore region. However, the direct reading current meter data off Visakhapatnam during June 1980 (Rao et al., 1987) showed a varying current between northwesterly to southwesterly. The ship drift data (Cutler and Swallow, 1984) also show a northeasterly flow. In short, the residual current observed in the surface layers in the present study agreed with the derived flow pattern of the earlier studies.

The hourly surface wind and current at 20 min interval at 10, 25, 50 and 85 m depths are shown as sticks (Fig. 4.7) for delineating the short-term variability in the subsurface current and the surface wind fields. The above data were smoothed with a 3 h moving average to explain clearly the well organized low frequency oscillations. The wind field was mostly southwesterly with speeds between 4 and 16 m/s. The currents in the mixed layer were southeasterly with fluctuations of speed from 15 to 45 cm/s. Current speed in the pycnocline was reduced and superposed with oscillations around 12 h periodicity. This 12 h periodicity indicated the importance of the internal tides. In the mixed layer the oscillations with 12 h periodicity were not conspicuous under the influence of mixing. The flow near the bottom was very weak due to friction.

Time series plots of temperature, salinity, U and V components of currents (all obtained from the Aanderaa current meters) are shown in Fig. 4.8 to explain the

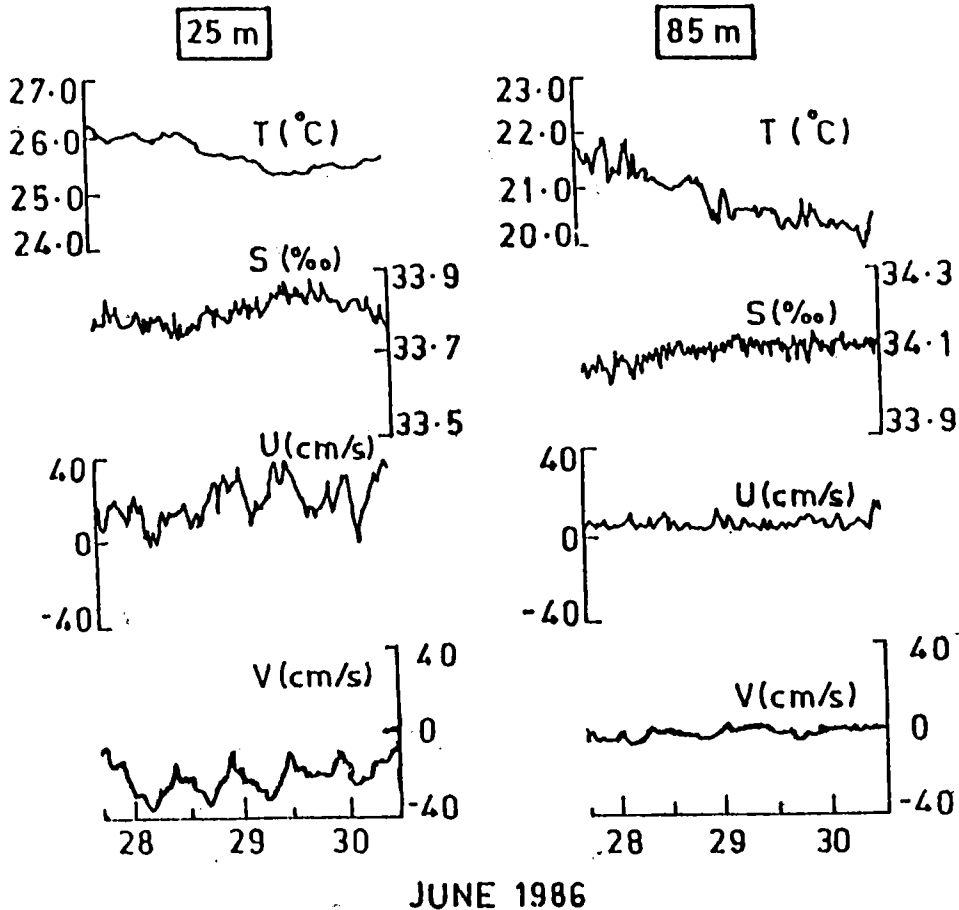
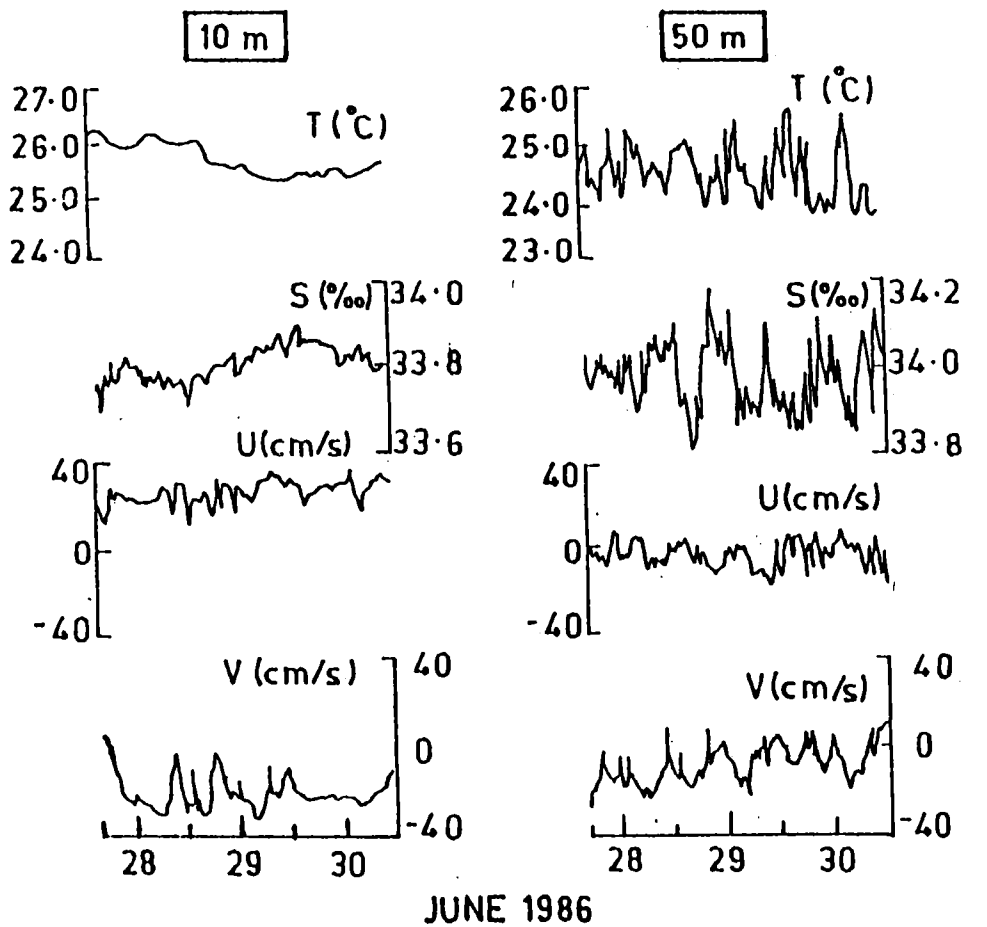


Fig. 4.8. Time series of temperature (T), salinity (S) and offshore (U) and alongshore (V) components of currents

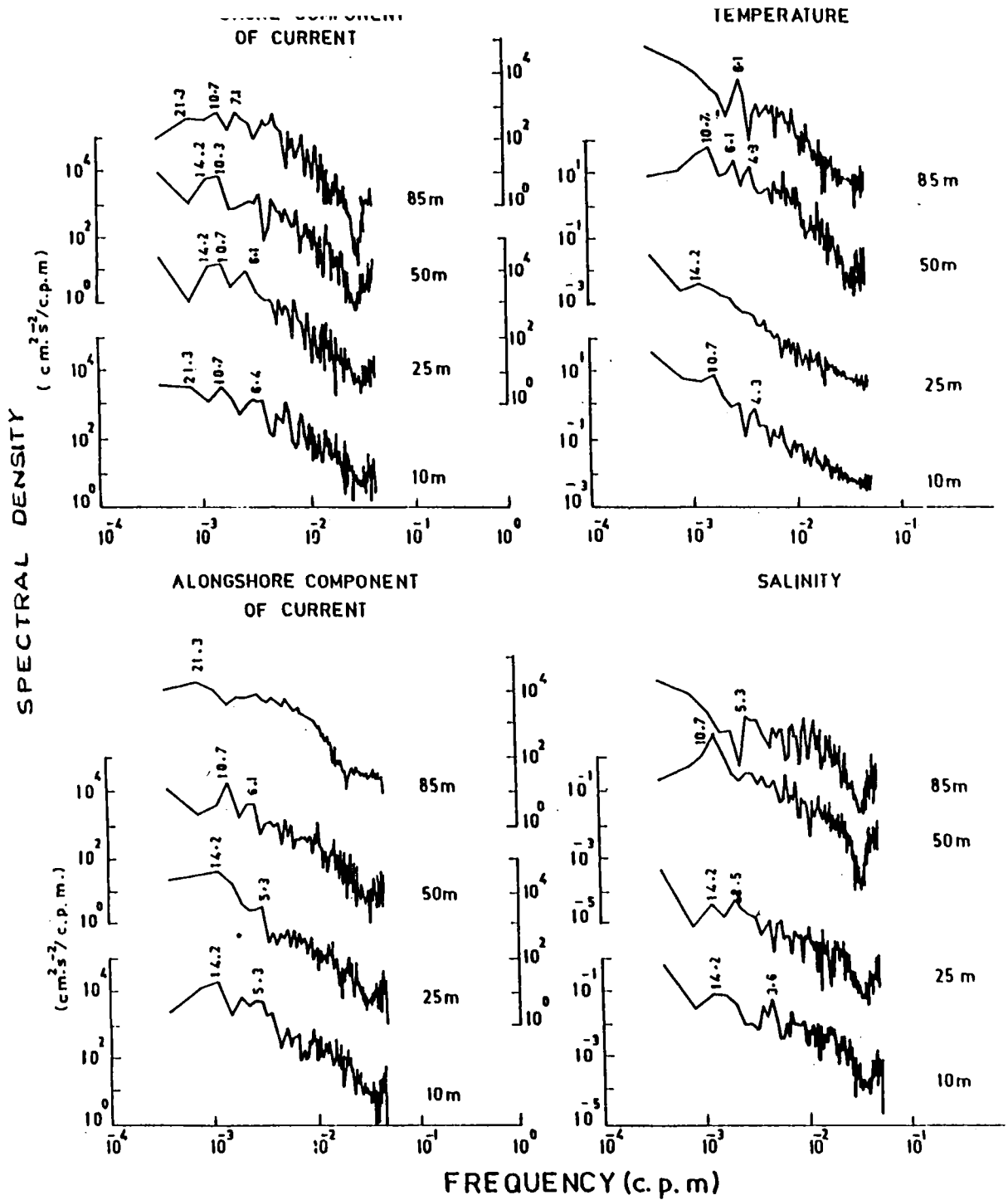


Fig. 4.9. Spectra of temperature (T), salinity (S), and offshore (U) and alongshore (V) components of currents.

short-term variability and the interrelationship between these parameters. Under the influence of upwelling, the temperature and salinity showed a decrease and increase respectively in the entire water column during all the 3 days. The temperature fluctuated between 25.3°C and 26.3°C with a decreasing trend in the surface layer. A marked decrease of 2°C in temperature was observed within the observational period at 85 m. The maximum amplitude of temperature and salinity variability was observed at 50 m due to strong gradients in the pycnocline. Temperature varied between 23.5°C and 28.5°C and salinity between 33.8 and 34.2 PSU at this depth. At all these depths an inverse relationship between temperature and salinity was observed. Positive values of U at 10, 25 and 85 m indicated offshore flow as a consequence of upwelling. But at 50 m, U was negative during most of the period. Southeasterly components (V negative) were seen during most of the observational period at all depths with exceptional appearance of positive V at 50 m occasionally. The occurrence of offshore flow at 10 and 25 m and onshore flow at 50 m with decreasing trend in temperature and increasing trend in salinity confirmed the upwelling process in the water column. At 50m (pycnocline), the internal waves also contributed to variation.

4.3.2.2. Spectral analysis: -

The prominent frequencies embedded in the offshore, alongshore, temperature and salinity fields were identified (Fig. 4.9). In all the elements at 10, 25, and 50 m, maximum energy was found to be concentrated between the frequencies 0.00117 cpm (14.2 h) and 0.00156 (10.7 h). These frequencies

are nearer to semi-diurnal tidal frequencies ($S_2 = 12$ and $M_2 = 12.4$ h). Because of the low resolution of the spectra in this analysis, the frequencies correspond to 12 and 12.4 h reflect in the frequency band 0.00117 to 0.00156 cpm. It is well known that the semi-diurnal tide is one of the major generating mechanisms to explain these periodic oscillations in the water column, especially in the coastal waters off Andhra coast (LaFond and Moore, 1972). Even in the north central Bay of Bengal (upto ~550 km away from the coast) tidal dominance was observed in the current structure (Chapter III). It is therefore concluded that the oscillations found in the frequency band, 0.00117 to 0.00156 cycles/min were generated due to tide. The wide spacing of the spectra of temperature and salinity between 25 and 50 m was due to the fact that the energy level was ~100 times greater at 50 m compared to 10 and 25 m. This is attributed to the greater amplitude of the internal waves in the temperature and salinity fields in the pycnocline. The different shape of spectra at 85 m implied the different forcing function at this level compared to those of the upper layers. In general, the energy peaks in the semi-diurnal tidal frequency were weak at 85 m due to frictional effects which damp most of these natural oscillations.

4.3.2.3. Mixing characteristics of the water column:-

The mixing characteristics of the water column are determined by density stratification and vertical momentum exchange through shear instability. Since the current meter data were available at greater depth intervals, values of Ri can differ much for individual levels. So in this Chapter, Ri

is used mainly to explain the relative importance of density stratification and shear flow in the mixing characteristics. Time series of Ri , N and S for 3 different layers viz. 10-25, 25-50 and 50-85 m representing surface, middle and bottom layers respectively, are given in Fig. 4.10. Since the energy in the high frequency band was negligibly small, the data were subjected to a 3 h moving average to bring out the major features. On an average N was increasing towards the subsurface layers due to increasing density gradient. In the surface layer, N varied between 0.6 and 2.6 cycles/h. But in the bottom layer N ranged from 4.7 to 6.3 cycles/h. Since the strength and variability in the current field were stronger in the surface and middle layers, S was also higher (0 to 0.02 sec^{-1}) in those layers with larger amplitude of variability. At the bottom layer, S ranged between 0.02 and 0.06 s^{-1} . In general, the Ri was very low (<0.25 , unstable layer) in the surface layer during the observational period. In the middle layer Ri dropped occasionally below 0.25 when the shear increased. The spells of instability occurred on 27 June 1986 night, between 28 June 1986 afternoon and 30 June 1986 and towards the end of observational period. During these periods, the current vectors at 50 m was almost opposing the current vectors at 25 m (Fig. 4.7). The observations showed that when the periodically oscillating currents (tidal periodicity) at thermocline opposed the stronger surface layer flow, sufficiently larger current shear was produced to bring down Ri below 0.25 across the mixed layer base. Presumably the vertical mixing between the pycnocline and mixed layer was enhanced by internal tides in a transient manner depending upon the phase of near-surface

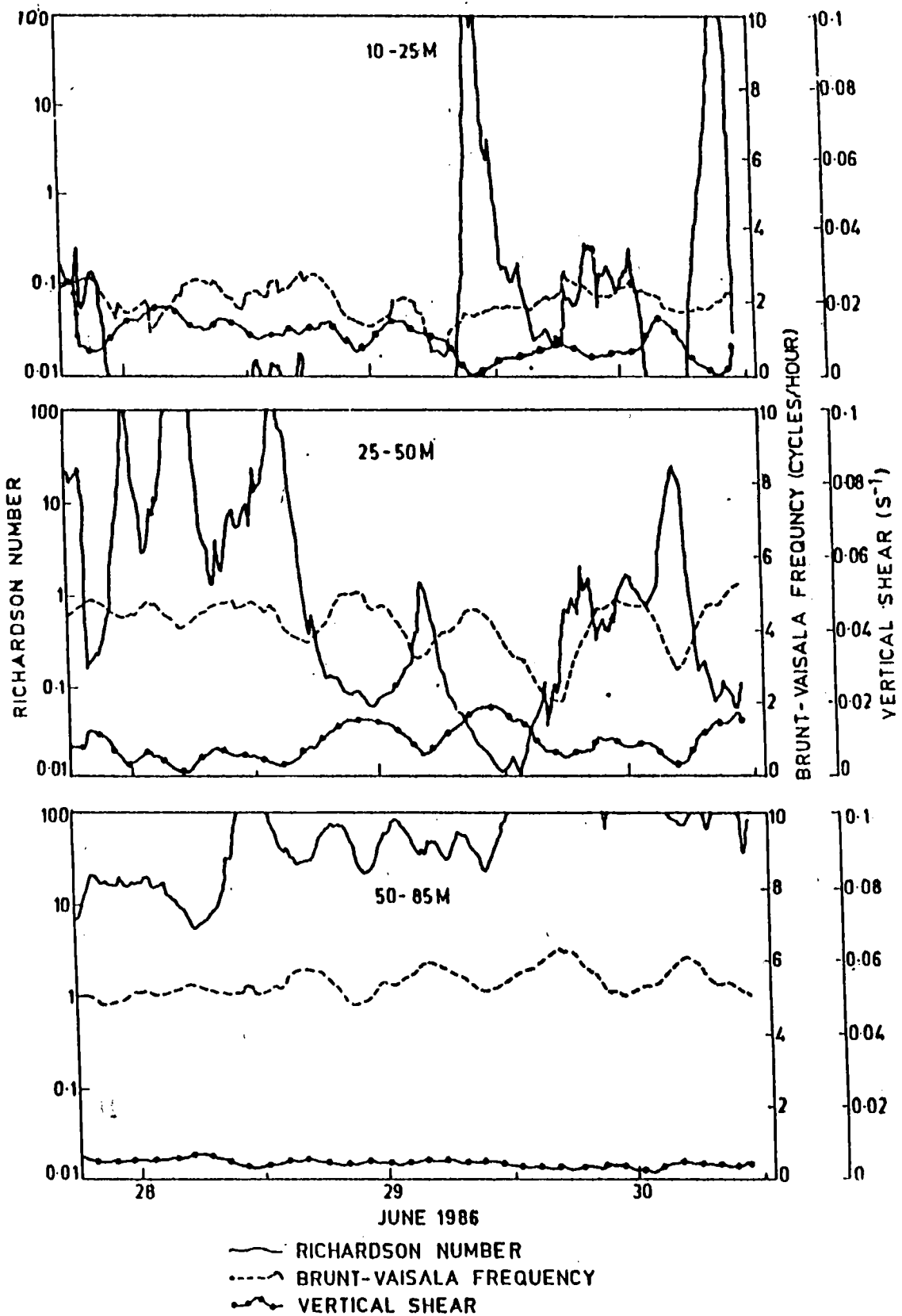


Fig. 4.10. Time series of Richardson number (Ri), Brunt Vaisala Frequency (N) and vertical current shear (SR) at TS2.

offshore flow and subsurface onshore flow. This unstable water column (in the vertical direction) might have caused to decrease the temperature and to increase the salinity in the surface mixed layer (Fig. 4.8) between 28 June afternoon and 30 June 1986. The Ri in the bottom layer indicates that the water column was dynamically stable.

4.3.2.4. Simulation of mixed layer characteristics:-

Following the methodology described in chapter II, a number of simulations were carried out with different combinations of m_1 and m_2 with NK and ' γ ' with KTDM models. The most suitable combination of m_1 and m_2 for both the stations (ST1 and ST2) was found when $m_1 = 0.39$ and $m_2 = 0.48$. This combination was selected from Davis et al. (1981). The most representative value of ' γ ' in KTDM was found when it was 0.0012 equivalent to Secchi disc depth 14 m. The results of these simulations along with the observed MLD and MLT are shown in Fig. 4.11. Observed MLD fluctuated within a wide range between 5 and 50 m. The shoaling/deepening of MLD corresponding to diurnal heating/cooling reflected at shallow station, but was not evident at deep station. The observed MLT also exhibited greater variability in the range 27.5°C and 28.8°C at TS1 compared to TS2. The diurnal heating/cooling was also not clearly resolved at both the stations. The results of the simulation showed that both NK and KTDM performed well in simulating MLD at the TS2 but poorly performed at TS1. The excursions in the simulated MLD were larger in the case of NK compared to KTDM because of the inclusion of the shear production term in NK. The oscillations in the observed temperature field were also not

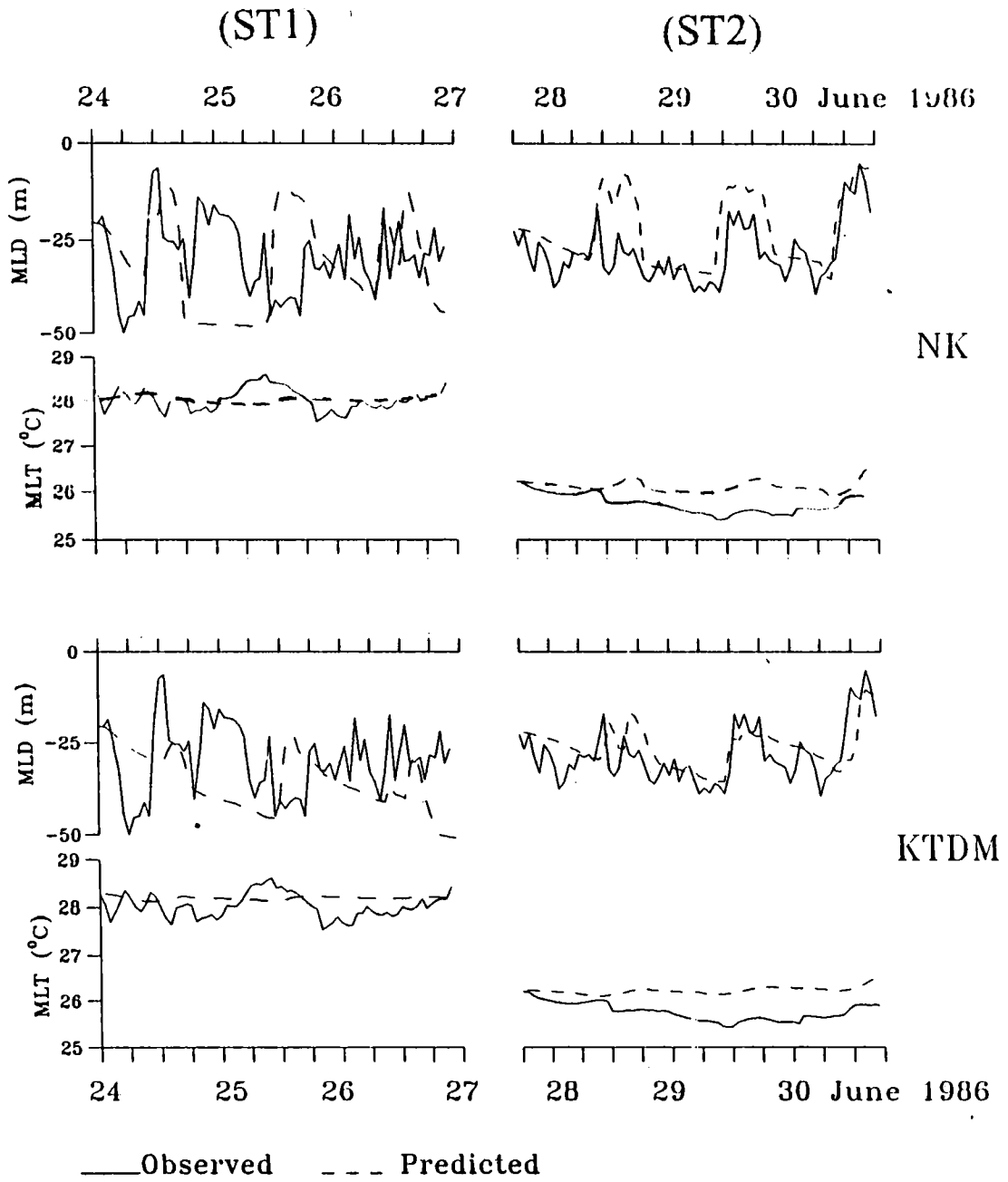


Fig. 4.11. Time series of mixed layer depth (MLD) and mixed layer temperature (MLT),

simulated well with both the models. The reasons for the wide departure between the observed and simulated MLD and MLT have to be viewed in terms of likely influence of offshore advection of upwelled cold water. If the surface heat exchange processes (buoyancy effect) are dominant in the variation of the thermal structure, an increase/decrease is expected in SST and thermal field with respect to the values of Q only. But from the above discussions, it was clear that such correlation was not revealed in the present case. Also the influence of the internal tide on the instability of the water column in the mixed layer was proved (spells of instability occurred on 27 June 1986 night, between 28 June 1986 afternoon and 30 June 1986 and towards the end of observational period) from Fig. 4.10 (section 4.3.2.3). Therefore, the greater departure between the observed and simulated MLD occurred during the 'spells of instability' at the shallow station using NK is obvious. This observation prompted to accept the better results of KTDM at shallow station with caution. The above observations suggest the physical processes other than the one dimensional processes (viz. upwelling, internal tide etc.) were dominant off Visakhapatnam during the observational period. At present those processes are not included in the 1D models. Thus the above result, necessitates a comprehensive study on the impact of oceanic internal processes in mixed layer dynamics.

CHAPTER V

THERMOHALINE AND CURRENT VARIABILITY OFF ANDAMAN
ISLANDS DURING PRE-MONSOON SEASON

5.1.Introduction

The eastern Bay of Bengal is enriched by a chain of islands emerging from the long range submerged Indonesian Archipelago. These islands are grouped into Andaman and Nicobar Islands. They extend from off Burma to off Sumatra or more precisely, spread between 6°N and 14°N and 91°E and 94°E . The portion of the Archipelago nearer to Burma, consists of extinct volcanoes of which some experience geothermal activity occasionally. These island chains provide a geographic identity to the Andaman Sea. The Andman Sea is a partially enclosed water body, extending east upto the continental margin of Myanmar, Thailand and Malaysia. It occupies an area of $6.02 \times 10^5 \text{ km}^2$ with an average depth of 1096 m. The sea is connected to the Bay of Bengal through several channels between the Islands. Among them three channels viz. (i) Preparis Channel in the north (ii) Ten Degree Channel along 10°N and (iii) the Great Channel in the south are the major ones. The southern Andaman Sea is also connected to the south China Sea through Malacca Strait.

Since the Andaman Sea is a partially enclosed basin and receives copious amount of fresh water from rainfall and river discharge from Irrawady and Salween, this basin exhibits estuarine characteristics with halocline very near to the surface layers (Ramesh Babu and Sastry, 1976). The water body also consists of the watermasses of the south China Sea and of the Bay of Bengal (Ramaraju et al., 1981; Murty et al., 1981). A mixture of these watermasses spread over to the western side of the island groups through several channels and can produce a complicated oceanographic structure there. These island groups are far away from the continental margins and act as a barrier to the free flow of

water bodies. Consequently, modifications in the flow pattern, stratification and mixing are expected in the waters around the Islands. It is well known that the seas around Andaman islands are areas of intense air-sea interaction. There is sufficient evidence for the genesis of the devastating cyclones over the Andaman Sea almost every year (INDIA METEOROLOGICAL DEPARTMENT, 1979; Subbaramayya and Rao, 1981). The complex interaction between the ocean and the atmosphere to trigger the genesis of these cyclones still remains unknown. Being an area under monsoonal influence, the surface winds and currents reverse their directions annually.

Despite all this importance, the studies on oceanographic conditions are very meagre on different spatial (LaViolette, 1967) and temporal scales. The pioneering expeditions covering the physical, chemical, biological and geological aspects, date back to 1913 to 1925 (Sewell, 1925 - 1935). However, after these expeditions, the seas continued to remain unexplored until International Indian Ocean Expedition during 1961 to 1964 (Ramesh Babu and Sastry, 1976, Wyrcki, 1971; Ramesh Babu and Sastry, 1981). During 1979 and 1980, National Institute of Oceanography, Goa conducted a few spatial surveys in the Andaman Sea (Rama Raju et al., 1981; Murty et al., 1981; Sen Gupta et al., 1981). A solitary attempt has been made to assess the short-term variability in the air-sea interaction in the Bay of Port Blair during a 12 h period (Shammi Raj et al., 1990). Some information is available on the thermohaline structure of the western side of the Islands during summer and winter monsoons (Murty et al., 1992; Suryanarayana et al., 1993). Scanty information on the currents is available from the ship drifts (Cutler and Swallow, 1984) and geostrophy (Wyrcki, 1971; Murty et al.,

1981). One study reported the internal solitons in the Andaman Sea (Osborne and Burch, 1980). Apart from the above studies, no information is available, especially on the short-term variability in currents, air-sea interaction and on the other oceanographic and meteorological properties. Thus the oceanographic setting around the Andaman Islands is very important to be probed and studied systematically.

In this chapter, the thermohaline structure around the Andaman Islands is described for a pre-monsoon period. The short-term variability in thermohaline fields, observed subsurface currents, mixing characteristics of the water column and air-sea interaction is studied at a western location off Andamans. An attempt is also made to simulate the ML characteristics using KTDM and NK models.

5.2. Data and methodology

RV Gaveshani covered a saw-tooth track around the Andaman Islands (Fig. 5.1 - dots represent the stations) from 14 to 24 May 1987 to collect data on temperature and salinity in the upper 1000 m/bottom using MICOM STDV (accuracy of sensors: temperature - 0.05°C ; salinity - 0.03 PSU; depth - 3 m for 100 m depth). In the STDV, V represents the sound velocity which is not presented in the present analysis. The ship was also anchored at a location off Andamans at $12^{\circ}28' \text{N}$ and $92^{\circ}32.6' \text{E}$ (depth 80 m) for three days from 11 to 13 May 1987. During this period, all the standard meteorological data, subsurface salinity and temperature profiles were collected at hourly interval. Five current meters of RCM-4S of Aanderaa make were moored at depths of 3, 18, 33, 45 and 58 m (accuracies of the sensors: speed - 4 cm/s; direction - 5° ; temperature - 0.05°C and salinity - 0.03 PSU). The data

were obtained at 5 min interval. Among the data, the temperature at 18 m and salinity at 18 and 58 m depths were found to be unreliable and were not considered for this analysis. The winds were recorded at 14 m height also recorded with an anemograph installed onboard for this cruise, in addition to the hourly observations from the shipborne anemometer.

The overall methods used in this analysis are adapted from Chapter 5.

5.3. Results and discussion

5.3.1. Thermohaline structure around the Islands:-

Temperature and salinity distribution around the Islands at different depths (viz. 0, 25, 50 and 75 m) are presented in Fig. 5.1. At the surface, the waters were quite warmer ($\approx 31^{\circ}\text{C}$) inspite of the sampling covered over seven diurnal cycles (14 to 21 May 1987). These warm water may be one of the favorable factors for the abundant cyclogenesis during May (INDIA METEOROLOGICAL DEPARTMENT, 1979; Subbaramayya and Rao, 1981) in the Andaman Sea. One of the climatological studies shows that the maximum SST (30°C) occurs during May (Wyrtki, 1971). In fact, the SST distribution is bimodal (Wyrtki, 1971; Colborn, 1975) with two maxima occurring during May (30°C) and October (29°C). The minima appear during January-February (26° - 27°C) and August-September (27° - 28°C). Temperature values higher than 30°C during May were not reported in the climatological studies due to the averaging of scanty data over large spatial and temporal scales. Relatively warmer waters were noticed on the western side of the Island chain at sub-surface levels in confirmity with climatology (Levitus,

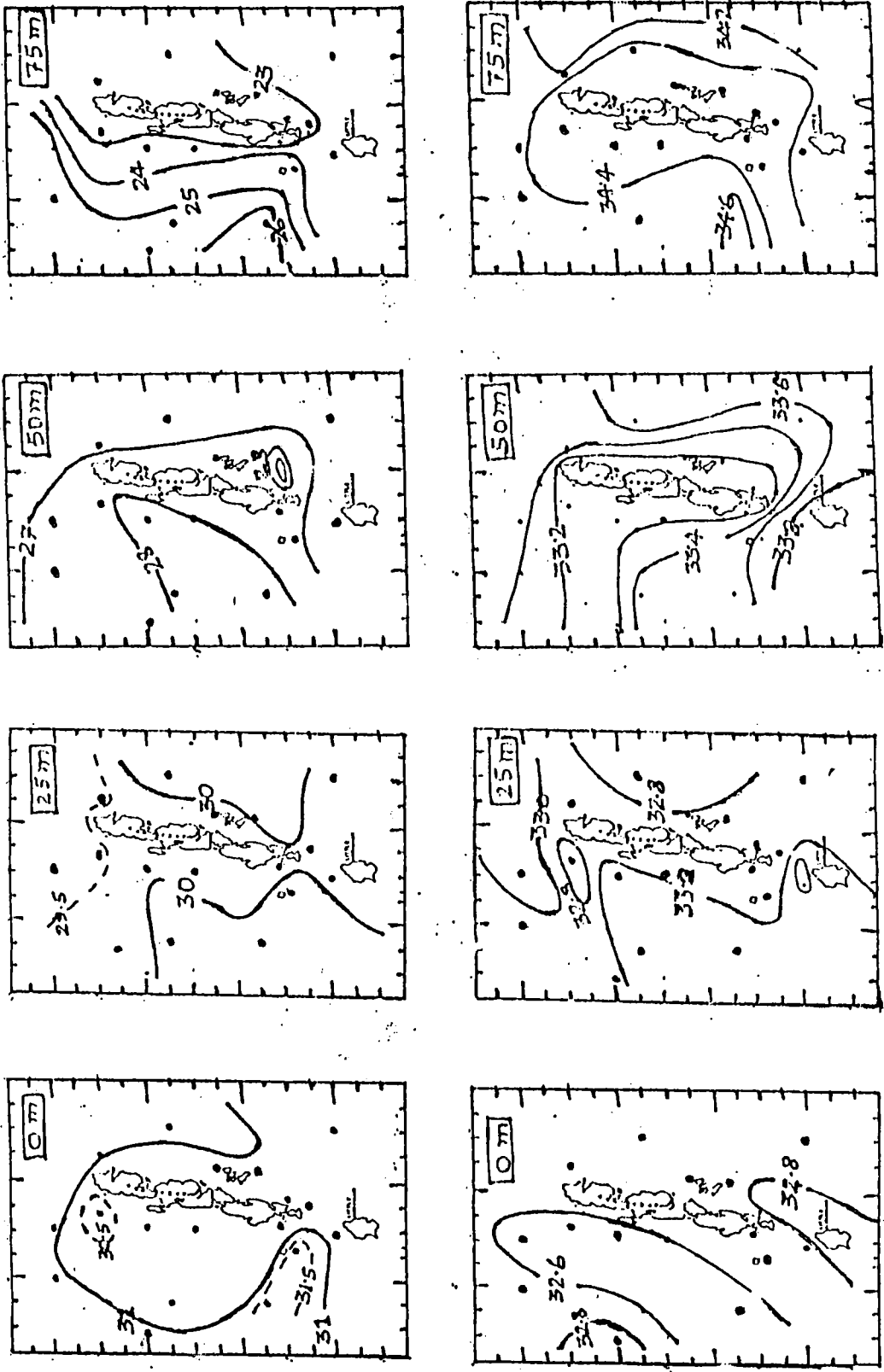


Fig. 5.1. Temperature and salinity distributions at different depths around the Andaman Islands.

1982).

In general, salinity increased from 32.6 to 34.6 PSU from surface to 75 m on the western side. This type of vertical salinity gradient produces stratification in the upper layers. Highly stratified upper layers are a characteristic feature of the Bay of Bengal.

5.3.2. Observations at the stationary location:-

Time series of standard marine meteorological parameters at hourly interval are presented in Fig. 5.2. Readings of the shipborne anemometer were reduced to 10 m height (Wu, 1980) for analysis. The atmospheric pressure (PR) showed an overall increase with embedded oscillations of amplitude ≈ 4 mb at semidiurnal period. The wind speed (FF) showed calm conditions with mean speed of ≈ 3 m/s. The cloud cover (CL) varied between 0 and 8 octa. The diurnal heating/cooling events were prominent in dry bulb (DB) and sea surface temperature (SST) data, but were absent in the wet bulb temperature (WB) record. In general, SST was greater than DB during most of the observational period and thus showed a condition for unstable overlying atmosphere.

Estimated heat budget components are presented in Fig. 5.3. As expected for the tropical oceans, the net heat flux (Q) mainly followed the incoming solar radiation (Q_I). The latent heat loss (Q_E) was the most dominant heat loss term. Effect of the sensible heat loss (Q_S) and long wave radiation (Q_B) was marginal. The diurnal peaks of Q and Q_I were always $> 1050 \text{ W/m}^2$ and $> 1100 \text{ W/m}^2$ respectively.

The effect of the net heat flux on the near-surface thermal structure can be noticed from the composite plot of temperature profiles. The occurrence of diurnal thermocline

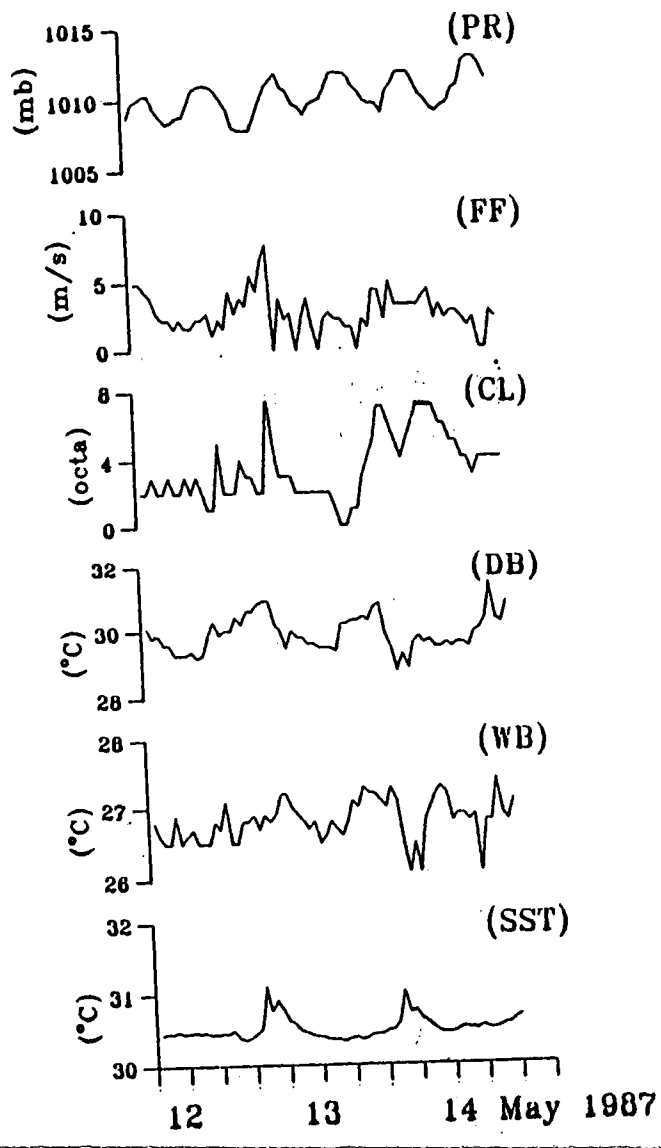


Fig. 5.2. Time series of meteorological elements.

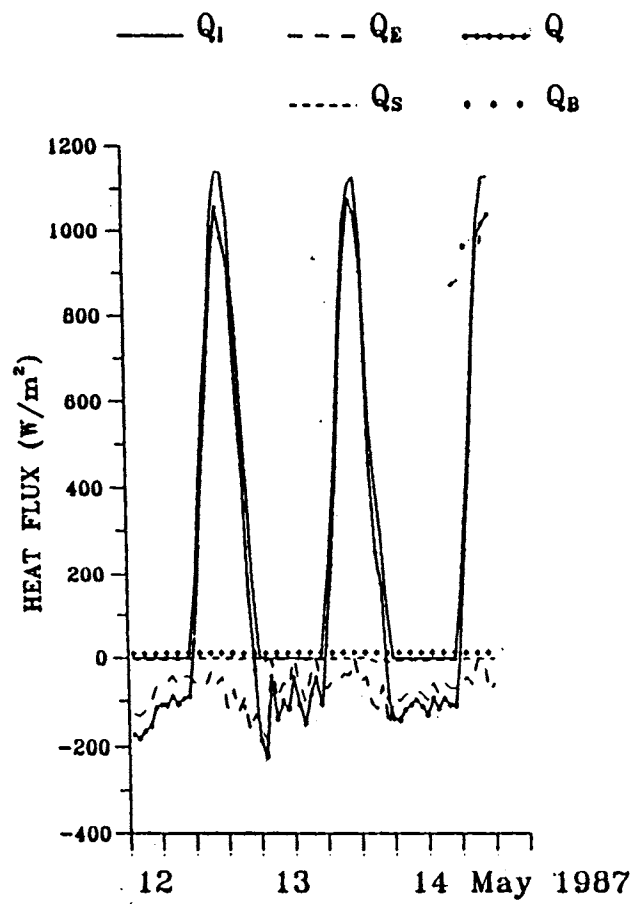


Fig. 5.3. Time series of heat budget components.

extending over the topmost 5 m water column is obvious (Fig. 5.4). This figure shows that the maxima of the isothermal and isohaline layer thickness were 25 m and 30 m respectively. The permanent thermocline was noticed below 25 m depth. The spreading of the isotherms between the depths 10 and 25 m, indicate the influence of the internal oscillations on MLD. Another feature of the temperature profiles was the occasional inversion of 0.2° to 0.6°C at subsurface layers, especially between 30 and 40 m. Due to the lack of closely sampled spatial data and current meters at closer intervals, the present data set is inadequate to investigate the reasons for these inversions. Inversions of 0.2° to 0.7°C in the upper layers were found as the characteristic feature of the Andaman Sea (Ramesh Babu and Sastry, 1976; Ramaraju et al., 1981; Murty et al., 1981). Contrary to the variability in the thermal structure, the isohaline layer thickness almost remained constant (≈ 30 m) throughout the observational period. The σ_t profiles mainly followed temperature profiles as expected in the open ocean.

Vertical sections of temperature and salinity are given in Fig. 5.5A to understand their temporal variability at different depths. In the upper 10 m, warmer pockets ($>31^{\circ}\text{C}$) were noticed due to diurnal heating effect. Below this depth the entire thermal structure fluctuates periodically under the influence of internal tides (periods ~ 12 h) with vertical displacements of 5 to 10 m. Within the thermocline a 20 m layer of weak stratification ($\approx 28^{\circ}\text{C}$) persists in the depth range of 30 - 50 m.

The salinity structure (Fig. 5.5B) showed diluted layers in the surface (<32.75 PSU) and a progressive increase towards the deeper layers. The oscillations in the isohalines

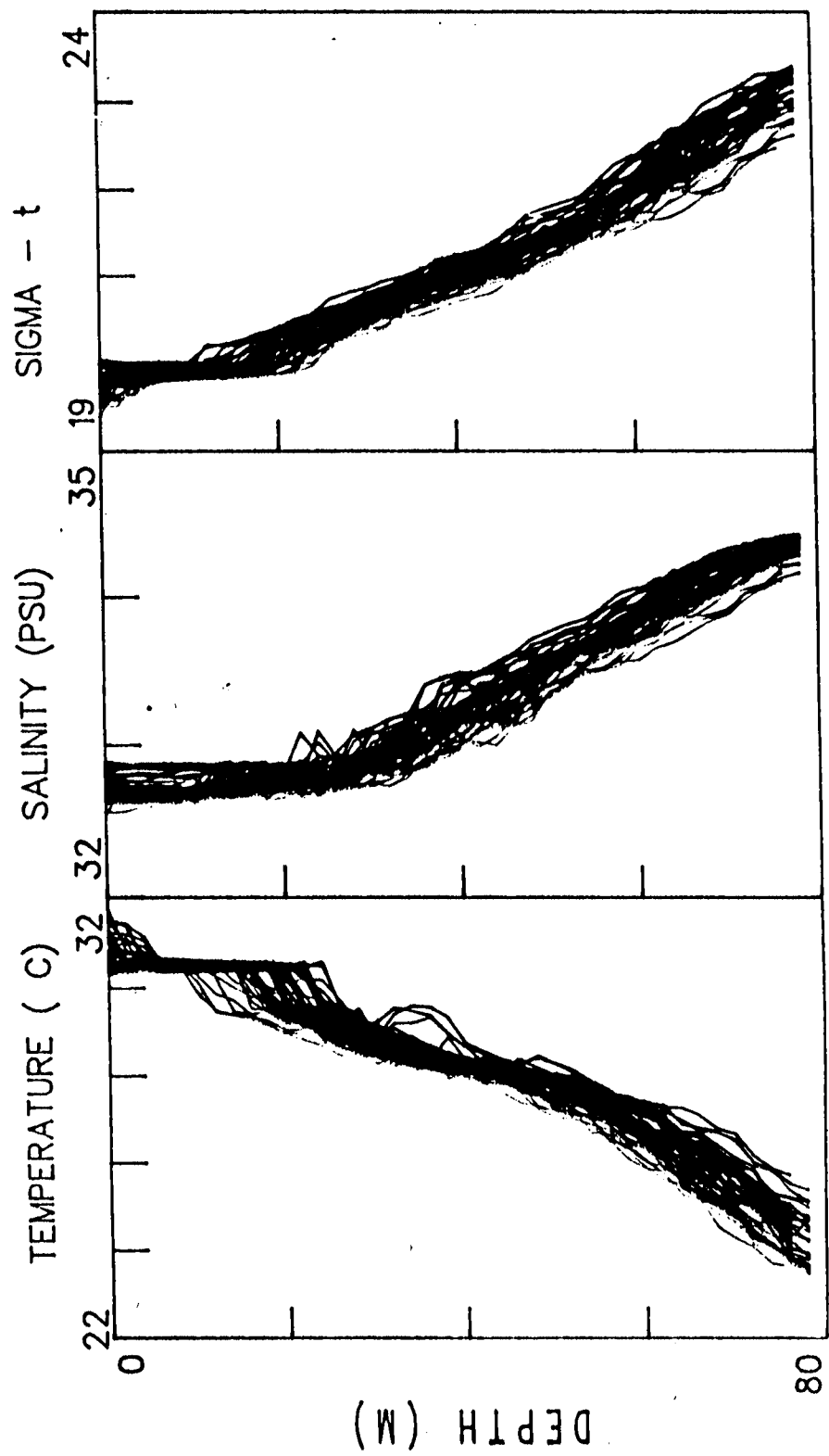


Fig. 5.4. Composit plot of temperature, salinity and σ_t

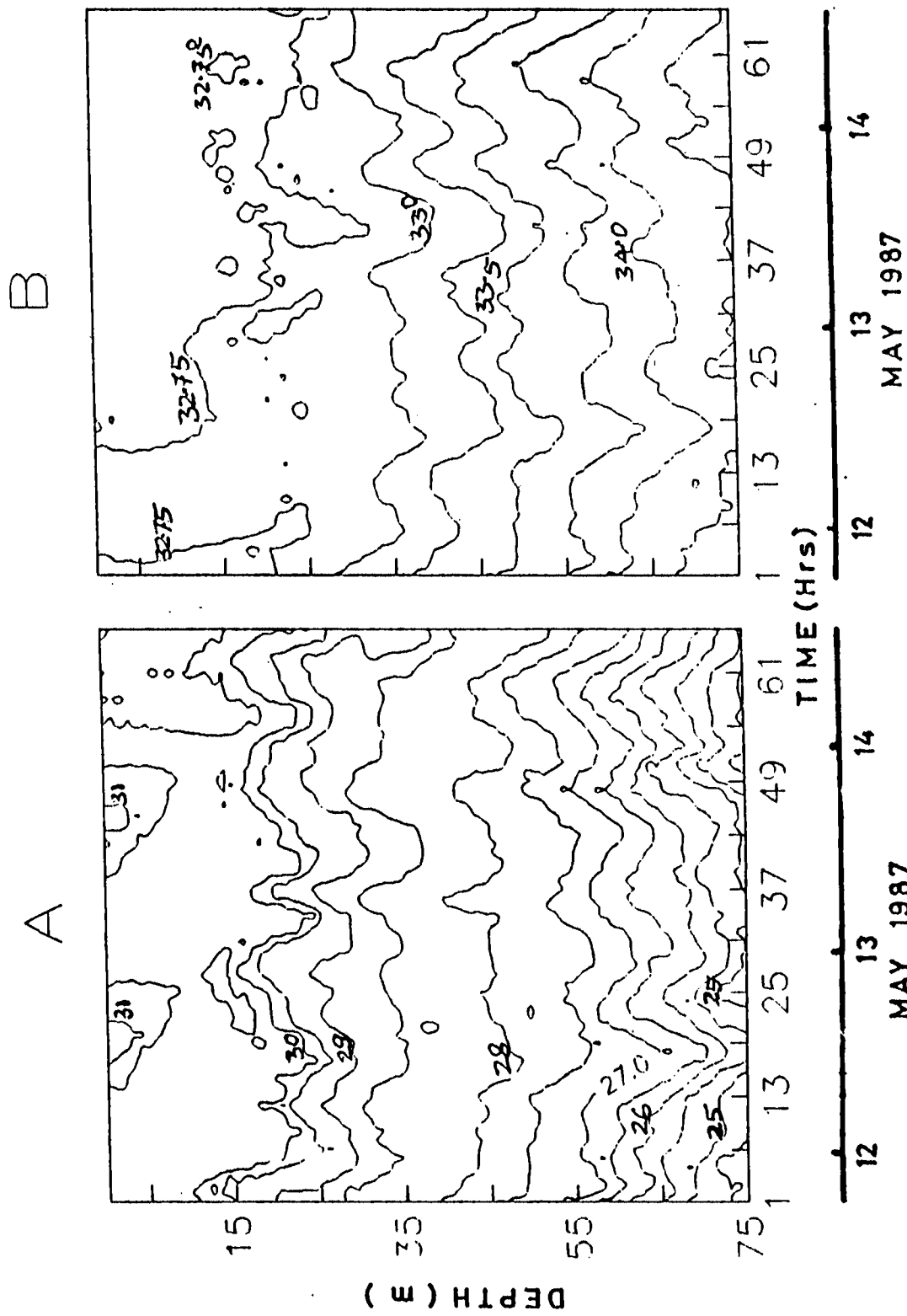


Fig. 5.5A. Depth-time section of temperature.

Fig. 5.5B. Depth-time section of salinity.

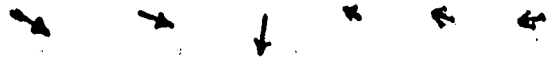
also resemble to those noticed in the thermal structure (Fig. 5.5A).

The surface winds recorded on the anemogram were digitized at 10 min interval and were used in the following analysis along with the subsurface current data. The winds at surface and currents at different levels were vectorially averaged and shown in Fig. 5.6A. This figure depicts the mean conditions at the observational site. The wind direction was northeasterly with an average speed around 3 m/s which is not in agreement with the climatological value (Hastenrath and Lamb, 1979). The currents at 3 m depth were almost in the same direction of the wind. But at 18 m depth they changed into westerly direction and thus showed a 90° rotation in the clockwise direction with respect to the current at 3 m. According to the Ekman theory, if the current is fully driven by the local wind, the surface current flow towards 45° right to the wind direction. Also the current vectors should diminish constantly towards deeper layers. In the present observations, the observed mean vectors at 3 and 18 m do not exactly fit into the Ekman Layer. Though the flow at 3 m was southerly, it had changed to westerly at 18 m and to northerly in the thermocline (33, 45 and 58 m). Thus the flow in the thermocline is opposite to the flow near the surface.

The digitized wind and current data are represented as stick plots (Fig. 5.6B) at 10 min interval to understand one to one correspondence. The data were smoothed by an hourly moving average to deduce the low frequency variability clearly. The winds were mostly northwesterly to northeasterly with moderate strength (≈ 5 m/s). The currents in general were stronger in the surface layers (3 and 18 m depths) and were weaker at the below layers (33, 45 and 58 m depths).

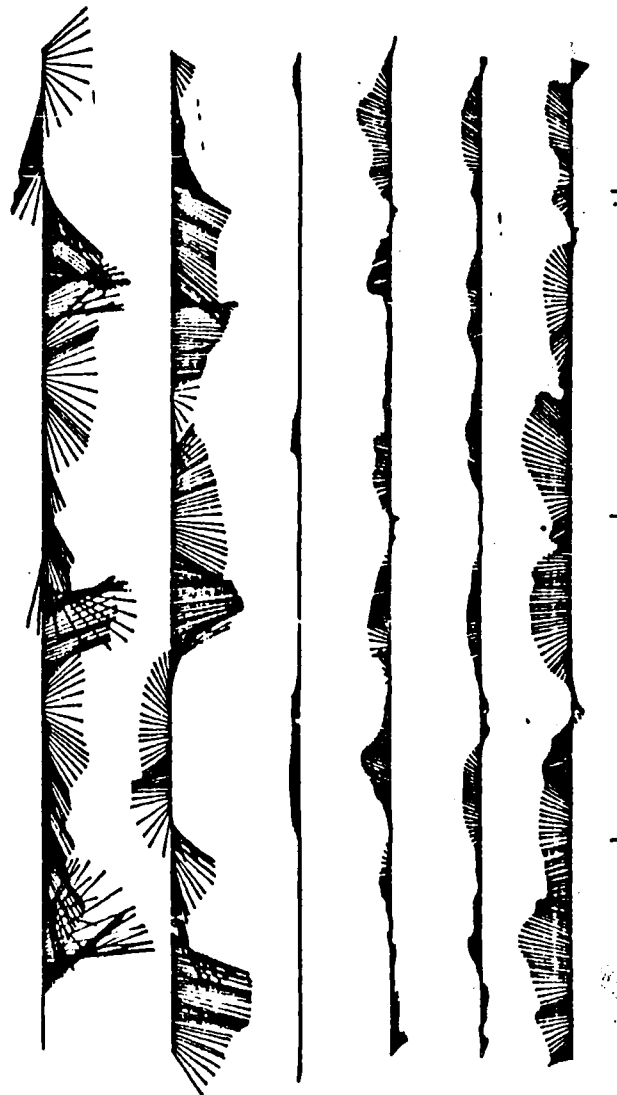
(A)

WIND
10 m/s



+10m
-3m
-18m
-33m
-45m
-58m

CURRENT
50 cm/s



12

13

14

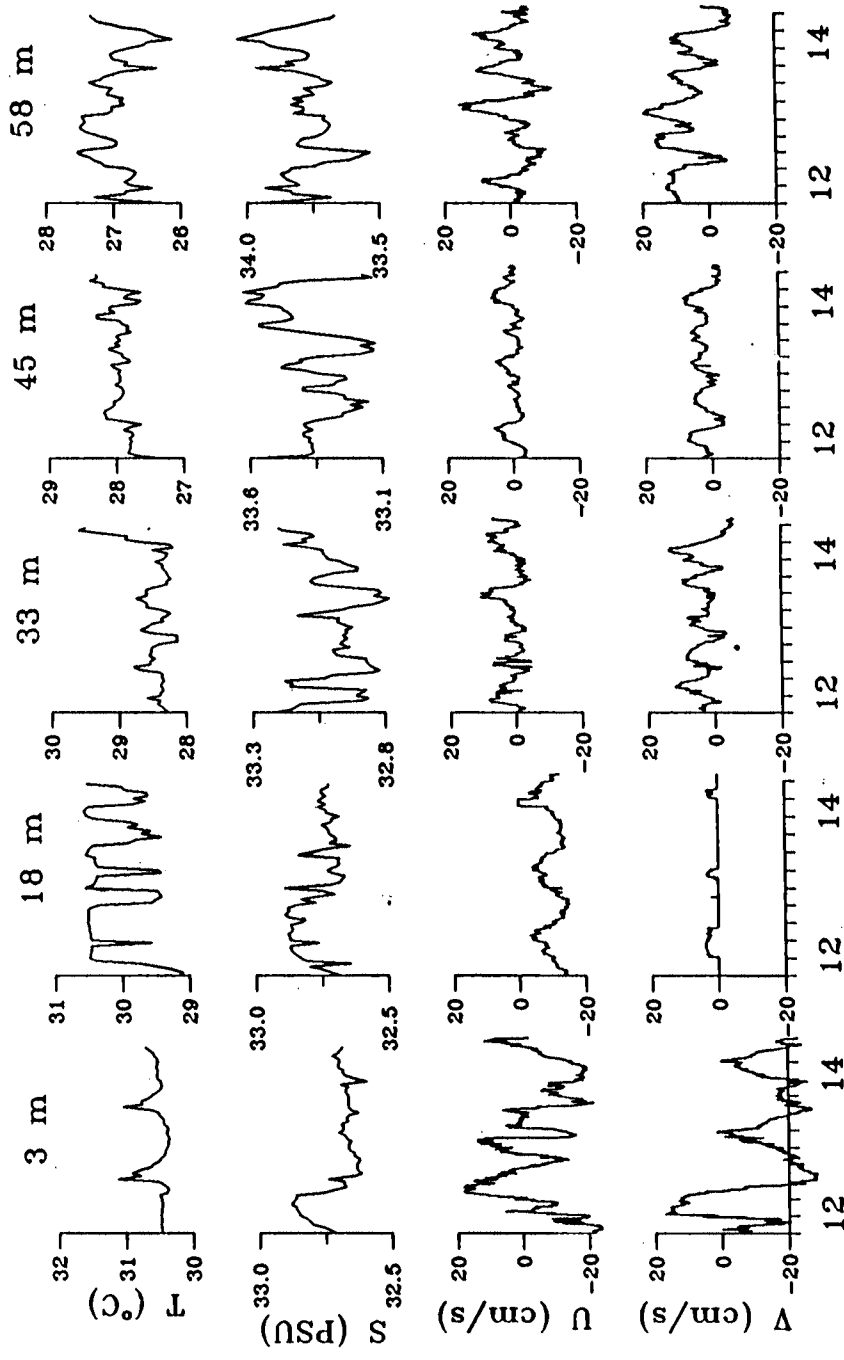
MAY 1987

Fig. 5.6A. Vectorially averaged surface wind and subsurface currents.

Fig. 5.6B. Stick plots of surface winds and subsurface currents

During most of the observational period, the surface current (at 3 m) oscillated between south-southeast and south-southwest with peak speeds around 30 cm/s. Although the winds at surface and currents at 3 m depth fluctuated nearly at diurnal and semi-diurnal tidal periods, they were mostly in phase. The currents at 18 m were not the weakest as they seem to be. Since the flow was mostly towards west, the vectors merged with the time axis. Strangely, the flow at the deepest level (at 58 m) was stronger at all the time due to unknown reasons (peak speeds 25 cm/s against 10 cm/s at 45 m and 15 cm/s at 33 m). A common feature among the currents at this site was that their speeds showed a modulation in response to the local internal tides.

Time series plots of temperature (T), salinity (S), east-west component (U) and north-south component (V) at different levels are given in Fig. 5.7 to examine the interrelationship between them. Since the temperature and salinity sensors of current meters had not worked at certain levels, those parameters sampled using MICOM STDV at hourly interval were considered here. The U and V components sampled at 5 min interval were averaged at hourly interval and presented to make compatible with T and S. At 3 m, the dominant oscillations were at semidiurnal periodicity in U and at diurnal periodicity in V. But T was mainly following diurnal heating/cooling cycle only. No particular periodicity was observed in the variability of S. At 18 m, variations in U and V components were mainly at diurnal periodicity with greater amplitude in U. The observed distribution of V at 18 m depth is quite intriguing. Maximum amplitude in the variability of T ($\approx 1.5^{\circ}\text{C}$) was observed at this level (at semidiurnal periodicity) due to the higher density



MAY 1987

Fig. 5.7. Time series of temperature (T), salinity (S) and east-west (U) and north-south (V) components of currents.

stratification between the mixed layer and thermocline. Correlation between currents, T and S were weak from the picture at 3 and 18 m levels. Contrary to the upper two levels (3 and 18 m), the deeper levels exhibited a close relationship between the variability in all the parameters. The most prominent oscillations were at semidiurnal periodicity and also they were in phase each other. However, T showed an inverse relationship with S, U and V. This implied that along with the northerly to easterly currents, the salinity increased and temperature decreased. Since the warmer water was found south of this observational site (Fig 5.1), the decrease in temperature with the increase of V was against the expectations of an increase in T with V. This prompted to believe that the only vertical oscillations due to internal tides were responsible for the decrease in temperature in the thermocline as seen from Fig. 5.5A.

5.3.2.1. Power Spectra: -

The power spectra were computed and presented in Fig. 5.8 to delineate the embedded periodic oscillations in the currents. For the spectral computations, 1024 points at 5 min. interval were used. All the major frequencies were marked at the respective peaks in hours also. Since the actually observed data length was not sufficient, zeroes were padded for deficient number of data points at the beginning and at the end of the zero centred series. As it was noticed from the time series plots (Figs. 5.5A and 5.7), semidiurnal tides were the most occurring periodic oscillations in the spectra of all the parameters. This showed the dominance of semi-diurnal tides at the observational area which is in agreement with the observations reported and discussed in

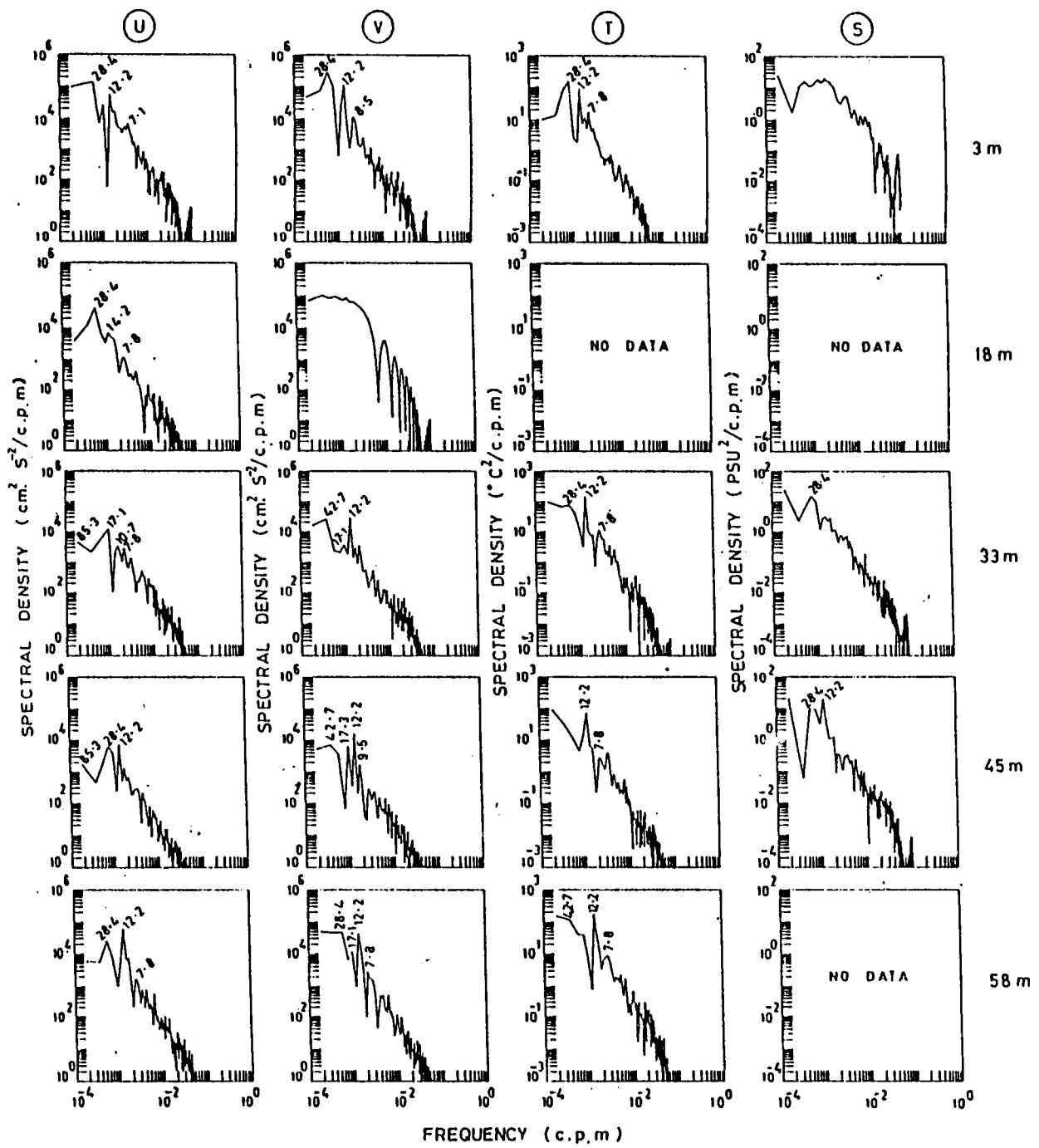


Fig. 5.8. Spectra of temperature (T), salinity (S), and east-west (U) and north-south (V) components of currents.

Chapters III, IV and V. The other most frequently occurring harmonic was 28.4 h. This might be due to the diurnal wave of 24 h periodicity. Since the resolving periodicity on both sides of 24 h are 21.3 h and 28.4 h, 24 h periodicity reflects either in 28.4 h or 21.3 h only. The diurnal heat wave was dominating over the semi-diurnal tidal oscillation in temperature at 3 m. But the heating effect had considerably decreased at 33 m and was absent at the other lower depths. The shape of all the spectra were more or less similar except those of 'S' at 3 m and 'V' at 18 m. This indicates that the causative factors for the periodic oscillations of these factors were different compared to those of the other parameters at other levels. The variability in S might have been aperiodic as it was revealed from time series plot (Fig. 5.7). The currents at 18 m came under the shearing zone (Fig. 5.6) of southerly flow near the surface (3 m) and northerly flow at 33 m depths. So the opposing flow in the meridional direction at either levels might have influenced and dampened the natural frequencies at 18 m resulting in a different shape of spectra.

5.3.2.2. Mixing Characteristics of the water column:-

Hourly temperature and salinity data collected by MICOM STDV and vectorially averaged current data at hourly intervals were used to make time series (Fig. 5.9) of Richardson Number (Ri), Brunt Vaisala Frequency (N) and vertical shear (SR) for different layers. The N widely fluctuated between 0 and 9 c.p.h. in the upper slab (3 to 18 m). But the range of variation was less (~5 c.p.h) in the middle and bottom layers where the values were always higher than 8 c.p.h.. The higher fluctuation in the surface layers

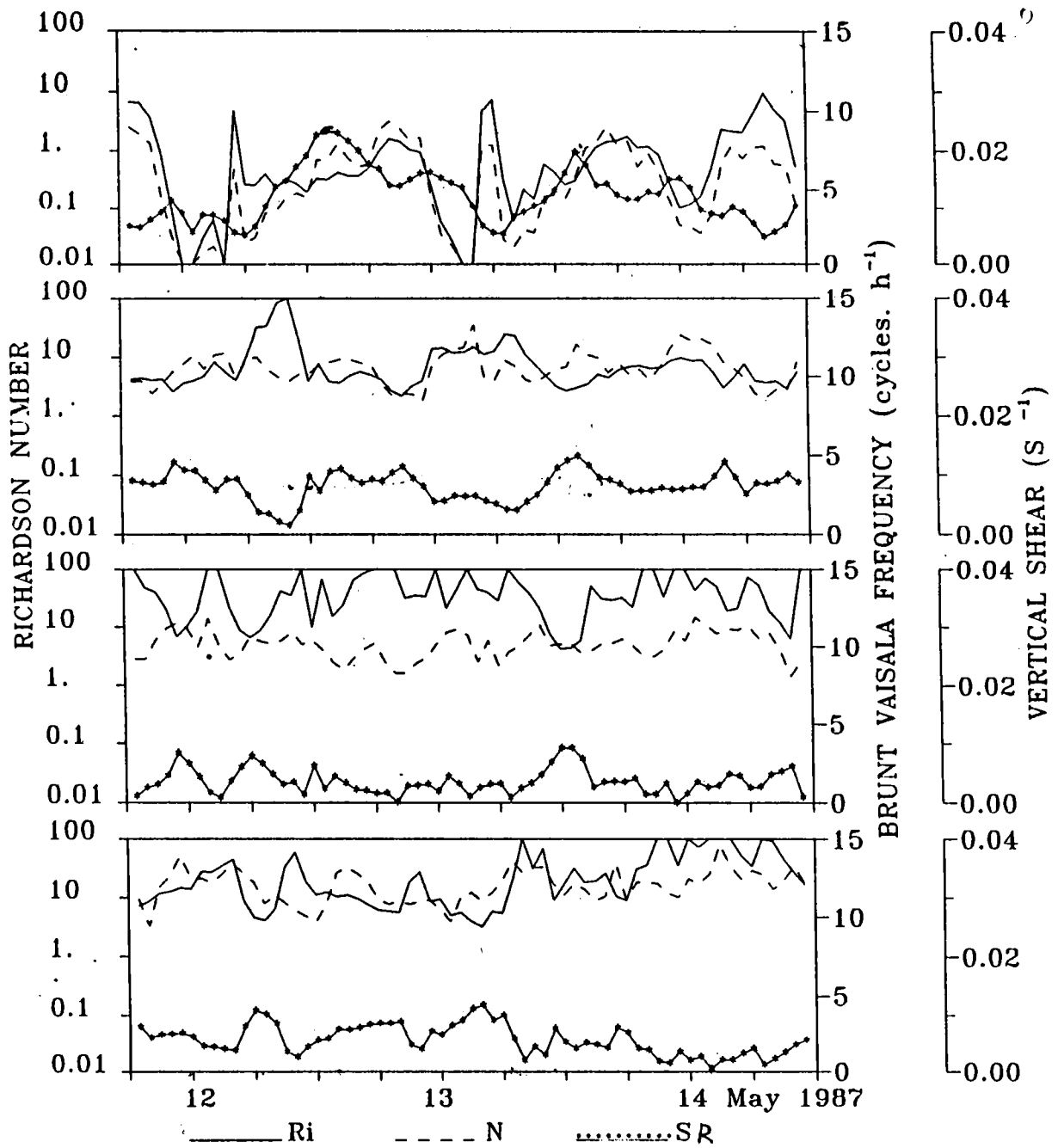


Fig. 5.9. Time series of Richardson number (Ri), Brunt Vaisala Frequency (N) and vertical current shear (SR).

was due to the oscillation of the pycnocline at the interface of the mixed layer and pycnocline. The SR was relatively higher (0.005 to 0.02 S^{-1}) in the upper slab compared to that of below layer slabs (0 to 0.01 S^{-1}). The relative importance of N and SR on Ri are discussed below. The Ri fell below 0.25 on three occasions which was conducive for instability in the upper slab. The lowest Ri occurred at night on all days when N was small. This observation proved that the instability in the upper slab had occurred due to very weak vertical density gradient during night followed by a deeper mixed layer. It is interesting to note that the deepening of mixed layer had occurred due to the intrusion of warmer water between 10 and 25 m and the disappearance of diurnal thermocline within the upper 10 m (Fig 5.4 and 5.5A). This feature is contrary to that of the other oceanic regions where the deepening of MLD during night is generally only due to cooling in the mixed layer. At this stage, it is useful to refer Fig. 5.7 again. Only diurnal component was most prominent in V component at 3 m and in U and V components at 18 m. Also the period of occurrence of the higher peaks in them coincided with the spells of instability in the upper slab. This proved that during the night time, the northerly currents were primarily responsible for the maintenance of higher temperature ($>30.5^{\circ}C$) at the upper slab. This inference was in agreement with the general distribution of temperature (Fig. 5.1) in which warmer water was observed in the southern region. Thus it can be concluded that in the upper 25 m, horizontal flow at diurnal periodicity was one of the major factors controlling the thermal and mixed layer characteristics. However, this inference is against that of in the thermocline (Fig. 5.5A)

where the vertical oscillations of semi-diurnal periodicity were found as the controlling factor. Thus it has proved the relative influence of horizontal currents and vertical oscillation of internal tide on the variability of the thermal field in the mixed layer and thermocline respectively. The Ri at the other 3 slabs (18-33, 33-45 and 45-58) was always higher than the critical value which showed stable layers throughout the observational period.

5.3.2.3. Simulation of the mixed layer characteristics:-

Simulation of the mixed layer characteristics (Fig. 5.10) was done following the methodology used in the Chapter V. Values of m_1 and m_2 in NK were found more appropriate when they were 0.39 and 0 respectively (a combination from Davis et al., 1981). The best simulation with KTDM was obtained when the value of ' γ ' and m was assigned 0.00085 and 0.009 respectively. The observed MLD fluctuated in a wide range between 5 and 25 m. The shallowest MLD occurred in the afternoon due to heating whereas the deepest MLD occurred during night time due to the intrusion of warmer waters at the subsurface layers (5.3.2.2). Time series of MLD, showed the dominance of other oscillations also. But, the observed MLD showed only one dominant periodic oscillation of diurnal heating/cooling cycle. The shoaling and heating events were simulated reasonably well by both the models. But some improvement can be seen in the case of NK. The deepening events could not be simulated by both the models. However, the amplitude of diurnal heating cycle were better reproduced by the MDKT model. From Figs. 5.3, 5.4 and 5.5A, the response of the near surface layers to the net heat flux was clearly revealed. Therefore, the present models driven by net

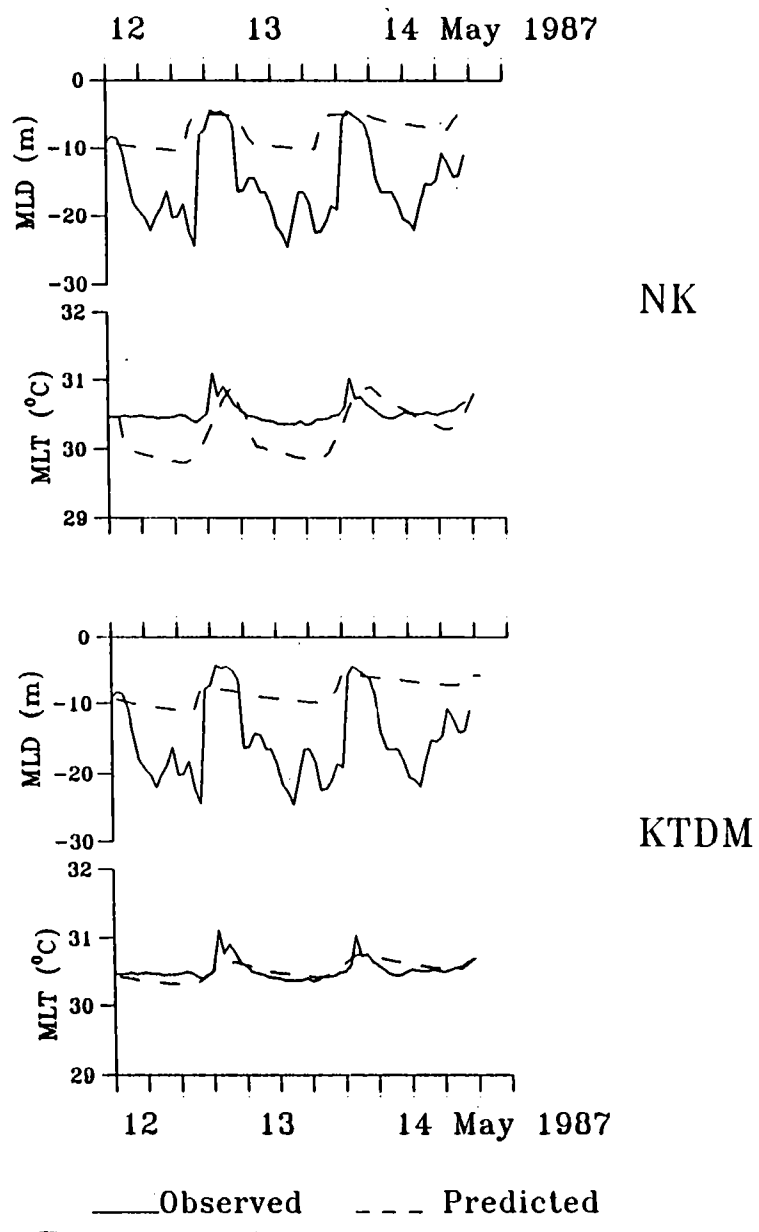


Fig. 5.10. Time series of mixed layer depth (MLD) and mixed layer temperature (MLT).

heat flux, performed well for the heating events. But it is seen from the Chapters IV and V that the parameterization for the solar absorption in the sea is better in NK than that of KTDM. Hence the simulated heating maxima were better with NK model. It is concluded in the section 5.3.2.2, that the deepening event had occurred due to the intrusion of warmer water during night time at diurnal periodicity at the subsurface layer (between 10 and 25 m). This process is not incorporated in the present models. Consequently wider departure between the observed and predicted values is noticed. The intrusion of warmer water maintained comparatively higher temperature during night time also. Therefore, it is to be expected simulated temperatures with the one dimensional models would be warmer. Considering this fact, NK seems to be more acceptable model eventhough the KTDM produced better matching during the cooling regime between the predicted and observed MLT. In short, this study also necessitates a comprehensive study of internal processes around Andaman Sea, as it is seen in Chapter V.

CHAPTER VI

THE HYDROGRAPHIC OBSERVATIONS ON THE WESTERN BOUNDARY
CURRENT OF THE BAY OF BENGAL DURING MARCH 1993

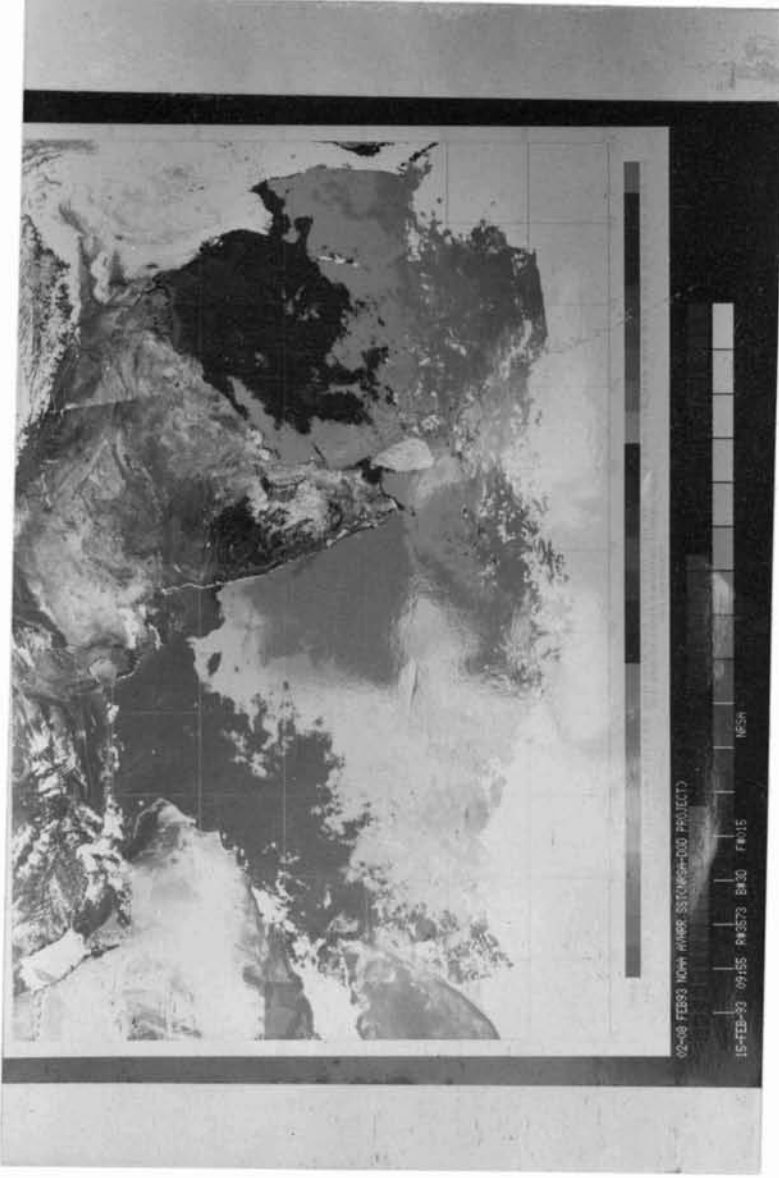


Fig. 6.0. SST of the north Indian Ocean during the first week of February 1993 derived from the infra-red imageries of NOAA satellites. The core of the warm water in the western boundary of the Bay of Bengal suggests a narrow poleward flow.

6.1.Introduction

Western Boundary Currents (WBC) in the major oceans have always fascinated the oceanographers by virtue of their well developed and intense flow patterns and associated thermohaline structure. Though numerous studies were made on WBCs of the Atlantic, Pacific and south Indian Oceans, such studies are meagre for the north Indian Ocean where the surface flow reverses seasonally. However, few studies were made on the Somali Current (Bruce, 1973; Brown et al., 1980; Evans and Brown, 1981; Leetma et al., 1982; Swallow et al., 1983; etc.) in the western Arabian Sea. Recently, Legeckis (1987) established the possibility of a WBC in the Bay of Bengal (BBWBC) during February 1985 based on the satellite infra-red imageries. He showed some similarities between the Gulf Stream and the currents off the east coast of India. The cross stream dimensions of the distinct core of warm water and the wave like perturbations with trailing filaments of warm water in the Gulf Stream were comparable to those of BBWBC. The major difference he pointed out was the abrupt fall of sea surface temperature (SST) of BBWBC contrary to continuous warm core of Gulf Stream and its slow dissipation. Even few decades back, very strong northeasterly currents (speed: 150 to 350 cm/s) were reported (LaFond and Rao, 1956; Varadachari et al., 1968) at certain areas off the east coast of India in the northern Bay of Bengal during early southwest monsoon. But those currents were then not identified as part of the BBWBC. More observational evidence began to pile up from the subsequent studies on BBWBC (Cutler and Swallow, 1984; Shcherbinin et al., 1979; Murty et al., 1993; Shetye et al., 1993). From the ship drift data in the

western Bay of Bengal, Cutler and Swallow (1984) showed, the occurrence of a clockwise gyre during February to July and anticlockwise gyre in the rest of the year with short transition periods in between these two circulation regimes. The BBWBC is viewed as the western rim of this clockwise gyre. The life cycle of the BBWBC can be inferred from Cutler and Swallow (1984) as follows. The BBWBC begins to form by February north of 8°N , strengthens upto May, weakens further and disappears by August. The temporal evolution of the BBWBC was reproduced by some numerical models driven by climatological surface winds (Potemra et al., 1991; and McCreary et al., 1993). However, the results of numerical models show that the BBWBC begins to form much early ie. by December/January itself which is found to be more reasonable by Shetye et al. (1993). McCreary et al. (1993) showed that by January the current reverses first at north of 15°N from southwesterly to northeasterly. This current extends all along the east coast of India and forms into well developed BBWBC by March/April and decays by June/July (Shetye et al., 1993; McCreary et al., 1993). Plausible forcing functions that cause the formation of the BBWBC are discussed at length in some of the recent works (Potemra et al., 1991; Yu et al., 1991; Johns and Ali, 1992; McCreary et al., 1993; Shetye et al., 1993). In this paper, the features of the circulation off the east coast of India during March 1993 are brought out from the observed thermohaline structure and estimated geostrophic flow patterns.

6.2.Data

FORV Sagar Sampada occupied 56 stations (Fig. 6.1) off

the east coast of India from 9 to 23 March 1993 (with a two day break in between for a port call at Madras) to collect data on thermohaline structure of the BBWBC. The stations were planned based on the available infra-red imagery of SST obtained from NOAA satellites during the first week of February 1993. These imageries had clearly shown a core of warm waters flowing parallel to the east coast of India (Fig. 6.0). At these stations, vertical profiles of temperature and salinity were measured upto 500 m depth/bottom using MICOM STD of TSK, Japan (accuracy of temperature is 0.05°C ; salinity is 0.03 PSU and depth is 1 % of the depth scale) at half degree interval along the zonal transects, spaced at one degree latitudinal interval between 11°N and 18°N (ie. from sections 1 to 8 of Fig. 6.1). But along sections 7 and 8, nearer to the coast, the stations were fixed at $15'$ interval to resolve the observed narrow warm core patches in the satellite infra-red imageries.

In addition, this study is also supplemented with the temperature and salinity data collected upto 500 m depth along 14°N at every 1° interval between 81° and 92°E using MICOM STDV (TSK, Japan. Accuracies of temperature 0.05°C ; salinity 0.03 PSU and depth 1% of the full scale) during the cruise of RV Gaveshani in May 1987.

6.3. Results

6.3.1. General hydrography

One of the major factors controlling the thermohaline modifications is the oceanic circulation. Therefore in this section, both the vertical and horizontal fields of temperature and salinity are utilized to describe the three

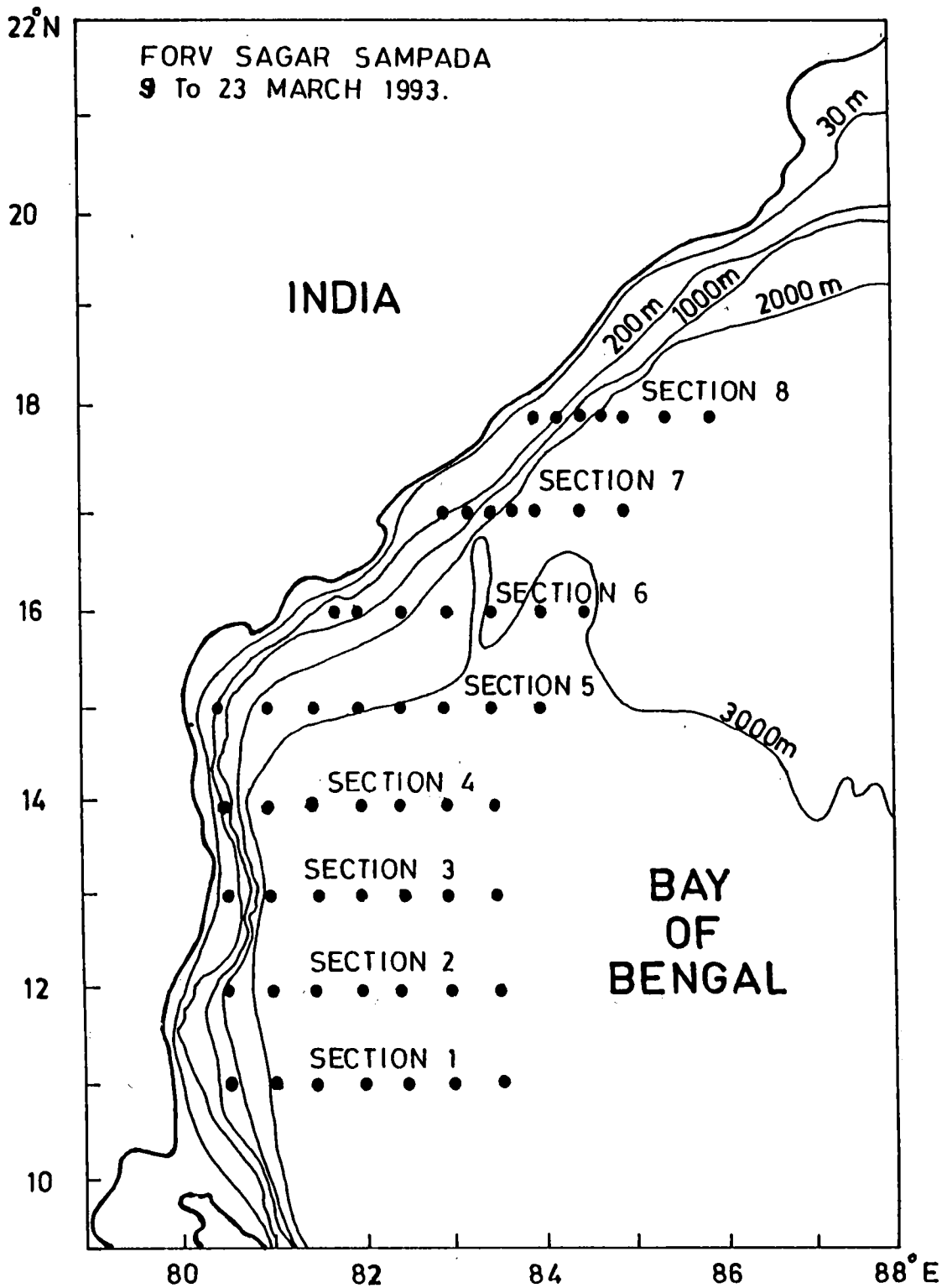


Fig. 6.1. Stations covered during March 1993 along the sections 1 (11°N) to 8 (18°N) at 1° interval.

dimensional structure of the BBWBC.

The SST (5 m depth) from MICOM STD and NOAA satellites (weekly averaged during the period from 15 to 22 March 1993) are presented (Fig. 6.2a and b) to show the surface thermal structure of the current regime. However, Fig. 6.2a is not discussed here, because the range of the variation is within the expected diurnal changes ($\sim 0.5^{\circ}\text{C}$). In general, throughout the study area a decrease in temperature from coast to offshore and from south to north was observed (Fig. 6.2b). The SST varied between 27.4°C and 28.2°C . The warmest water ($>28.2^{\circ}\text{C}$) was found at the southwestern region and the coldest water ($<27.4^{\circ}\text{C}$) was found at the eastern region north of 14°N as a cold core tongue. The surface salinity distribution (Fig. 6.2c) also showed a low saline tongue (hatched area, salinity < 32.8 PSU) offshore following the cold core between 14°N and 17°N . The appearance of cold and low saline waters north of 14°N suggests a westerly to southwesterly flow in the offshore region originating from the head of the Bay which matches with the derived flow from the climatological winds (Potemra et al., 1991; Shetye et al., 1993) and from satellite infrared imageries (Legeckis, 1987). This cold and low saline water might have been originated from the river discharges of the Ganges (Legeckis, 1987). As described in the SST distribution, salinity also increased towards the coast north of 14°N . Thus the Fig. 6.2b and c show warmer and saline waters near the coast north of 14°N as a manifestation of the BBWBC. But south of 14°N , surface waters are more saline. In general, north of 14°N , surface salinity decreased from 33.6 PSU to 32.8 PSU from south to north except near the coast.

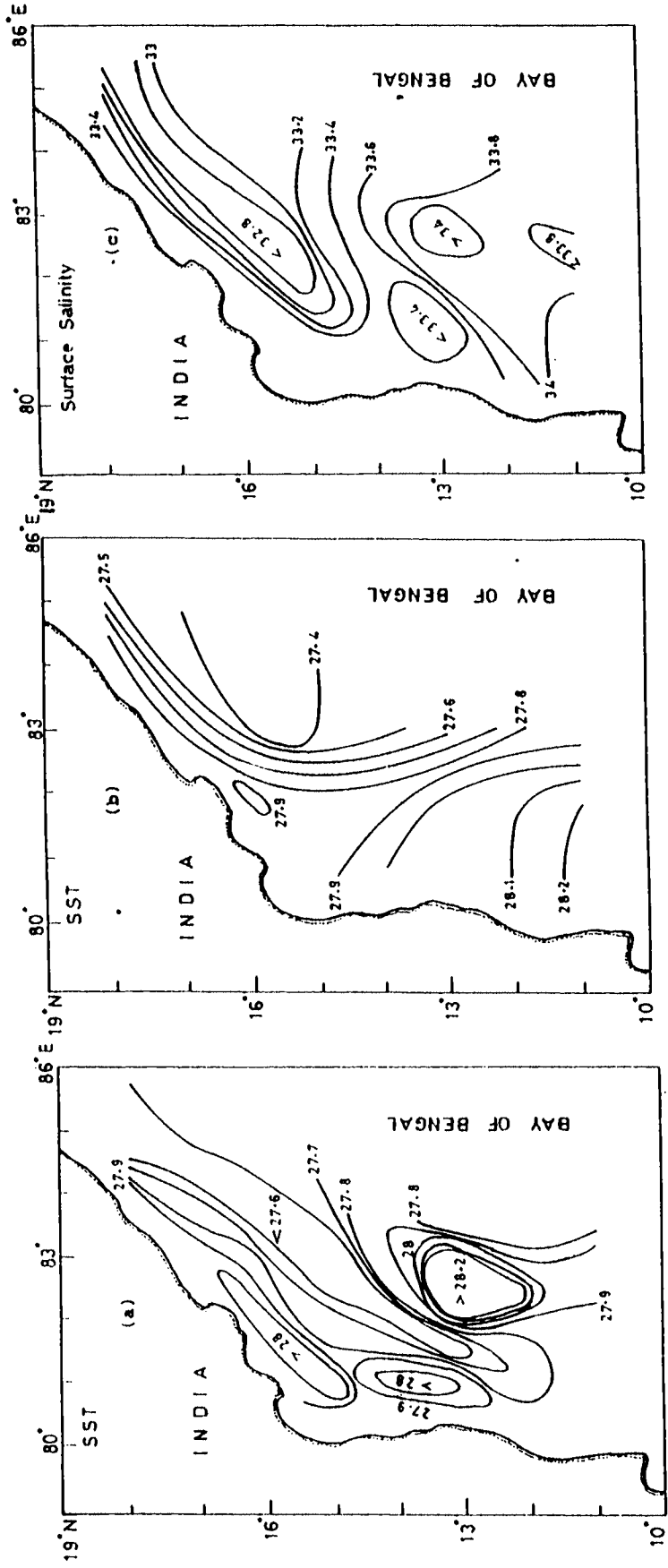


Fig.6.2.(a) The sea truth SST obtained from MICOM SID (9 - 23 March 1993)
 (b) Weekly averaged SST derived from the infrared imageries of NOAA satellites (15 - 22 March 1993)
 (c) surface (5m) salinity. Contour interval is 0.2 PSU (9 - 23 March 1993).

The meridional salinity gradient in the Bay is well known (Sastry et al., 1985; Sarma et al., 1988; Varkey and Sastry, 1992, etc.).

In general, the temperature of the near-surface layer was around 27°C with occasional appearance of warmer pockets ($>28^{\circ}\text{C}$) due to diurnal heating (Fig. 6.3). Thermocline depth increased offshore and was deeper (>50 m) at southern and northern regions (sections 1,2,7 and 8); whereas it was shallower (<50 m) in the middle region (sections 3 to 6). The isotherms exhibit a downward slope (more prominently in the deeper layers below 100 m) from the coast to 82.5°E and thereafter an upward slope towards offshore at sections 1 and 2. These slopes indicate a northerly flow westward of 82.5°E and a southerly flow on the eastward of 82.5°E . A dome shaped formation in the isotherms was noticed near the coast at sections 3 and 4 throughout the water column which indicated the presence of a cyclonic eddy of diameter ≈ 200 km. The downward sloping of the isotherms from the coast in the upper 150 m along section 7 and in the entire water column along section 8, indicates a northerly flow. An interesting feature along section 7 was a dip in the isotherms below 250 m around 83.5°E . This showed a strong convergence zone probably resulted from opposing currents with relatively stronger northerly flow near to the coast below 250 m across section 7.

The salinity sections (Fig. 6.4) showed increased dilution in the upper layers towards north due to the river discharges in the head of the Bay. As noticed in the temperature sections, the isohalines also showed offshore downslope with greater magnitude towards the northern Bay.

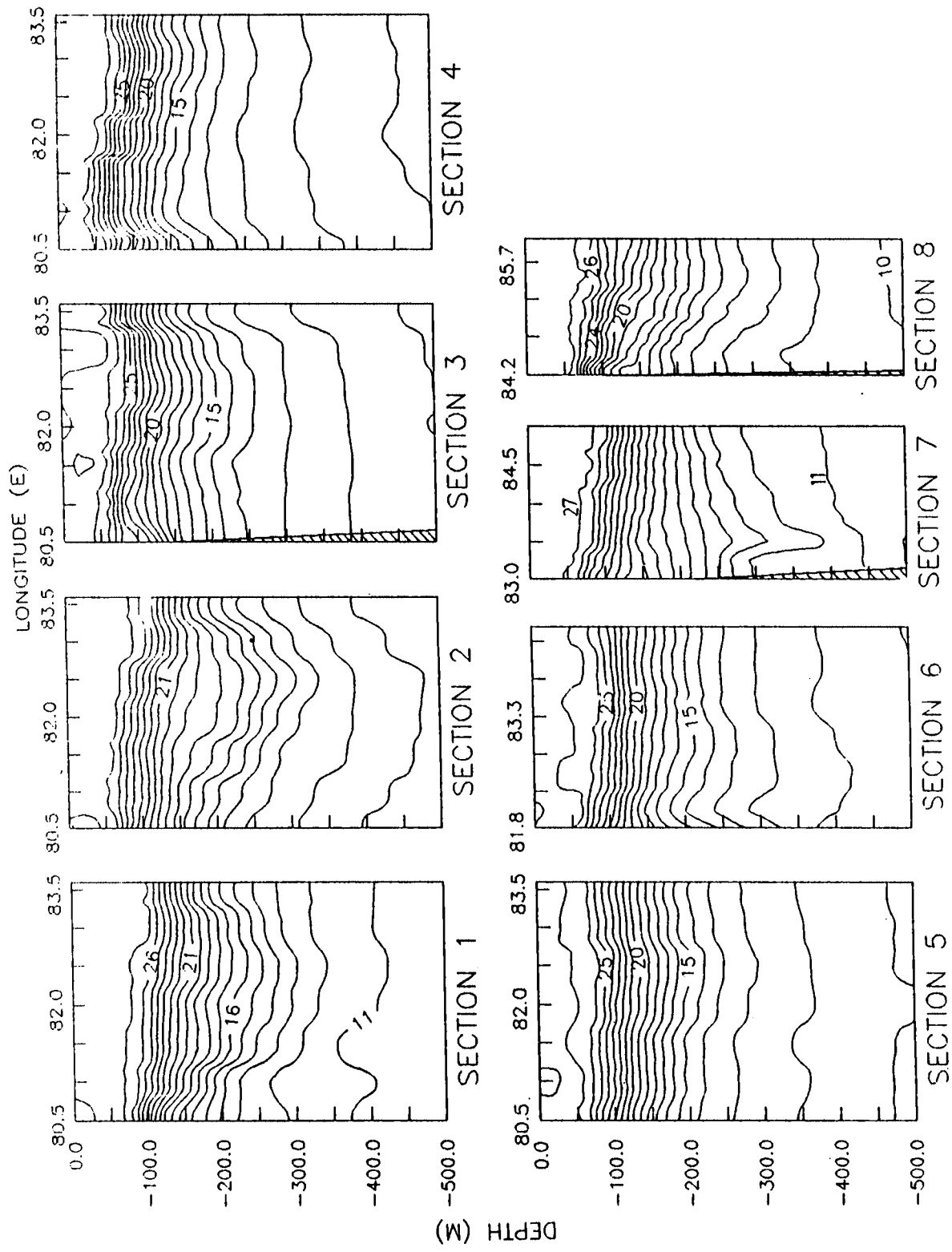


Fig. 6.3. Vertical sections of temperature along sections 1 to 8. Contour interval is 1°C.

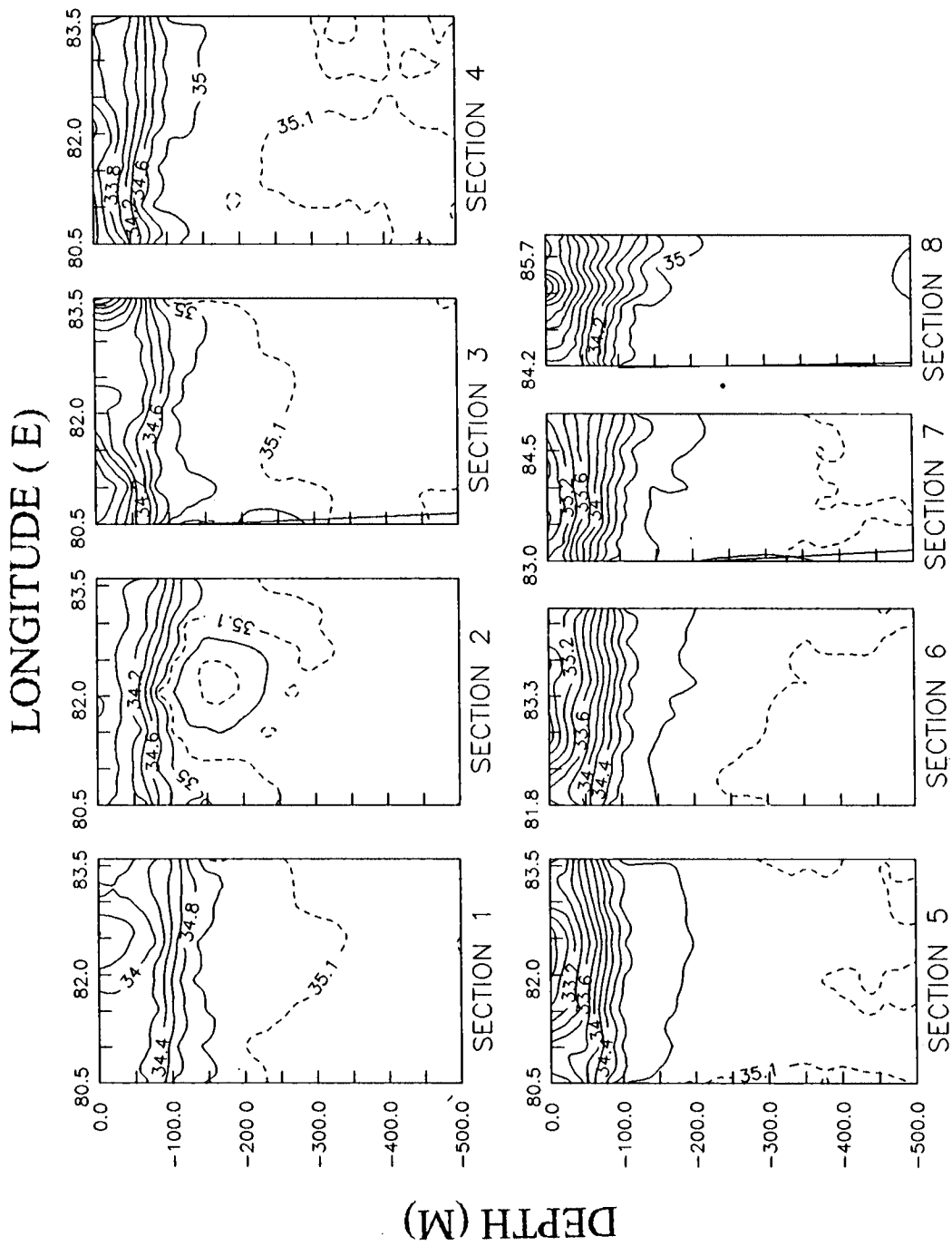


Fig. 6.4. Vertical sections of salinity along sections 1 to 8. Contour interval is 0.2 PSU. Broken lines represent 0.1 PSU contour interval.

Such a variable gradient would suggest the importance of salinity on the strength of the BBWBC of this region. Another notable feature is the appearance of a high salinity core (>35.2 PSU; hatched area) between 100 m and 250 m depths at section 2 around 82.5°E where the corresponding thermal structure also showed a diffused thermocline.

6.3.2. Geostrophic circulation:-

Dynamic topography charts for various levels viz. surface (5db), 100 and 200 db relative to 500 db are presented to describe the flow characteristics (Fig. 6.5a to c). Since the readings of initial few metres of MICOM STD are not reliable, data at 5 db is considered for the surface level.

During the observational period, the surface circulation in the western Bay between 11°N and 18°N (Fig. 6.5a) is characterized by few embedded eddy type cells. The closed contours of dynamic topography between 13°N and 15°N nearer to the coast, suggest the presence of a cyclonic eddy of diameter $\simeq 200$ km which can also be seen in Fig. 6.3 (section 4). South of 13°N , the circulation appears to be the part of an anticyclonic eddy with its northerly flow west of 83°E . The speed of this northerly flow was $\simeq 40$ cm/s which is in close agreement with the ship drift data of Cutler and Swallow (1984). The poleward flow was very weak and meandering between 13°N and 15°N due to the presence of cyclonic shear. The northeasterly flow north of 15°N showed the highest speed (>90 cm/s) within a narrow cross stream dimension of 30 km (revealed by the crowding of isolines). The vertical extent of this intense flow in deeper layers can

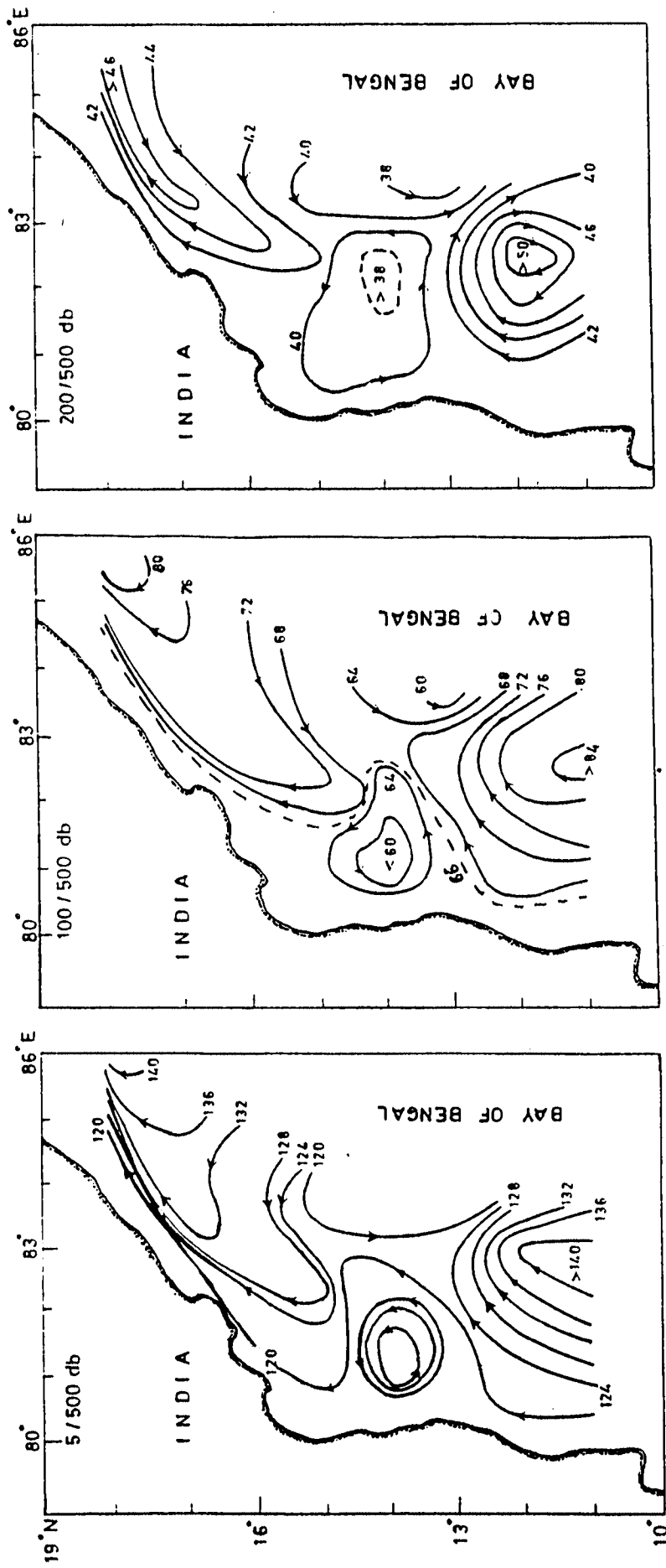


Fig. 6.5. Dynamic topography charts relative to 500 db at (a) surface (5 db), (b) 100 db and (c) 200 db. Please note the change in the contour interval at 200 db.

be traced even upto 500 m depth from the concave shape of the isotherms at sections 6, 7 and 8 (Fig. 6.3). This poleward flow can be regarded as the BBWBC during March 1993. The southerly flow observed east of 83°E between 11°N and 15°N may be viewed as a segment of an independent flow.

Although the flow pattern at 100 db level (Fig. 6.5b) resembled the surface circulation, strength of the flow reduced considerably at this level. The cyclonic eddy near the coast was found distorted. An important feature at 200 db level (Fig. 6.5c), was that the anticyclonic eddy at the southern region which was elliptical in the upper layers, became nearly circular. The cyclonic eddy at 14°N and 81.5°E was distorted more due to the influence of peripheral circulations and became weak. The overall current speed at this level reduced by 50 % when compared to those at 100 db.

6.3.3. Geostrophic volume transport:-

Depth integrated geostrophic volume transport across each latitude from 11°N to 18°N is shown in Fig. 6.6. Northward transport (positive values) was >12 Sv (Sv - Sverdrup) south of 12°N while it was between 3 and 9 Sv north of 13°N . Southward transport (negative values) is nearly zero north of 15°N . Between 13° and 14°N , the southward transport near the coast has resulted from the southward component of the cyclonic eddy observed there. Maximum values of the southward transport were observed (6 to 9 Sv) south of 13°N at the eastern side of the observational area which was mainly due to the southerly flow associated with the anticyclonic eddy there. The northward transport across 12°N in the present study (12 Sv) shows a good agreement with the

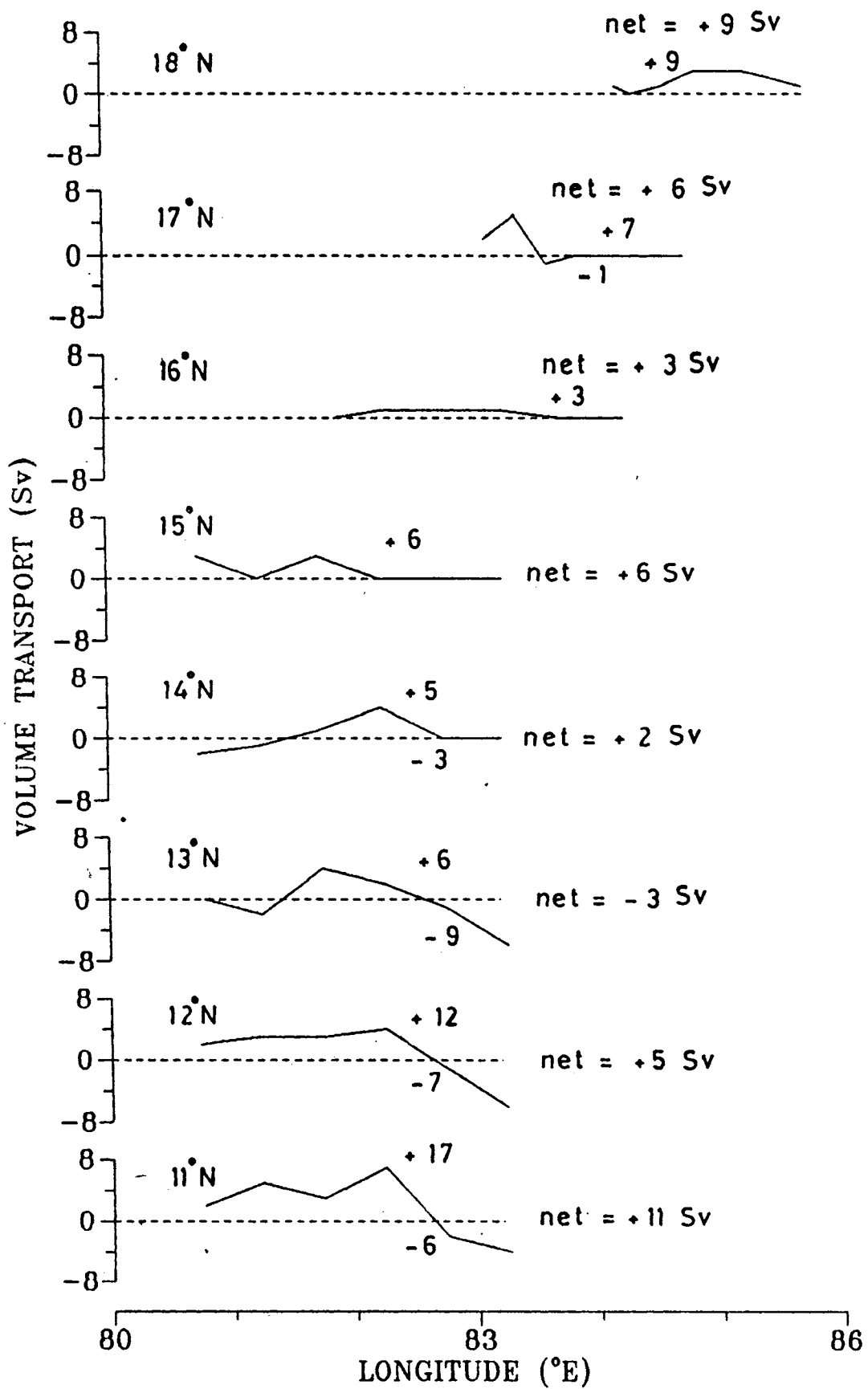


Fig. 6.6. Geostrophic volume transport across the sections 1 to 8

observations of Murty et al. (1993) during April 1987.

6.3.4. TS characteristics:-

The TS characteristics for four regions are shown in Fig. 6.7a to d. The regions are categorized on the basis of surface flow pattern and salinity distribution. Since it is assumed that a branch of south equatorial current joins the BBWBC in the southern Bay (Cutler and Swallow, 1984), a different TS characteristics can be expected in this poleward flow region. Therefore the area is divided into two regions - one as the region of poleward current and the other as the region outside the poleward current. But from the salinity distribution, it is quite evident that north of 15°N the surface salinity is very much dominated with low saline waters and thus clearly shows two distinct modes - north of 15°N and south of 14°N . Combining the above factors, four regions are identified viz. (i) region I (poleward current region south of 14°N) (ii) region II (outside the poleward current region south of 14°N) (iii) region III (poleward current region north of 15°N) and (iv) region IV (outside the poleward current region north of 15°N).

A salinity minimum 'A' and maximum 'E' were common at all the four regions. The lowest salinities (< 33 PSU) were observed in the regions III and IV (Fig 6.7c and d). Another salinity minimum 'B' has appeared in the region IV. Two prominent maxima 'C' and 'D' were noticed in the region I (Fig. 6.7a). These maxima were not very prominent in the other regions. However, the presence of salinity maximum 'C' has weakly appeared in region II (Fig. 6.7b) where one of the branches of poleward current turned to equatorward current.

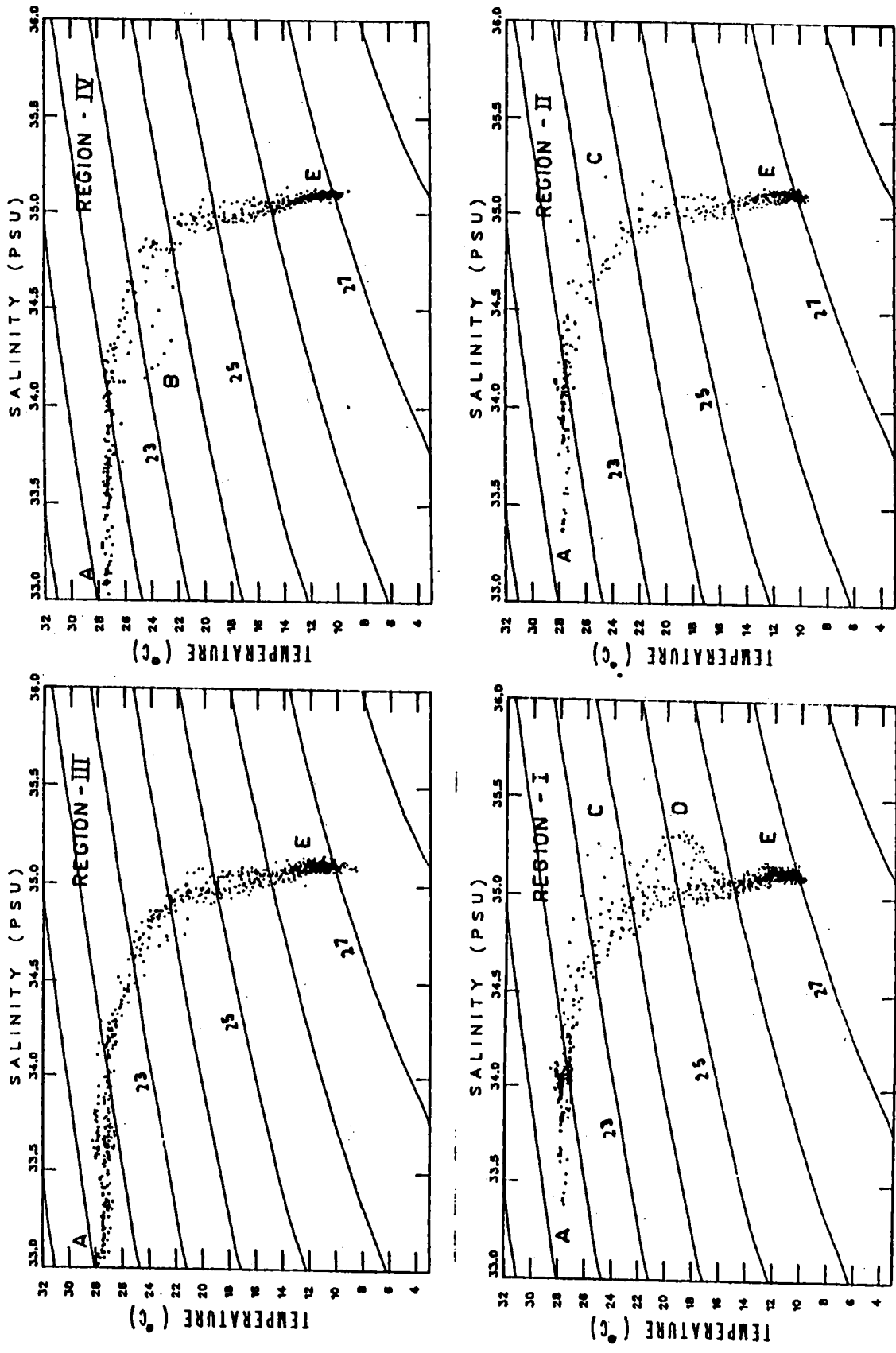


Fig. 6.7. TS diagrams for (a) region I, (b) region II, (c) region III and (d) region IV.

In fact, all the three maxima (including 'C' and 'E') were most prominent at 12°N and 82°E. Therefore the corresponding temperature and salinity profiles are given in Fig. 6.8 to elucidate these maxima. Modifications on the temperature profile due to the presence of 'D' and 'E' were conspicuous from this figure. Watermass characteristics associated to all salinity minima/maxima points are summarised in table 6.1.

Table 6.1

Characteristics of watermasses at the salinity minima/maxima					
Salinity minima/maxima	temperature (°C)	salinity (PSU)	depth (m)	σ_t (CGS)	regions of occurrence
A	> 27	< 33.5	surface	<21.25	I, II, III, IV
B	22.95	34.28	120	23.42	IV
C	25.	35.25	90	23.55	I, II
D	19.21	35.3	170	25.24	I
E	12.88	35.11	>260	26.52	I, II, III, IV

The low saline watermass 'A' is well known in the Bay of Bengal due to the conspicuous dilution in the upper layers (Sastry et al., 1985; Levitus, 1986; Shetye, 1993). Similarly, the occurrence of high saline watermass 'E' between the depth 200 and 900 m is also well described earlier (Sastry et al., 1985; Premchand et al., 1986b; Murty

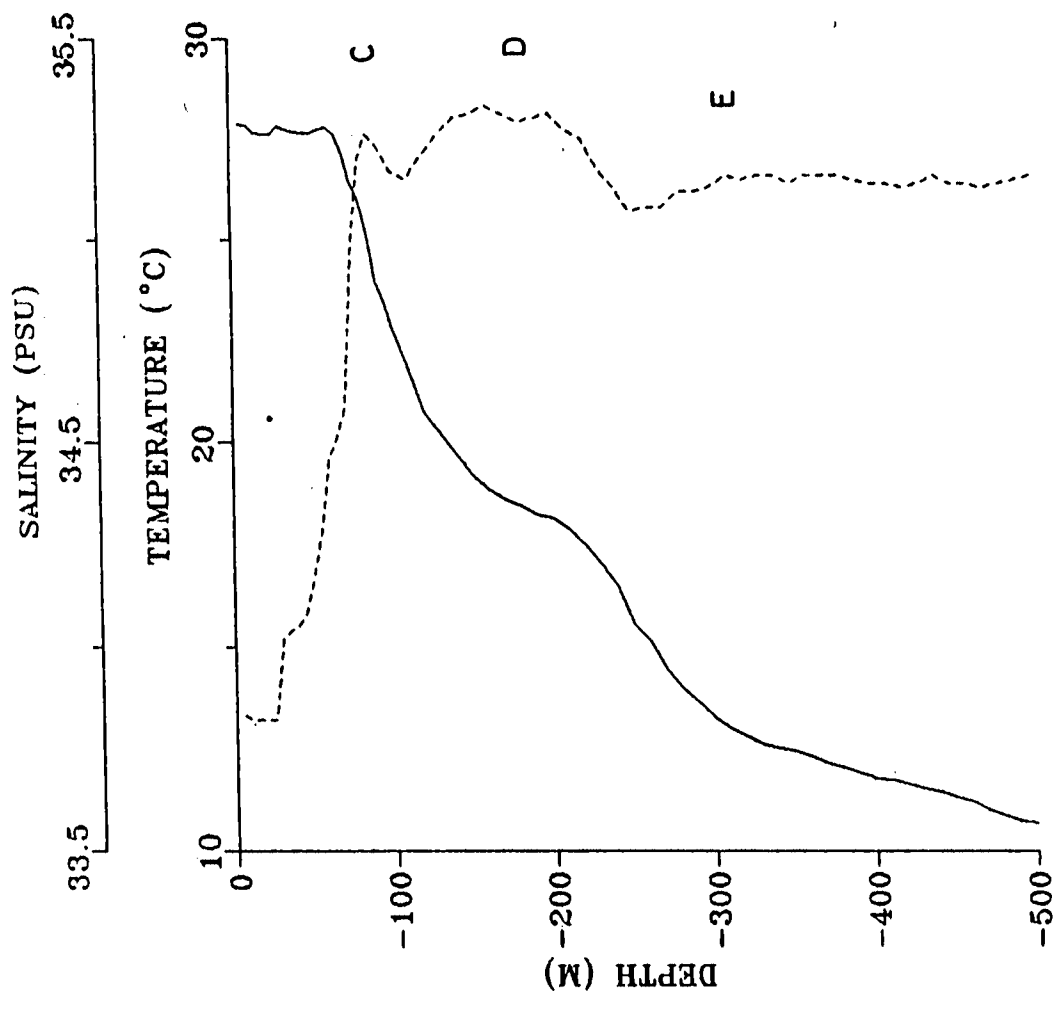


Fig. 6.8. Temperature and salinity profiles at 12°N and 82°E.

et al., 1992). This watermass is a combination of the Persian Gulf and Red Sea watermasses. The number of data points on the watermasses 'B', 'C' and 'D' are too inadequate for a detailed discussion.

6.3.5. Observations during May 1987 along 14°N:-

6.3.5.1. Temperature, salinity, $\sigma_{s,t,p}$ and meridional flow:-

The most conspicuous feature in temperature, salinity and $\sigma_{s,t,p}$ sections (Fig. 6.9) was the occurrence of a very sharp gradient between 82° and 84°E. Correspondingly the meridional geostrophic flow (relative to 500 db) showed maximum velocity (>80 cm/s) within a narrow cross stream dimension of 100 km. It is obvious from the temperature section that the influence of this strong current extended at least upto 500 m depth. However, the currents were very weaker, shallower and wider from 84°E to 92°E as seen in the subtropical gyres of the other oceans. Thus the sections (Fig. 6.9) showed the characteristics of a well developed WBC compared to those of March 1993.

The dome shaped temperature contours near the coast indicate the presence of a cyclonic eddy of diameter of about 200 km. The geographic location and dimensions of this eddy exactly coincided to the eddy observed during March 1993. The major difference noticed was its vertical extent. The May 1987 section showed much deeper extent (≈ 500 m) while March 1993 section showed only a shallower extent (≈ 100 m). Murty et al. (1993) also observed this eddy during March to June 1987. The consistency of the existence of this eddy during different months of the year suggests its quasi-permanent nature during the period of BBWBC. However, this eddy was

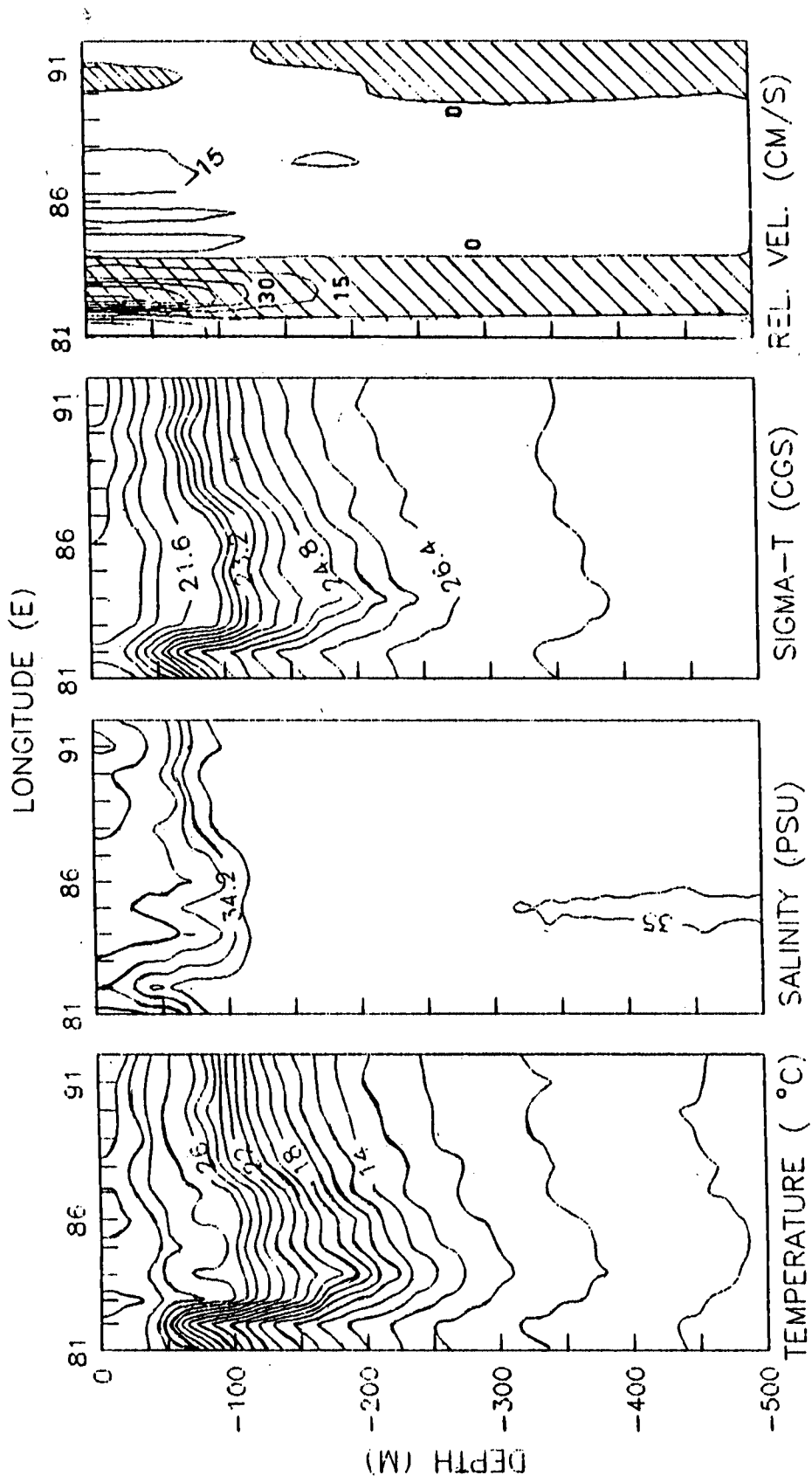


Fig. 6.9. Temperature, salinity, $\sigma_{t,p}$ and meridional flow along 14°N during May 1987.

found to be shifted to ~200 km northwards during March/April 1991 (Shetye et al., 1993). Therefore, year to year variability of the location of this eddy is also possible.

6.3.5.2. Geostrophic volume transport across 14° N:-

The volume transport in the region of BBWBC is 16 Sv whereas the total southward transport across the latitude is only 13 Sv (Fig. 6.10). This shows the remarkable flow associated with the BBWBC. During May 1987, geostrophic volume transport of BBWBC was considerably higher when compared to those of March 1993 (5 Sv).

6.4. Discussion

Recent numerical experiments (Potemra et al., 1991; Yu et al., 1991; Johns and Ali, 1992; McCreary et al., 1993) examined the possibilities of remote forcing on the formation of a WBC in the Bay of Bengal. Kelvin waves are found to be generated in the equator as the result of wind forcing along the equator (Potemra et al., 1991; Yu et al., 1991). These waves move eastward and reflect towards north along the eastern boundary of the Bay. While travelling northward, these coastal Kelvin waves generate long Rossby waves which propagate westward and cause the formation of the BBWBC during winter. This hypothesis of remote forcing from equatorial wave guide was tested by McCreary et al. (1993) using a 2.5 layer model and found it is not an important factor in the formation of the BBWBC. They suggested another forcing mechanism within the Bay itself to drive the poleward current off the east coast by January onwards. Northeast monsoon winds can generate upwelling favourable

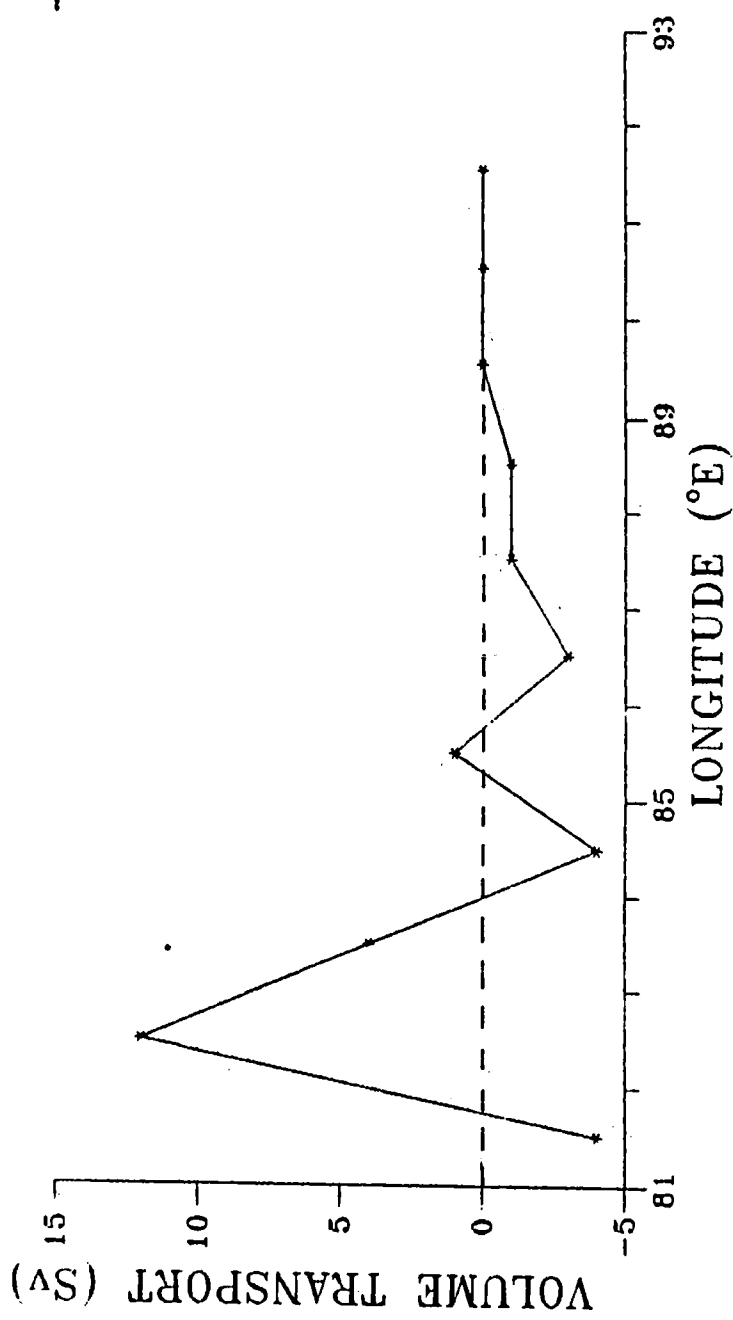


Fig. 6.10. Geostrophic volume transport across 14°N.

Kelvin waves along the northeastern corner of the Bay. When these waves reach at the east coast of India after travelling along the northern boundary of the Bay, they can support a poleward current off the east coast. This current appears first in the northern part of the Bay and extends towards south all along the coast within few months. By March, negative wind stress curl with in the Bay will also reinforce the process. However, Shetye et al. (1993) suggested the negative wind curl alone is sufficient to drive an anticyclonic sub-tropical gyre with in the Bay. The resultant current will appear all along the east coast north of 10°N by January itself and develops to full strength before April. Johns and Ali (1992) have carried out another numerical experiment by introducing a factor of northward flow at the southern open boundary (at the latitudes of Sri Lanka) along with the westward propagating Rossby waves generated within the Bay during the winter monsoon. This experiment showed that the BBWBC can be formed along the east coast of India on a 4 day time scale and the intermittency in the strength can occur according to the strength of the inflow across the southern boundary. The main lacuna is the lack of sufficient observational evidence to evaluate these model simulations.

In the present study, organised BBWBC was found only north of 15°N during March 1993. The poleward geostrophic volume transport also showed a progressive increase from 16°N to 18°N . This result prompts one to view that the BBWBC first forms at northern Bay and progresses equatorward as proposed by McCreary et al. (1993). According to their hypothesis, negative wind stress curl begins to intensify the BBWBC all along the east coast only during March. This may be the

reason for the inferred weak currents during this study (March) south of 15°N whereas north of 15°N the process might have already started (Kelvin wave propagation).

The boundary current inferred in the present study during 9 to 23 March 1993 differs in many respects from those of Shetye et al. (1993) during 14 March to 7 April 1991. The present study shows that the flow was weaker (< 40 cm/s) and shallower (upto 100 db only) south of 15°N whereas north of 15°N , the flow was stronger (> 90 cm/s) and deeper (upto 500 m). Contrary to the present observations, Shetye et al. (1993) found nearly uniform, faster (90 cm/s) and deeper BBWBC (extending beyond 200 m depth) all along the east coast of India. The anticyclonic cell north of 15°N during March 1993 is replaced by a steady northerly current spanning over the complete observational area between 15° and 18°N transects (Shetye et al., 1993). Another study by Murty et al. (1993) during March to June 1987 also showed more or less faster (90 cm/s), broader and nearly uniform surface flow throughout off the east coast of India similar to those of Shetye et al. (1993). During May 1987 (in the present study), along 14°N , the flow showed a pattern of an intense and well developed poleward BBWBC between 82°E and 84°E and a slower compensatory equatorward flow east of the boundary current. Also from the numerical study of McCreary et al. (1993), the life cycle of BBWBC was found to begin at the northwestern Bay by January, extending all along the coast in the succeeding few months and persists upto June/July. When all this information is put together, it is quite evident that the poleward, deeper, narrower and faster currents observed nearer the coast in the northern Bay and the slower, broader

and meandering currents in the southern Bay can be regarded as the formative stage of the BBWBC before the flow eventually builds up into a well developed BBWBC as seen in the later periods (Shetye et al., 1993; Murty et al., 1993).

All WBCs show an onshore "cold wall" and a haline front (shoreward drastic decrease in temperature and increase in salinity respectively). In certain regions of the Gulf Stream, 18°C drop in temperature and 2 PSU increase in salinity was noticed within 200 km from core of WBC. Though such prominent variations do not exist at surface levels in the present study, development of sloping up of isotherms and isohalines was noticed below mixed layer in sections 1, 2, 6, 7 and 8 (Figs. 6.3 and 6.4) where the poleward flow came closer and parallel to the coast. The poleward flow was stronger in the northern Bay as the slopes in the isolines were also more in the upper layers at sections 6, 7 and 8 compared to those of sections 1 and 2. Along sections 3 and 4, surface layers near the shore were dominated by the presence of the cyclonic eddy. However, at these sections the poleward flow was found offshore. Therefore the cold wall is expected in the onshore of the western edge of the poleward flow. A clear upward slope in the isolines associated with the poleward flow can be seen at 82°E in section 3 and 4 from the depths of surface mixed layer. In the study of Shetye et al. (1993) during March/April 1991, shoreward decrease of 2°C in temperature within 50 km appeared in the surface layers along 14°N followed by a salinity increase of 2 PSU as a result of the BBWBC. This result suggests that in the later stages of the BBWBC, onshore "cold wall" and haline front develop.

CHAPTER VII

SUMMARY AND CONCLUSIONS

The Bay of Bengal is unique among the world oceanic regions by virtue of its characteristic oceanographic features. However, certain features viz. short-term variability in the oceanographic parameters, oceanic conditions during the genesis of monsoon depressions, ephemeral Western Boundary Current system etc. are not adequately understood. Understanding such features has got utmost importance in several oceanographic applications. In the recent past considerable effort has been put forward to simulate the mixed layer characteristics at different parts of world oceanic regions using 1-dimensional numerical models. Such attempts lack for the Bay of Bengal. To understand all the above aspects, specific cruises were conducted and all the available relevant data sets were pooled up. The efficacy of the 1-dimensional numerical models KTDM (Kraus and Turner, 1967 - Denman, 1973 - Miller, 1976) and NK (Niiler, 1975 - Niiler and Kraus, 1977) were diagnostically analysed under the influence of the revealed oceanographic variability at four typical locations.

7.1. Thermohaline variability in the northern Bay of Bengal during the MONsoon Trough Boundary Layer EXperiment (MONTBLEX-90)

The short-term variability in the thermohaline structure of the upper layers of the northern Bay of Bengal during the period of MONTBLEX-90 is studied. The surface thermal structure showed the occurrence of intermittent distinct isolated mini warm pockets with temperatures in excess of 29°C , extending from surface to about 30m depth. These warm pockets showed an excellent coincidence with the formation of meteorological lows/depression over the head of the Bay of Bengal. Heat content with respect to 28.7°C

isotherm also exhibited a close correspondence with the formation of the meteorological disturbances. Whenever the heat content exceeded $0.4 \times 10^8 \text{ J/m}^2$, the ocean released energy and consequently low pressure systems formed.

In general, the signatures of the atmospheric disturbances were best noticed in the time series of surface pressure, wind direction, speed and sea surface temperature. The SST showed an inverse relationship with the surface pressure with an approximate time lag of two days. A broad correspondence between strengthening winds and lowering SST was also noticed during disturbed weather conditions. The insolation was mostly in excess of 200 W/m^2 with occasional reduction during disturbed days. The latent heat flux Q_E showed large variations between disturbed and undisturbed conditions. On the whole the ocean gained heat during the entire observational record with the only exceptions on disturbed days.

Spatial survey showed that the near surface thermal structure of the Bay was characterized by strong thermocline and eddy features. The depth-time sections of temperature and salinity fields also suggested the possibility of transient eddy circulation in the head of the Bay of Bengal. A great deal of small scale structure was noticed both in the temperature and salinity profiles during September 90 compared to August 90.

The two numerical models, KTDM and NK, broadly captured the observed features of the mixed layer variability. In the KTDM model the choice of the extinction coefficient ' γ ' was found to be quite sensitive in simulating the observed variability of the mixed layer thickness and temperature. On the other hand the model

response was less sensitive to the imposed variations of the mixing efficiency coefficient ' m_0 '. The performance of the NK model was found to be the better when large values of wind and shear mixing coefficients were replaced. This implies that the parametrization for the faster response to the mixing forces, helped for realistic simulation under intermittent calm and disturbed environmental conditions. The response to the faster environmental changes were found to be poor in KTDM. Shoaling events were also better simulated with the NK. In short, it can be concluded that the NK is more suitable for the northern Bay during summer monsoon season.

7.2. Salinity and Currents in the northern Bay of Bengal during the Summer Monsoon Experiments:-

Short term variability in the salinity and current fields of the upper layers of the northern Bay of Bengal at four locations is examined utilising the data sets collected during MONSOON-77 and MONEX-79 field experiments. Density in the upper layers was found controlled by salinity rather than the temperature. Large differences in the salinity field in the upper 100m were noticed within an area of 440 x 440 km². The upper layer salinity was relatively lower during M-77 compared to that of M-79, especially at northern location. At the northern location during M-77, rapid temporal variability of 8 PSU change within one week's time was also noticed. The influence of a heavy rainfall event was confined only to the topmost 20 - 30 m water column lasting for few hours. Strong vertical stratification which was variable in the northern Bay of Bengal appeared to be influenced by the upper ocean flow.

The flow regime during M-79 suggests the presence of a

clockwise eddy. However, such a feature was not noticed during M-77 when the monsoon was stronger. The flow weakened rapidly with depth during M-77 when the stratification was larger particularly at the northeastern sector of the polygon compared to such features during M-79. Relatively stronger flow was noticed throughout the top 200m water column at all locations during M-79. Evidence for Ekman balance in the current structure was rather weak suggesting the importance of baroclinic mode. The rotary spectra indicated that the energy levels were about an order higher in the clockwise spectra compared to those of anticlockwise spectra. This indicated the dominance of clockwise flow during both M-77 and M-79. The inertial, diurnal and semidiurnal frequencies were prominent in the clockwise spectra during M-77 and M-79. The inertial peak was insignificant in the anticlockwise spectra as inertial oscillations are known to be clockwise in the northern hemisphere. The spectral peaks at periods 128 hr in the clockwise spectra and 85 hr in the anticlockwise spectra during M-79 suggest approximately 3-5 day oscillations in the flow field.

7.3. Thermohaline and current variability off Visakhapatnam during summer monsoon season

A comparative study of thermohaline variability at a deep and shallow stations off Visakhapatnam during summer monsoon season is presented. Short-term variability in the current structure was also studied at the shallow station. Typical monsoon conditions like strong winds (>10 m/s), overcast sky etc. were observed during most of the observational period. Due to upwelling at the shallow

station, SST was always lower than dry bulb temperature (DB) and thus formed a condition for a stable overlying atmosphere. Following the overcast sky, peaks of net heat flux (Q) were less than 800 W/m^2 during most of the days. The thermal structure at both the stations revealed the importance of the internal tide.

The mean observed surface current agreed with the derived flow pattern of the earlier studies. The vertical current structure also qualitatively followed the Ekman spiral. Inter-relationship between the current and thermohaline field were found to be quite significant. From the spectral analysis, semi-diurnal tide was found as the dominant periodic oscillation embedded in the water column. Its influence on the mixing processes was also established from the stability computations.

Both the NK and KTDM models simulated the ML characteristics at the shallow station reasonably well whereas they poorly performed at the deep station. It is proved that one of the reasons for wide departure between the observed and simulated values at the shallow station was the spells of instability occurred due to internal tides.

7.4. Thermohaline and current variability off the Andaman Islands during pre-monsoon season

Short-term variability in the thermohaline and current structure at a station on the western side of the Andaman Island is studied. Temperature and salinity distributions around the Islands are also presented here. High SST ($>30.5^\circ\text{C}$) was observed around the Islands. On the western side of the Island group, temperature and salinity were found increasing from north to south at all depths.

At the stationary location, surface meteorological elements showed calm conditions during the observational period. The diurnal peaks of net heat flux (Q) and insolation (Q_I) were always >1050 and >1100 W/m^2 respectively. The influence of day time heating was reflected on the thermal profiles as diurnal thermocline within the upper 10 m. The MLD was found to be highly influenced by internal oscillations of ~ 15 m amplitude. Thermal inversions were noticed in the thermocline, especially between 30 and 40 m depth. Flow in the ML was stronger, southerly and was influenced by diurnal oscillations. But it was weaker, northerly and was influenced by semi-diurnal oscillations in the thermocline. Correlation between current and thermohaline variability due to internal tide was evident in the thermocline whereas that was weak with in the ML. Spectral analysis revealed the dominance of diurnal and semi-diurnal tides in the current and thermohaline fields. Stability computations proved that the deepening of ML was mainly due to the intrusion of warmer water between 10 and 25 m carried by the horizontal currents.

Both the models simulated the shoaling events reasonably well. But the simulation of the deepening events were discouraging due to the dominance of internal processes at the ML base at diurnal periodicity.

7.5. The Hydrographic observations on the Western Boundary Current of the Bay of Bengal during March 1993

The characteristics of the western boundary current of the Bay of Bengal (BBWBC) are studied utilising MICOM STD profiles collected during 9 to 23 March 1993 onboard FORV Sagar Sampada from an area bounded by $11^\circ N$ and $18^\circ N$ and from

coastline to ~400 km offshore. North of 15°N , the waters nearer to the coast were warmer and high saline with a cross shore gradient as seen in an alongshore current regime. A cold core and a low saline tongue of water body was noticed north of 15°N in the offshore. In general, the isotherms in the vertical zonal sections from 11°N to 18°N showed an offshore deepening indicating a northerly flow. The near shore isotherms and isohalines along 13° and 14°N were dome shaped indicating the presence of a cyclonic eddy. The dilution was more in the northern Bay north of 14°N . A high salinity pocket (> 35.2 PSU) was found between 100 and 250 m depths around 12°N and 82.5°E .

The geostrophic flow regime was dominated by the presence of few eddy type cells. The poleward flow was stronger (> 90 cm/s) with in a narrow cross stream of dimension 30 km width and deeper (500 m) in the northwestern Bay whereas it was diffused between 13°N and 15°N due to cyclonic shear. South of 13°N , the poleward flow appeared as the part of an anticyclonic eddy with a speed of ≈ 40 cm/s. The stronger poleward flow in the northwestern Bay was regarded as the BBWBC during March 1993. The volume transport showed a poleward flow across all the sections which varied between 3 and 17 Sv ($1 \text{ Sv} = 10^6 \text{ m}^3/\text{s}$). Southward transport of 3 Sv was observed nearer to the coast along 14°N due to the cyclonic eddy.

The TS characteristics revealed the presence of three salinity maxima and two minima. Among them one minimum and maximum are identified as the well known Bay of Bengal low salinity Watermass and the mixture of Red Sea and Persian Gulf Watermasses respectively.

The hydrographic features along a section from off Madras

to Andamans during May 1987, exhibited the characteristics of a well developed WBC of a subtropical gyre. The volume transport in the BBWBC region was found to be considerably higher during May 1987 (16 Sv) compared to that of March 1993 (5 Sv).

It is concluded that the flow regime inferred in the western Bay during March 1993 represented the developing phase of the western boundary current system which appeared first at the northwestern Bay as suggested by McCREARY et al. (1993). Though a "cold wall" and a haline front occur on the shoreward side of all WBCs, the same had not yet appeared at the surface level by March, but their development was clear below the mixed layer.

7.6. Future scope of the work

The correlation between the thermal field and the genesis of the meteorological systems, suggests a practical weather forecasting application. Moored telemetering buoys with thermistor chains in the areas of cyclogenesis, are to be deployed to monitor the evolution of SST and heat content of the ocean in relation to the formation of meteorological systems. Such advanced knowledge would be useful for forecasting depressions and cyclonic storms.

Short-term variability in the surface salinity in the northern Bay was found to be very conspicuous during summer monsoon which may affect the ML, stratification etc.. So this study proved the importance of the salinity which is to be monitored systematically at closer spatial and time interval in the northern Bay during summer monsoon season.

Relative importance of the coefficients for shear and wind mixing parameterization are found to be variable for

different environmental conditions in NK model. Therefore, the bench mark conditions for choosing the appropriate values for those coefficients are to be established with a number of time series data sets of different environmental settings.

Importance of the internal processes on the variability of ML characteristics was revealed from the present work. At present knowledge on the internal processes is not enough to incorporate into any operational models described in the above Chapters. This awareness necessitates a comprehensive study on the internal processes in the Bay of Bengal.

Unanswered questions about the BBWBC are many. Few of them have been described below. Observed evidence on the spatio-temporal evolution of this current system and the associated eddies and thermohaline structure is very essential but is inadequate now. Systematic spatial surveys at regular intervals off the east coast of India are to be organised to collect systematic data sets. Such surveys can also throw light on the coastal upwelling, river discharge and other dynamics of the system. Since the sharp density fronts form at the western boundary, acoustic propagation across the current system is also an aspect to be investigated in detail. Finally all the information can be utilized to model the BBWBC which is essential for the long term predictions of ML characteristics, weather forecasting, navigation, fisheries and underwater acoustic characteristics.

REFERENCES

- Ahmad N. and T. Natarajan. 1983. *Discrete time signals and systems*, Prentice Hall, New York, 398 pp.
- Alexander R. C. and J. W. Kim. 1976. Diagnostic model study of mixed layer depths in the summer north Pacific. *J. Phys. Oceanogr.*, 6, 293-298.
- Amos A. F., M. G. Langseth and R. G. Markel. 1972. *Visible oceanic saline fronts in studies*. In: *Physical Oceanography* Ed. A. L. Gordon, Gordon and Breach, New York, 49-62.
- Anon. 1978. Weather. *Indian J. Met. Hydrol. and Geophys.*, 29, 573-582.
- Anjaneyulu T. S. S. 1969. On the estimates of heat and moisture over the Indian monsoon trough zone. *Tellus*, 21, 64-75.
- Anto A. F., L. V. G. Rao and Y. K. Somayajulu 1982. Surface layer conditions of the atmosphere over the western Bay of Bengal during MONEX. *Indian J. of Mar. Sci.*, 11, 15-20.
- Anto A. F. and Y. K. Somayajulu. 1985. Structure of the oceanic mixed layer in western Bay of Bengal during MONEX. *Mausam*, 36, 519-524.
- Antony M. K., C. S. Murty, G. V. Reddy and K. H. Rao. 1985. Sub-surface temperature oscillations and associated flow in the western Bay of Bengal. *Estuar. Coast. and Shelf Sci.*, 21, 823-834.
- Awade S.T., M. Y. Totagy, and S. M. Bawiskar. 1986. Large scale features of the summer monsoon during 1979. *Mausam*, 37, 441-450.
- Babu M. T., S. P. Kumar and D. P. Rao. 1991. A subsurface cyclonic eddy in the Bay of Bengal. *J. Mar. Res.*, 49, 403-410.
- Bahulayan N. and V. V. R. Varadachari. 1986. Numerical model for wind driven circulation in the Bay of Bengal. *Indian J. Mar. Sci.*, 15, 8-12.

- Balaramamurty C. 1957. Watermasses of the western central Bay of Bengal during November. *Curr. Sci.*, 26, 80.
- Banse K. 1990. Remarks on oceanographic observations off the east coast of India. *Mahasagar*, 23, 75-84.
- Berliand M. E. and T. G. Berliand. 1952. Measurement of the effective radiation of the earth with varying cloud amounts (in Russian). *Izv. Akad. Nauk SSSR Ser. Geofiz.* No. 1.
- Borowski M. R. and J. R. Goulat. 1971. Comparison of methods for interpolating oceanographic data. *Deep-Sea Res.*, 18, 260-274.
- Brown O. B., J. G. Bruce and R. Evans. 1980. Evolution of sea surface temperature in the Somali basin during the southwest monsoon of 1979. *Science*, 209, 595-597.
- Bruce J. G. 1973. Large scale variations of the Somali current during the southwest monsoon 1970. *Deep-Sea Res.*, 20, 837-846.
- Bush N. E. 1977. Fluxes in the surface boundary layer over the sea. In: *Modeling and prediction of the upper layers of the ocean*, Ed. E. B. Kraus, Pergamon Press, Oxford 72-91 pp.
- Colborn J.G. 1975. *The Thermal Structure of the Indian Ocean*. East-West Centre Press, University of Hawaii, 173pp.
- Cooper N. S. 1988. The effect of salinity on tropical ocean models. *J. Phys. Oceanogr.*, 18, 697-707.
- Curray J. R. and D. G. Moore. 1971. Growth of the Bengal deep sea fan and denudation in the Himalayas. *Geological Society of America Bulletin*, 82, 563-572.
- Cutler A. N. and J. C. Swallow. 1984. *Surface currents of the Indian Ocean (to 25oS, 100oE): Compiled from historic data archived by the Meteorological Office, Bracknell (UK)*. Institute of Oceanographic Sciences, Report No. 187, 8pp and 36 charts.

- Davis R. E., DeZoeke and P. P. Niiler. 1981. Variability in the upper ocean during MILE. Part II. Modeling the mixed layer response. *Deep-Sea Research*, 28, 1453-1475.
- Deardorff J. W., G. E. Willis and D. K. Lilly. 1969. Laboratory investigation of non-steady penetrative convection. *J. Fluid Mechan.*, 35, 7-31.
- Denman K. L. 1973. A time dependent model of the upper ocean. *J. of Phys. Oceanogr.*, 3, 173-184.
- Denman K. L. and M. Miyake. 1973. Upper layer modification at ocean station PAPA: Observations and simulation. *J. of Phys. Oceanogr.*, 3, 185-186.
- Dobson F. W. and S. D. Smith. 1988. Bulk models of solar radiation at sea. *Quarterly Journal of Royal Meteorological Society*, 114, 165-182.
- Duing W. 1970. *The monsoon regime of currents in the Indian Ocean*. East-West Center Press, Honolulu, 68pp.
- Elsberry R.L., T.S. Fraim and R.N. Trapnell Jr. 1976. A mixed layer model of the oceanic thermal response to hurricanes. *J. Geophys. Res.*, 81, 1153-1162.
- Evans R. M. and O. B. Brown. 1981. Propagation of thermal fronts in the Somali current system. *Deep-Sea Res.*, 28, 521-527.
- Friehe C. A. and K. F. Schmitt. 1976. Parameterisation of air-sea interface fluxes of sensible heat and moisture by bulk aerodyn 801-809.
- Frohlich C. and J. London. 1986. *Revised instruction manual on radiation instruments and measurements*, World Meteorological Organisation, Geneva. WCRP Pub. ser. 7.
- Fuglister, F. C. 1972. *Cyclonic rings formed by the Gulf Stream 1965-66*. In studies in Physical Oceanography. A tribute to Georg Wust on his 80th birthday, A. L. Gordon ed., Gordon and Breach, New York, 1, 137-168.

- Fung I. Y., D. E. Harrison and A. A. Lacis. 1984. On the variability of the net longwave radiation at the ocean surface. *Reviews of Geophysics and Space Physics*, 22, 177- 193.
- Gadgil S., N. V. Joshi and P. V. Joseph. 1984. Ocean - atmosphere coupling over monsoon regimes. *Nature*. 312, 141-143.
- Ganapati P. N. and V. S. Murthy. 1954. Salinity and temperature variations of the surface waters off Visakhapatnam coast. *Andhra Uni. Mem. Oceanogr.*, 1, 125-142.
- Garwood R. W. 1977. An oceanic mixed layer capable of simulating cyclic states. *J. Phys. Oceanogr.*, 7, 455-468.
- Goel M. and H. N. Srivastava. 1990. Monsoon trough boundary layer experiment (MONTBLEX). *Bulletin of the American Meteorological Society*, 71, 1594-1599.
- Gonella, J. 1972. A rotary-component method for analysing meteorological and oceanographic vector time series. *Deep- Sea Res.*, 19, 833-848.
- Gopalakrishna, V.V. and J. S. Sastry. 1986. Surface circulation over the shelf off the east coast of India during the south west monsoon. *Indian Jour. Mar. Sci.*, 14, 60-65.
- Gopalakrishna, V.V., Y.Sadhuram, V. Ramesh Babu and M. V. Rao. 1988. Variability of windstress and currents at selected locations over the north Indian Ocean during 1977 and 1979 summer monsoon seasons. *Mausam*, 39, 159-166.
- Graham N. E. and Barnet T. P. 1987. Sea surface temperature, surface wind divergence and convection over tropical oceans. *Science*, 238, 657-659.
- Gray W. M. 1975. Tropical cyclone genesis. *Dept. Atmos. Sci., Paper 232*, Colorado State University, Ft. Collins Co., 121 pp.

- Hareesh Kumar P. V., T. Pradeep Kumar, B. Mathew and M. X. Joseph. 1990. Upper ocean thermal structure off Karwar (west coast of India) during the withdrawal phase of monsoon-1987. *Indian Journal of Marine Sciences*, 19, 36-41.
- Harenduprakash L. and A. K. Mitra. 1988. Vertical turbulent mean flux below the sea surface and air-sea interaction-monsoon regime of the Indian Ocean. *Deep-Sea Res.*, 35, 333-346.
- Hastenrath S. and L. L. Greischar. 1989. *Climatic Atlas of the Indian Ocean - Part III: Upper-Ocean Structure*. University of Wisconsin press, Wisconsin.
- Hastenrath S. and P. J. Lamb. 1979. *Climatic Atlas of the Indian Ocean. Part I. Surface climate and atmospheric circulation*. University of Wisconsin press, Madison.
- Holeman J. N. 1968. The sediment yield of major rivers of the world. *Water Resources Res.*, 4, 787-799.
- Holt T. and Sethuraman. 1986. Observations of the mean and turbulence structure of the marine boundary layer over the Bay of Bengal during MONEX-79. *Monthly Weather Review*, 114, 2176-2190.
- INDIA METEOROLOGICAL DEPARTMENT 1979. *Tracks of storms and depressions in the Bay of Bengal and Arabian Sea (1987-1970)*, New-Delhi, India.
- Johns, B. and A. Ali. 1992. On the formation of a western boundary current in the Bay of Bengal. *J. Mar. Sys.*, 3, 267-278.
- Johns, B., A. D. Rao and G. S. Rao. 1992. On the occurrence of upwelling along the east coast of India. *Estuarine, Coast. and Shel. Sci.*, 35, 75-90.
- Joseph M. G., P. V. Hareesh Kumar and M. X. Joseph. 1992. Deep and shallow water characteristics of mixed layer response to momentum and buoyancy fluxes off Bombay, west coast of India, during winter. *Cont. Shel. Res.*, 12, 661-673.

- Kato H. and O. M. Phillips. 1969. On the penetration of a turbulent layer into stratified fluid. *Journal of Fluid Mechanics*, 37, 643-655.
- Kim J. W. 1976. A generalised bulk model of the oceanic mixed layer. *J. Phys. Oceanogr.*, 6, 686-695.
- KNMI. 1952. *Indische Ocean Oceanographische and Meteorologische gegevens*. 2 Ed. Publ. No.135, I, 31pp and II, 24 charts.
- Kraus E. B. and J. S. Turner. 1967. A one dimensional model of the seasonal thermocline: II. The general theory and its consequences. *Tellus*, 19, 98-106.
- Krishnamurti T. N. and H. N. Balme. 1976. Oscillations of a monsoon system, I: Observational aspects. *J. Atmos. Sci.*, 33, 1937-1954.
- Kumar S. P., M. T. Babu and D. P. Rao. 1992. Energy and generating mechanism of a subsurface, cold core eddy in the Bay of Bengal. *Indian J. Mar. Sci.*, 21, 140-142.
- LaFond E. C. 1954. On upwelling and sinking off the east coast of India. *Andhra Univ. Memo. in Oceanogr.*, 1, 117-121.
- LaFond E. C. 1957. Oceanographic studies in the Bay of Bengal. *Proc. Indian Aca. Sci.*, XLVI (B), 1-46.
- LaFond E. C. 1958a. On the circulation of the surface layers of the east coast of India. *Andhra Uni. Mem. Ocean.*, 2, 1-11.
- LaFond E. C. 1958b. Seasonal cycle of SST and salinity along the East Coast of India. *Andhra Uni. Mem. Ocean.*, 2, 12-21.
- LaFond E. C. 1972. Tidal currents and their relation to the shelf zone of the continental shelf off Waltair. *Indian J. Mar. Sci.*, 1, 66-73.
- LaFond E. C. and A. T. Moore. 1972. Sea temperature variations off the east coast of India. *Indian J. Mar. Sci.*, 1, 63-65.

- LaFond E. C. and Rao C. P. 1954. Vertical oscillations of tidal periods in the temperature structure of the sea. *Andhra Univ. Mem.*, 1, 109-116.
- LaFond E. C. and K. G. LaFond. 1968. Studies of oceanic circulation in the Bay of Bengal. *Bulletin of National Institute of Sciences of India*, 38, 164-183.
- LaFond, E. C. and R. P. Rao. 1956. On the erosion of the beach at Uppada. *Port Engr.*, 5, 2-7.
- Lau K. M. and P. H. Chan. 1988. Intraseasonal and interannual variations of tropical convection: a possible link between the 40 day mode and ENSO. *J. Atmos. Sci.*, 45, 950-972.
- LaViolette P. E. 1967. *Temperature, salinity and density of the world's seas. Bay of Bengal and Andaman Sea.* U. S. Naval Oceanographic Office, Washington D.C., Rept. No. IR-67-57.
- Leetmaa, A., D. R. Quadfasel and D. Wilson. 1982. Development of the flow field during the onset of the Somali current, 1979. *J. Phys. Oceanogr.*, 12, 1325-1342.
- Legeckis R. 1987. Satellite observations of a western boundary current in the Bay of Bengal. *J. Geophys. Res.*, 92, 12974-12979.
- Legeckis R. 1991. Personal communication.
- Levitus S. 1982. *Climatological atlas of the world ocean.* NOAA Prof. Paper No.13. U. S. Government Printing Office, (Washington D. C.), 173 pp.
- Levitus S. 1986. Annual cycle of salinity and salt storage in the world ocean. *J. of Phys. Oceanogr.*, 16, 320-343.
- Lumb F. E. 1964 The influence of clouds on hourly amounts of total solar radiation at the sea surface. *Quarterly Journal of Royal Meteorological Society*, 90, 43-56.

- Mathew B. 1983. Studies on upwelling and sinking in the seas around India, Ph.D Thesis, University of Cochin, pp 159.
- McCreary J. and P. K. Kundu. 1985. Western boundary circulation driven by an alongshore wind: With application to the Somali current system. *J. Mar. Res.*, 43, 493-516.
- McCreary J. and P. K. Kundu. 1989. A numerical Investigation of Sea Surface Temperature Variability in the Arabian Sea. *Journal of Geophysical Research*, 94, 16097-16114.114.
- McCreary, J. P., P. K. Kundu and R. L. Molinari. 1993. A numerical investigation of dynamics, thermodynamics and mixed-layer processes in the Indian Ocean. *Prog. Oceanogr.*, 31, 181-244.
- Mellor G. L. and P. A. Durbin. 1975. The structure and dynamics of the ocean surface layer. *Journal of Physical Oceanography*, 5, 718-728.
- Miller J. R. 1976. The salinity effect in a mixed layer ocean model. *Journal of Physical Oceanography*, 6, 29-35.
- Mooley D. A. and J. Shukla. 1989. Index of the monsoon trough over India. *Mausam*, 40, 247-258.
- Munk W. M. 1966. Abyssal Recipes. *Deep-Sea Res.*, 13, 707-730.
- Murthy P. G. K. and P. V. Hareesh Kumar. 1991. Response of coastal waters off Karwar to a deep depression. *Continental Shelf Research*, 11, 239-250.
- Murty C. B. 1958. On the temperature and salinity structure of the Bay of Bengal. *Curr. Sci.*, 27, 249.
- Murty C. S. and V. V. R. Varadachari. 1968. Upwelling along the east coast of India. *Bull. Natl. Inst. Sci. India.* , 38, 80-86.

- Murty C. S., P. K. Das and A. D. Gouveia. 1981. Some physical aspects of the surface waters around the Little Andaman island. *Indian J. Mar. Sci.*, 10, 221-227.
- Murty V. S. N., A. Suryanarayana and D. P. Rao. 1993. Current structure and volume transport across 12°N in the Bay of Bengal. *Indian J. Mar. Sci.*, 22, 12-16.
- Murty V. S. N. and D. P. Rao. 1992. Potential vorticity field in the Bay of Bengal during southwest monsoon. *Proc. First Convention Indian Society for Physical Sciences of the Ocean*, 63-68.
- Murty V. S. N., Y. V. B. Sarma, D. P. Rao and C. S. Murty. 1992. Water characteristics, mixing and circulation in the Bay of Bengal during southwest monsoon. *J. Mar. Res.*, 50, 207-228.
- Nieuwolt S. N. 1977. *Tropical climatology*. John Wiley & Sons, 82-83.
- Niiler P. P. 1975. Deepening of the wind mixed layer. *Journal of Marine Research*, 33, 405-422.
- Niiler P. P. and E. B. Kraus. 1977. *One dimensional models of the upper ocean*. In: *Modelling and prediction of the upper layers of the ocean*, E. B. Kraus, Editor, Pergamon Press, Oxford, pp 143-172.
- Oke T. R. 1987. *Boundary Layer Climatology*. Methuen, USA, pp 435.
- Osborne A. R. and T. L. Burch. 1980. Internal solitons in the Andaman Sea. *Science*, 208, 451-460.
- Paulson C A and J J Simpson. 1977. Irradiance measurements in the upper ocean. *Journal of Physical Oceanography*, 7, 952-956.
- Payne R E. 1972. Albedo of sea surface. *Journal of Atmospheric Sciences*, 29, 959-970.
- Pickard G. and W. J. Emery. 1990. *Descriptive Physical Oceanography. An Introduction*. Pergamon Press,

Oxford, 249pp.

- Phyllips O. M. 1966. *Dynamics of the Upper Ocean*. Cambridge University Press, Cambridge, 261 pp.
- Pisharoty P. R. 1964. Monsoon pulses. *Proc. WMO Sympos. on Topical Meteorology*, Rotorua, New Zealand, pp 373-378.
- Pollard R. T., R. B. Rhines and R. O. R. Y. Thompson. 1973. The deepening of the wind mixed layer. *Geophysical Fluid Dynamics*, 4, 381-404.
- Pollard, R.T. and R. C. Millard. 1970. Comparison between observed and simulated inertial oscillations. *Deep-Sea Res.*, 17, 813-821.
- Potemra, J. T., M. E. Luther and J. J. O'Brien. 1991. The seasonal circulation of the upper ocean in the Bay of Bengal. *J. Geophys. Res.*, 96, 12667-12683.
- Premchand, K., J. S. Sastry and C. S. Murty. 1986a. Watermass structure in the western Indian Ocean - Part II: The spreading and transformation of Persian Gulf Water. *Mausam*, 37, 179-186.
- Premchand, K., J. S. Sastry and C. S. Murty. 1986b. Watermass structure in the western Indian Ocean - Part III: The spreading and transformation of Red Sea Watermass. *Mausam*, 37, 317-324.
- Price, J.F. and R.A. Weller. 1986. Diurnal cycling: observations and models of the upper ocean response to diurnal heating, cooling and wind mixing, *J. Geophys. Res.*, 91, 8411-8427.
- Price J. F., C. N. K. Mooers and J. C. Van Leer. 1978. Observation and Simulation of Storm Induced Mixed Layer Deepening. *J. Phys. Oceanogr.*, 8, 582-599.
- Price, J.F., R.A. Weller, C.M. Bowers and M.G. Briscoe. 1987. Diurnal response of sea surface temperature observed at the long-term upper ocean study (34 N, 70 W) in the Sargasso Sea. *J. Geophys. Res.*, 92, 14480-14490.

- Price J. F., R. A. Weller and R. Pinkel. 1986. Diurnal cycling : Observations and models of the upper ocean response to diurnal heating, cooling and wind mixing. *J. Geophys. Res.*, 91, 8411-8427.
- Raghavan K. 1973. Break monsoon over India. *Monthly Weather Review*, 101, 33-43.
- Raju V. S. R., V. V. Sarma, B. P. Rao and V. S. Rao. 1992. Watermasses of Visakhapatnam shelf waters. *Proc. First Convention Indian Society for Physical Sciences of the Ocean*, 75-78.
- Raman C. R. V., Y. P. Rao, S. K. Subrahmaniyam and Z. E. Shaikh. 1978. Wind shear in monsoon depression. *Nature*, 275, 53-53.
- Rama Raju D. V., Gouveia A. D. and Murty C. S. 1981. Some physical characteristics of Andaman sea waters during winter. *Indian J. Mar. Sci.*, 10, 211-218.
- Ramasastri A. A. and C. B. Murty. 1957. Thermal field and oceanic circulation along the east coast of India. *Proc. Indian. Aca. Sci.*, XLVI.
- Ramesh Babu V. and Sastry J. S. 1976. Hydrography of the Andaman sea during late winter. *Indian J. Mar. Sci.*, 5, 179-189.
- Ramesh Babu V. and Sastry J. S. 1981. Heat storage in the Andaman sea. *Mausam*, 32, 145-150.
- Rao A. D., P. C. Sinha, S. K. Dube and S. Chamarthi. 1993. Numerical simulation of upwelling off Visakhapatnam on east coast of India during pre-monsoon months. *Proc. Indian Acad. Sci.*, 102, 465-486.
- Rao C. P. 1956a. Currents off Visakhapatnam Coast in March. *Indian J Met. Geophys.*, 7, 377-379.
- Rao C. P. 1956b. Watermasses in the Bay of Bengal. *Curr. Sci.*, 25, 51-53.

- Rao D. P. and J. S. Sastry. 1981. Circulation and distribution of some hydrographical properties during the late winter in the Bay of Bengal. *Mahasagar*, 14, 1-16.
- Rao D.S., and R. R. Rao. 1986. A case study on the genesis of a monsoon low and the thermal structure of the upper northern Bay of Bengal during MONEX-79. *Mahasagar*, 19, 1-9.
- Rao, K. H., M. K. Antony, C. S. Murty and G. V. Reddy. 1986. Gyres in the northwestern Bay of Bengal - some observed evidences. *Indian J. Mar. Sci.*, 16, 9-14.
- Rao P. B., V. R. Babu and P. Chandramohan. 1987. Seasonal and diurnal variability of thermal structure in the coastal waters off Visakhapatnam. *Proc. Indian Aca. Sci. (Earth and Plan. Sci.)*, 96, 69-79.
- Rao P. B. and Y. Sadhuram. 1992. Seasonal variability of heat flux divergence in the coastal waters of Visakhapatnam. *Proc. First Conv. Indian Soc. Physical Sci. of Ocean*, held at Goa, 1990, 1-5.
- Rao P. K. 1974. Surface circulation features in the Bay of Bengal as seen in ERTS imageries. *Mahasagar*, 7, 1-13.
- Rao R. R. 1986. Cooling and deepening of the mixed layer in the central Arabian Sea during MONSOON - 77: Observations and simulations. *Deep - Sea Research*, 33, 1413-1424.
- Rao R. R. 1987. Further analysis on the thermal response of the upper Bay of Bengal to a pre-monsoon cyclonic storm and summer monsoonal onset during MONEX-79. *Mausam*, 38, 142-156.
- Rao R. R. and B. Mathew. 1988. On the observed synoptic variability in the thermal structure of the upper northern Bay of Bengal during MONEX-79. *Proceedings of Indian Academy of Sciences*, 94, 21-34.
- Rao R. R. and B. Mathew. 1990. A case study on the mixed layer variability in the south central Arabian Sea during the onset phase of MONEX- 79. *Deep-Sea*

Research, 37, 227-243.

- Rao R. R., B. Mathew and P. V. Hareesh Kumar. 1993. A summary of results on thermohaline variability in the upper layers of the east central Arabian Sea and Bay of Bengal during summer monsoon experiments. *Deep-Sea Res.*, 40, 1647-1672.
- Rao R. R., D. S. Rao, P. G. K. Murthy and M. X. Joseph. 1983. A preliminary investigation on the summer monsoonal forcing on the thermal structure of upper Bay of Bengal during MONEX-79. *Mausam*. 34, 239-250.
- Rao R.R., K.V.S. Ramam, D.S. Rao and M.X. Joseph. 1985. Surface heat budget estimates at selected areas of the north Indian Ocean during MONSOON-77. *Mausam*, 36, 21-32.
- Rao R. R., R. L. Molinari and J. F. Festa. 1989. Evolution of the climatological near-surface thermal structure of the tropical Indian Ocean. Part I: Description of mean monthly mixed-layer depth and sea-surface temperature, surface current and surface meteorological fields. *J. Geophys. Res.*, 94, 10801-10815.
- Rao R. R., R. L. Molinari and J. F. Festa. 1991. *Surface meteorological and near surface oceanographic atlas of the tropical Indian Ocean*. NOAA Tech. Memo. ERL AOML-69.
- Rao R. R., S. V. S. Somanadham, S. S. V. S. Ramakrishna and R. Ramanadham. 1987. A case study on the genesis of a monsoon depression in the northern Bay of Bengal during MONSOON 77 experiment. *Mausam*, 38, 387-394.
- Rao R.R., V. V. Gopalakrishna and S. V. Babu. 1981. A case study on the northern Bay of Bengal subsurface thermal structure and ocean mixed layer depth in relation to surface energy processes. *Mausam*, 32, 85-92.
- Rao T. V. N., D. P. Rao, B. P. Rao and V. S. R. Raju. 1986. Upwelling and sinking along Visakhapatnam coast. *Indian Journal of Marine Sciences*, 15, 84-87.

- Rao Y. P. 1976. *Southwest monsoons, Meteorological Monographs, Synoptic Meteorology.* India Meteorological Department, Delhi, India, 367 pp.
- Robinson M.K., R.A. Baur and E.H. Schroeder. 1979. *Atlas of North Atlantic-Indian Ocean monthly mean temperature and mean salinities of the surface layer.* Naval Oceanographic Office Reference Publication 18, Department of the Navy, Washington, D.C., 20373, 213pp.
- Rochford D. J. 1964. Salinity maxima in the upper 100 m of the North Indian Ocean. *Aust. J. Mar. Fresh Water Res.*, 15, 1-24.
- Sanil Kumar K. V., K. D. K. M. Sarma, M. X. Joseph and N. K. Viswambharan. 1989. Variability of current and thermohaline structure off Visakhapatnam during late June 1986. *Indian J. Mar. Sci.*, 18, 232-237.
- Sanil Kumar K. V., N. Mohankumar, M. X. Joseph and R. R. Rao. 1995a. Genesis of meteorological disturbances and thermohaline variability of the upper layers in the head of the Bay of Bengal during Monsoon Trough Boundary Layer Experiment (MONTBLEX-90) *Deep-Sea Res.*, (under publication).
- Sanil Kumar K. V., P. Madhusoodhanan, M. G. Joseph and Basil Mathew. 1991. Mixed layer variability in the east central Arabian Sea. *Indian J. Mar. Sci.*, 20, 239-243.
- Sanil Kumar K. V., P. V. Hareesh Kumar and M. X. Joseph. 1993. Observations and simulations of the mixed layer characteristics off Bombay, west coast of India during the summer monsoon of 1988. *Estuar. Coast. Shelf Sci.* 36, 59-69.
- Sanil Kumar K. V., T. V. Kuruvilla, Jogendranath D. and R. R. Rao. 1995b. On the western boundary current of the Bay of Bengal. *Deep-Sea Res.*, (under publication).
- Sarma K. D. K. M., B. Mathew and R. R. Rao. 1988. Observed salinity field in the upper layers of the Bay of

- Bengal during summer monsoon experiments. *Mahasagar*, 21, 75-83.
- Sarma M. S. S. and L. V. G. Rao. 1986. Currents and temperature structure off Godavari (east coast of India) during September 1980. *Indian J. Mar.*, 15, 88-91.
- Sarma Y. V. B., M. S. S. Sarma, R. J. Krishnamacharyulu and D. P. Rao. 1991. Subsurface oscillations at an oceanic station in the Bay of Bengal. *Indian J. Mar. Sci.*, 20, 204-207.
- Sastry J. S., D. P. Rao, V. S. N. Murty, Y. V. B. Sarma, A. Suryanarayana and M. T. Babu. 1985. Watermass structure in the Bay of Bengal. *Mahasagar - Bull. Natl. Inst. Oceanogr.*, 18, 153-162.
- Sastry J. S., K. Premchand and C. S. Murty. 1986. Watermass structure in the western Indian Ocean:- Part I Watermasses and their thermohaline indices. *Mausam*, 37, 107-140.
- Schott F. 1983. Monsoon response of the Somali Current and associated upwelling. *Progr. Oceanogr.*, 12, 357-381.
- Sen Gupta R., C. Moraes, M. D. George, T. W. Kureishy and R. J. Noronha. 1981. Chemistry and hydrography of the Andaman sea. *Indian J. Mar. Sci.*, 10, 208-233.
- Sewell R. B. S. 1925-1935. *Memoirs of the Asiatic Society of Bengal*, 9, Nos 1-8.
- Shammi Raj P. V. Varkeyachan and A. V. S. Murty. 1989. Diel variations of heat fluxes across the air-sea interface from the Bay of Port Blair. *Proc. first workshop on Scientific results of FORV Sagar Sampada*, June, 1993, Cochin 11-14.
- Shcherbinin A. D., V. S. Arsen'yev and Yu. A. Gol'din. 1979. The western boundary current of the Bay of Bengal. *Dokl. Acad. Sci. USSR, Earth Sciences Section*. English Translation, 244, 167-168.
- Shetye S. R. 1993. The movement and implications of the Ganges-Brahmaputra runoff on entering the Bay of

Bengal. *Current Sci.*, **64**, 32-38.

Shetye S. R. and S. S. C. Shenoi. 1988. Seasonal Cycle of surface circulation in the North Indian Ocean. *Proc. Indian Aca. Sci. (Earth and Planet. Sci.)*, **97**, 53-62.

Shetye S. R., S. S. C. Shenoi, A. D. Gouveia, G. S. Michael, D. Sundar and G. Nampoothori. 1991. Wind-driven coastal upwelling along the western boundary of the Bay of Bengal during the southwest monsoon. *Cont. Shelf Res.*, **11**, 1397-1408.

Shetye S. R., A. D. Gouveia, S. S. C. Shenoi, D. Sundar, G. S. Michael and G. Nampoothori. 1993. The western boundary current of the seasonal subtropical gyre in the Bay of Bengal. *J. Geophys. Res.*, **98**, 945-954.

Sprintall J. and M. Tomczak. 1990. Salinity considerations in the oceans' mixed layer. *Ocean Sciences*, Institute Rept. No. 36, Univ. of Sydney, 170 pp.

Stevenson J. W. and P. P. Niiler. 1983. Upper ocean heat budget during Hawaii to Tahiti shuttle experiment. *J. Phys. Oceanogr.*, **13**, 1894-1907.

Subbaramayya I. and M. S. Rao. 1981. Cyclone climatology of North Indian Ocean. *Indian J. Mar. Sci.*, **10**, 366-368.

Suryanarayana A. and D. P. Rao. 1992. Coastal circulation and upwelling index along the east coast of India. *Proc. First Conv. Indian Soc. Physical Sci. of Ocean*, held at Goa, 1990, 125-129.

Suryanarayana A., V. S. N. Murty and D. P. Rao. 1993. Hydrography and circulation of the Bay of Bengal during early winter, 1983. *Deep-Sea Res.*, **40**, 205-217.

Swallow J. C. 1983. *Eddies in the Indian Ocean*. In: *Eddies in Marine Sciences*, A. R. Robinson, Editor, Springer-Verlag, Berlin, pp. 200-218.

Swallow J. C., R. L. Molinari, J. G. Bruce, O. B. Brown and R. H. Evans. 1983. Development of near-surface

- flow patterns and water-mass distribution in the Somali Basin in response to the southwest monsoon, 1979. *J. Phys. Oceanogr.*, 13, 1398-1415.
- Thompson R. O. R. Y. 1976. Climatological numerical models of the surface mixed layer of the ocean. *J. Phys. Oceanogr.*, 6, 496-503.
- Toole J. M. and M. E. Raymer. 1985. Heat and fresh water budgets of the Indian Ocean - revisited. *Deep-Sea Res.*, 32, 917-925.
- Turner J. S. 1969. A note on wind mixing at the seasonal thermocline. *Deep-Sea Res.*, 16 (Supplement), 297-300.
- UNESCO. 1988. *River inputs to ocean systems: status and recommendations for research.* Unesco Technical Papers in Marine Science, No. 55, Final report of SCOR Working Group 46, Paris, 25 pp.
- Unnikrishnan A. S. and N. Bahulayan. 1991. Simulation of barotropic wind driven circulation in the Bay of Bengal and Andaman Sea during pre-monsoon and post-monsoon seasons. *Indian J. Mar. Sci.*, 20, 97-101.
- U.S. Navy. 1976. *Marine Climatic Atlas of the World*, Vol III, Indian Ocean, 248pp.
- Varadachari V. V. R., C. S. Murty and P. K. Das. 1968a. On the level of least motion and the circulation in the upper layers of the Bay of Bengal. *Bull. Natl. Inst. Sci. India*, 38, 301-307.
- Varadachari V. V. R., C. S. Murty and C. V. G. Reddy. 1968b. Salinity maxima associated with some sub-surface water masses in the upper layers of the Bay of Bengal. *Bull. Natl. Inst. Sci. India*, 38, 338-343.
- Varkey M. J. 1986. *Salt balance and mixing in the Bay of Bengal.* Ph. D. Thesis, Uni. Kerala, 109 pp.
- Varkey M. J. and J. S. Sastry. 1992. Estimates of runoff evaporation and precipitation for Bay of Bengal on

seasonal basis. *Proc. First Conv. Indian Society for Physical Sciences of the Ocean, held at Goa*, 43-45.

Wu J. 1980. Wind-stress coefficient over sea surface near neutral conditions - a revisit. *J. Phys. Oceanogr.*, 10, 727-740.

Wyrtki K. 1971. *Oceanographic Atlas of the International Indian Ocean Expedition*. National Science Foundation, Washington, D.C., 531pp.

Yu L., J. J. O'Brien and J. Yang. 1992. On the remote forcing of the circulation in the Bay of Bengal. *J. Geophys. Res.*, 96, 20449-20454.